

**TOXICITY OF ENGINEERED NANOPARTICLES TOWARDS
VERTEBRATE CELLS *IN VITRO***

Kumulative Dissertation

Zur Erlangung des akademischen Grades
Doctor rerum naturalium (Dr. rer. nat.)
der Naturwissenschaftlichen Fakultät I - Biowissenschaften
der Martin-Luther-Universität Halle-Wittenberg

vorgelegt von
Frau Diplom-Ingenieurin (FH) für Biotechnologie
Wibke Busch

Gutachter: Prof. Kristin Schirmer
Prof. Gerd-Joachim Krauß
Prof. Heidi Foth

eingereicht am: 08.07.2010

mündliche Prüfung am: 08.12.2010

Leipzig/Halle 2010

Diese Doktorarbeit wurde angefertigt am
Helmholtz – Zentrum für Umweltforschung - UFZ
in Leipzig,
im Department Zelltoxikologie (jetzt Department Bioanalytische Ökotoxikologie)
unter der Betreuung von Prof. Kristin Schirmer (jetzt EAWAG, Schweizer
Wasserforschungsinstitut) und Dr. Stefan Scholz

Von Seiten der Universität erfolgte die Betreuung durch
Prof. Dr. Gerd-Joachim Krauß,
Institut für Biochemie und Biotechnologie,
Abteilung Ökologische und Pflanzen-Biochemie
Martin-Luther-Universität Halle-Wittenberg

Diese Arbeit wurde als Teil des Verbundprojekts
„Identifizierung und Bewertung von Gesundheits- und Umweltauswirkungen
von technischen nanoskaligen Partikeln (INOS)“
„Arbeitspaket IV (UFZ): Toxikologische Analyse von Nanopartikeln und
Identifizierung von Wirkmechanismen“
durchgeführt. INOS wurde durch das Bundesministerium für Bildung und
Forschung (BMBF) im Rahmen der Förderrichtlinie „NanoChem – Chemische
Nanotechnologien für neue Werkstoffe und Produkte“ innerhalb des
Rahmenprogramms „Werkstoffinnovationen für Industrie und Gesellschaft -
WING“ (FKZ 03X0013C) gefördert. Zusätzliche Förderung erfolgte durch die Max
Buchner Forschungsstiftung.

TABLE OF CONTENTS

Chapter 1	General Introduction	7
Chapter 2	Internalisation of engineered nanoparticles into mammalian cells <i>in vitro</i> : influence of cell type and particle properties	21
Chapter 3	Toxicity of tungsten carbide and cobalt-doped tungsten carbide nanoparticles in mammalian cells <i>in vitro</i>	49
Chapter 4	Agglomeration of tungsten carbide nanoparticles in exposure medium does not prevent uptake and toxicity toward a rainbow trout gill cell line	67
Chapter 5	Tungsten carbide cobalt nanoparticles exert hypoxia-like effects on the gene expression level in human keratinocytes	87
Chapter 6	Summary and Conclusion	113
	Zusammenfassung	119
	References	125
	Appendix	139
	Authors' contributions to the manuscripts	143
	Curriculum vitae	145
	Eidesstattliche Erklärung	147
	Danksagung	149

Chapter 1

General Introduction

Nanotechnology is one of the most promising and emerging technologies today. The amazing potential of this new technology, however, also comes with novel risks and uncertainties. The assessment of risks evolving from a new technology is a great challenge and should be carried out in parallel to the technological developments. The research of this thesis concentrated on the toxicological assessment of engineered nanoparticles which are under development for industrial applications. As part of an interdisciplinary project, the work presented in this thesis demonstrates new knowledge about nanoparticle toxicity, evidence for modes of action and methods for toxicological assessment of nanoparticles.

Nanotechnology and Nanomaterials

In 1959, the physicist Richard Feynman summarised his vision on rearranging atoms, miniaturising computers and the ability to understand, produce and apply smaller and smaller building blocks of nature as “There’s plenty of room at the bottom” (Feynman 1991). Today, in the 21st century, nanotechnology is an emerging technology that promises revolutionary improvement of products and materials for new applications. Materials at the “nano” scale are characterised by having at least one dimension below 100 nm. At this size, materials show different behaviour and physico-chemical properties compared to the same material of larger size (bulk material), particularly with respect to conductivity, density, hardness, surface area, and surface layer composition but also other properties. These special characteristics are based on two features occurring at the nanoscale. The first is the increased surface to volume ratio, which results in a higher proportion of atoms at the surface (Nel et al. 2006). Based on this feature, chemical reactivity of the materials can be increased, turning nanomaterials into effective catalysts. A second feature of the nanoscale is the dominance of physical quantum effects which influences properties like transparency or conductivity. Due to these specific properties, nanostructures are used in products ranging from computer chips, composites, and coatings, to cosmetics, medicine, food and beverages.

Nanotechnology-based industries are developing rapidly. The production of engineered nanoparticles based on e.g. carbon, tungsten, titanium, silver, zinc, silicon, gold and cobalt constitutes the greatest part of nano-technological production so far. Resulting nanomaterials, such as metal oxides (TiO₂, SiO₂, ZnO), metals (Ag, Au), ceramics (WC-Co, TiN, SiC) or carbon nanotubes and fullerenes are not only used for industrial applications in their raw form or as composites, but also for consumer products (The Royal Society and the Royal Academy of Engineering 2004). For example, the production volumes for titanium nanoparticles were estimated to reach several hundreds of tons every year (Mueller & Nowack 2008, Gottschalk et al. 2009). For silver and carbon nanotubes, current estimations of the production volumes are lower (10 to 100 t/a in the U.S. for both materials; (Gottschalk et al. 2009)); data about total production volumes of other kinds of nanoparticles are hardly available. However, the fact that over 1000 consumer products were listed in august 2009 by the “Project on Emerging

Nanotechnologies” as containing nanomaterials suggests high production volumes for several kinds of nanoparticles (www.nanotechproject.org).

Potential influence of nanomaterials on human health and the environment

Nanomaterials are produced and applied for products that improve our daily life (e.g. medical products, cleaning products, cosmetics, computer technique) and also for industrial applications (e.g. paintings, coatings, powders and fibres for the production of materials with new properties). However, increased production levels inevitably lead to increasing incidence of the materials in the environment and to the exposure of humans even though this might not be intended. Experiences, e.g. with pharmaceuticals or industrial chemicals, showed that substances produced and used in high amounts are deposited into the environment and can be found in water, air and soil and even in regions far from the production sites (Muir et al. 1988, Muir & Norstrom 2000). Based on these experiences, the U.S. Environmental Protection Agency (U.S. EPA) published a scheme of potential human and environmental exposure paths and the ways of dispersal of nanomaterials into the environment (Figure 1).

Indeed, some pharmaceuticals and industrial chemicals were found to cause several drastic effects in the environment long time after the start of their industrial large-scale production. An example was the declining population of vultures in Pakistan due to diclofenac, a widely used drug for livestock treatment (Oaks et al. 2004). Another example are endocrine disruptions of fish or snail populations due to chemicals in the environment (Jobling & Tyler 2003, Oetken et al. 2004). Whether nanomaterials in the environment carry a similar hazardous potential is still unknown. However, the occurrence of engineered nanomaterials, especially those present as free particles, in the environment is most likely. Products with a high potential for release of nanoparticles into the aquatic environment include sunscreens, which contain titanium dioxide nanoparticles. They may be washed off during swimming or showering. Toothpaste contains nano-silicon and titanium dioxide as a polishing component. Many sealing products for car glass, household surfaces or shoes are already on the market. They are all able to form thin films on the surfaces (lotus effect) in order to make them moisture and dirt resistant. During

their usage or after disposal, nanoparticles may leach and finally be released to the environment via surface runoff or waste waters.

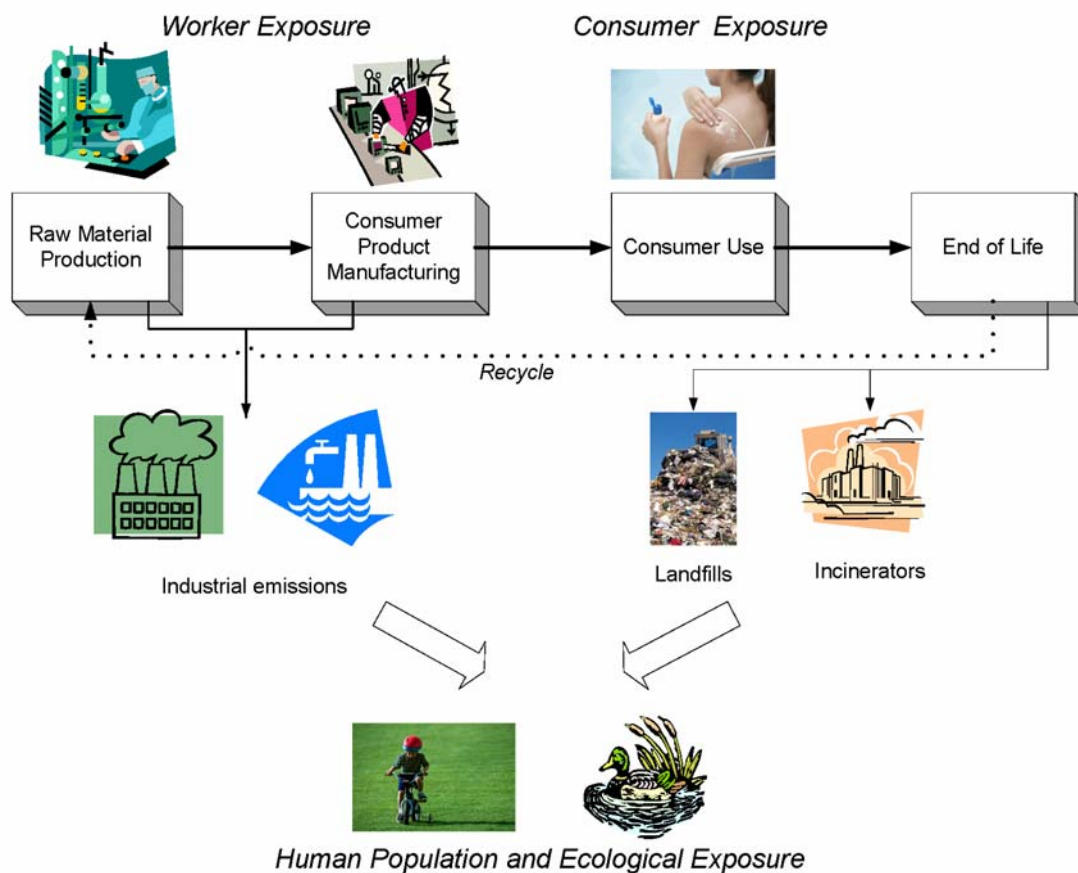


Figure 1. Life cycle perspective of nanomaterials. Picture was taken from U.S. EPA Nanotechnology, White Paper, February 2007.

An environmental contamination is an exposure path for humans as well. Moreover, exposure of humans occurs occupationally via consumer products or the ambient air. Nanomaterials might be inhaled, ingested, or enter the organism via the skin. Therefore, the lung, the intestine tract and the skin could be particularly affected by unintended exposure of humans to nanomaterials. Because non-immobilized nanomaterials in particulate form may be transported via air or liquids, inhaled, ingested or absorbed, they are considered the most relevant group of nanomaterials from a risk assessment point of view. The hazard assessment of such nanomaterials, namely engineered nanoparticles for industrial applications, was the subject of this thesis.

Nanoparticles exhibit a size in the range much smaller than cells but in the same order of magnitude as biological molecules such as proteins and DNA (Figure 2). On the one

hand, this small size carries a great potential for medical and industrial applications but it is the same feature that, on the other hand, gives reason for concerns.

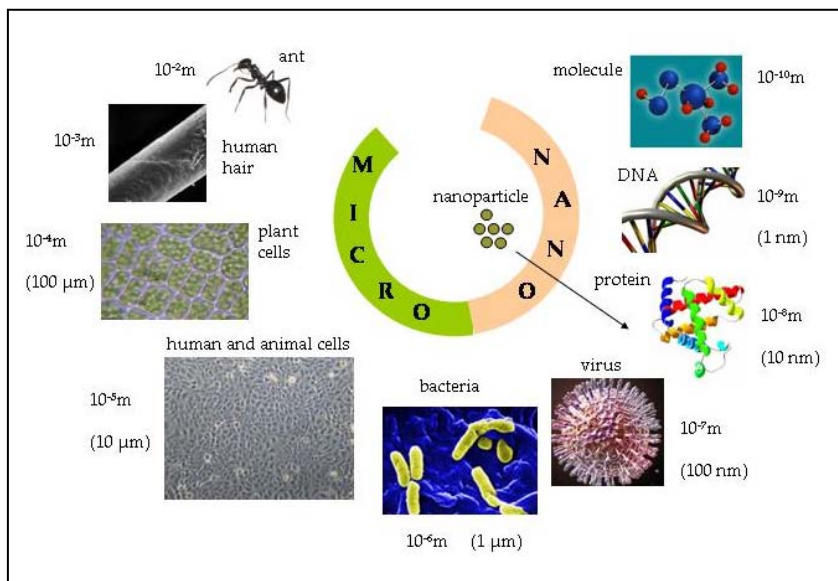


Figure 2. The micro and the nano scale. Nanoparticles are much smaller than a human hair or cell. The nanoparticles' size range coincides with that of biological molecules.

Nanoparticles for medical applications are specifically designed to be able to reach and enter target cells. In fact, improvements in cancer treatment, cell imaging or drug delivery applications demonstrate examples for the positive potential of nanoparticles on human health (Salata 2004, Nie et al. 2007, Blanco et al. 2009).

However, industrial non-medical nanoparticles, which are not designed for biological interactions, might enter cells unintentionally because of their small size and cause undesired effects. Indeed, past experiences with micro-scaled fibres and particles, such as asbestos and crystalline silica, as well as current debates about dust pollution and particulate matter, give rise to concerns about the potential hazardous effects of nanoparticles. Severe lung diseases (such as mesothelioma, lung cancer, or pulmonary fibrosis) provoked by fibres or/and particles occur long time after exposure e.g. as a result of chronic inflammation. Particulate matter in ambient air arising from industrial combustion processes and traffic is still problematic and increasing worldwide. Several epidemiological studies have linked increased morbidity and mortality with exposure to particulate matter (Seaton et al. 1995, Peters et al. 2000, Pope et al. 2002). Translocation of ultrafine particles within rats into several organs, including the brain, after inhalation has been shown in a few studies (Takenaka et al. 2001, Oberdörster et al. 2004, Semmler et al. 2004).

Engineered nanoparticles now comprise additional anthropogenic products that are even smaller than most particles considered so far (Maynard & Kuempel 2005, Maynard

et al. 2006). They are produced in large amounts as powders for various applications. Increasing production and use may lead to a release of significant amounts of nanoparticles either during production processes, use or waste disposal. Thus, an occupational or environmental exposure cannot be excluded and interactions with biota might result in possible hazardous undesired effects. Currently, data regarding production quantities and the relative amounts of nanomaterials released from production plants is rare and the occupational and environmental exposure values are hard to estimate. However, a few studies regarding the life cycle assessment of industrial nanoparticles are available. These studies estimated significant releases of nanoparticles (namely TiO₂, Silver, ZnO, and carbon nanotubes) from production sites into the ambient air and the environment (Mueller & Nowack 2008, Gottschalk et al. 2009).

Nevertheless, recommendations for work place safety or waste disposal are still lacking. To date, a special safety assessment for nanoparticles is not included in the new European regulation law for chemicals (REACH) and there is still a lack of knowledge about the practicability of toxicological standard tests. Furthermore, no special regulations respecting risk assessment and hazard identifications of industrial nanoparticles are available up to now. Whether special regulations and risk assessment strategies are necessary for nanoparticles is one of the major current questions.

Objectives of the thesis

In view of the rapid development of nanotechnology industries and the associated uncertainties regarding risks posed by nanomaterials, this thesis aimed to elucidate the toxicological impacts of a set of engineered nanoparticles to vertebrate cells *in vitro*. The specific questions addressed are:

1. Are different engineered nanoparticles able to enter several types of vertebrate cells?
2. Do engineered nanoparticles influence the vitality of human and fish cells *in vitro* and what is the role of particle constituents, such as metal ions, in nanoparticle toxicity?
3. Is nanoparticle uptake and toxicity detectable on the transcriptomic level and can genome-wide gene expression pattern give evidence for potential modes of action?

The research undertaken in this thesis was part of the research project INOS (“Identification and assessment of the effects of engineered nanoparticles on human and environmental health”; financed by the German Federal Ministry of Education and Research (BMBF)). A specific set of particles was selected for this study (discussed in more detail below) but the greatest attention was given to assessing the uptake and effects towards human and fish cells of tungsten carbide (WC) and tungsten carbide cobalt (WC-Co) nanoparticles.

INOS was designed to integrate the different disciplines required to characterise nanoparticle behaviour and interactions with vertebrate cells. Thus, the research team comprised chemists and particle experts from the Fraunhofer Institute Dresden - IKTS, biologists and medical scientists from the field of neurotoxicology as well as experts for electron microscopy from the Technical University Dresden, and biologists working in the field of human and ecotoxicology from the Helmholtz Centre for Environmental Research Leipzig - UFZ. In order to characterise potential adverse effects and to identify their underlying modes of action, a suite of *in vitro* methods, ranging from the study of particle behaviour, internalisation, and interaction with intracellular molecules to cell toxic effects, were applied.

For my Ph.D. research, several decisions had to be made with regard to the material to be studied, the selection of cell culture models and methods used to be able to answer the research questions stated above. The options considered and the rationale for the decisions made is summarized below to provide the general background. Detailed information regarding the individual materials and methods is provided in the respective chapters of the thesis.

Selection of Nanoparticles

Several engineered nanoparticles are of occupational and environmental relevance because they are produced in large amounts in non-closed systems. Such particles were subjects of the research described in this thesis. The particles which were investigated in the different studies are summarised in Table 1 and were all provided and characterised by the Fraunhofer Institute for Ceramic Technologies and Systems (IKTS) Dresden.

Table 1. Types of engineered nanoparticles investigated in this thesis.

Particle name	Industrial applications	Endpoints studied
Tungsten carbide large (WCL)	Hard metals	Particle uptake, acute toxicity, gene expression
Tungsten carbide small (WCS)	Hard metals	Particle uptake
Tungsten carbide cobalt (WC-Co)	Hard metals	Particle uptake, acute toxicity, gene expression
Titanium nitride (TiN)	Hard metals, ceramics	Particle uptake
Titanium dioxide (TiO ₂)	Pigments, emery substance	Particle uptake
Diamond	Polishing agents	Particle uptake

Tungsten carbide (WC) based particles are widely used in hard metal industries for the production of hard metals and tools. During the sintering process, particles stick together under high pressure and heat. This process needs less energy by using nano-sized powders and the structures of the resulting tools are better and firmer as with coarser powders. The production of such powders in the nanometer scale was difficult in the past but is technologically possible and therewith applied now. While WC is brittle, cobalt is more ductile and the combination of both is particularly useful for achieving the high stability.

The knowledge on WC and WC-Co nanoparticles toxicology is scarce, therefore these particles were chosen for detailed toxicological studies. So far, only reports on the effect of microsized particles are available published in several studies by a Belgian research group around Dominique Lison. It was found that WC-Co microparticles exhibit an enhanced toxicity if compared to the same amounts of WC or cobalt. Their findings (described and discussed in detail in Chapter 3) together with results of other groups, led to the classification of cobalt as 'possibly carcinogenic' and WC-Co as 'probably carcinogenic' by the International Agency for Research on Cancer (2006). Whether nanoparticles behave differently was one of the major questions of this thesis.

Titanium nitride (TiN) is an extremely hard ceramic material, often used as a coating on titanium alloys, steel, carbide, and aluminium components to improve the substrate's surface properties. All these materials become strong and tight bulk materials after sintering, but before that step particle powders in the nanometre size range have to be handled.

Titanium dioxide (TiO₂) exemplifies a metal oxide. Metal oxides are frequently used in consumer products. TiO₂ specifically is used as pigment or emery substance in, e.g., sunscreens, toothpaste or paints.

Diamond nanoparticles are mainly used as polishing agents for industrial applications.

The toxicological analyses of TiN, TiO₂, and diamond nanoparticles were performed by collaborators of the INOS project. For my studies these particles were chosen for investigations regarding the particle uptake into cells with the aim to compare particle internalisation ability of cells dependent on particle properties.

Characterisation of nanoparticles

Nanoparticles may aggregate and change their properties during environmental release and uptake into organisms. To know exactly how particles behave in the exposure system and what the cells or test organisms are really exposed to, knowledge on particle behaviour is essential for the interpretation of toxicological results. Therefore, all particles investigated in this project were carefully characterised regarding their physico-chemical properties and behaviour in physiological media by the researchers of the IKTS. Most engineered particle powders never exist as primary particles. Two important processes determining particle size in this regard are agglomeration and aggregation (Jiang et al. 2009). In solutions, such as cell culture media, particles tend to bind to each other and build agglomerates which are characterised by the hydrodynamic diameter (Figure 3).

The stability of nanoparticle dispersions and their tendency to agglomerate can be considered in the context of electrostatic, steric, and van der Waals forces between particles. Surface characteristics affect agglomeration in dispersions and the nanoparticle hydrodynamic size distributions can be altered by changes of the particle surface charge. If a particle has an ionic surface or highly polar bonds, multiply charged ions may be adsorbed by the particle in an aqueous environment, leading to an increase in particle surface charge. Adsorbed multiply charged ions and polymer coatings on nanoparticle surfaces as well as changes of the pH or the ionic strength of the aqueous solution can suppress agglomeration and stabilise nanoparticle dispersions (Jiang et al. 2009).

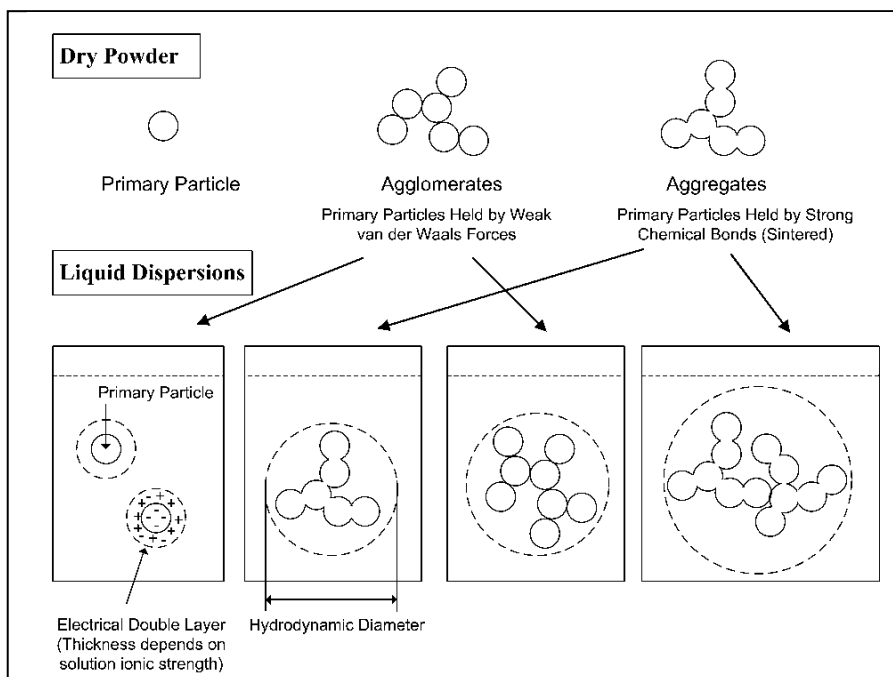


Figure 3. Nanoparticles tend to agglomerate in physiological fluids but may also build stable aggregates. Agglomerates and aggregates are characterised by the hydrodynamic diameter that can differ significantly from the primary particle diameter. Figure taken from (Jiang et al. 2009).

Since technical nanoparticles occur in a range of sizes, rather than having one exact single diameter, averages of the size distribution curves are used to represent and compare particle sizes. This is exemplarily demonstrated in Figure 4 for the particles investigated in this thesis.

Not only characteristics, such as size, surface area, or charge might be relevant for toxicological effects. Furthermore, indirect, secondary effects can be provoked by catalytic activities due to reactive particle surfaces and/or chemical interactions within the cells. Particles entering the cell may enhance the intracellular exposure to leaching ions, which would otherwise – due to their charge – not enter the cytoplasm. Consequently, an enhanced toxicity based on the leached ions might be observed. This was first hypothesised by Limbach and colleagues (Limbach et al. 2007) and described as the “Trojan Horse” effect.

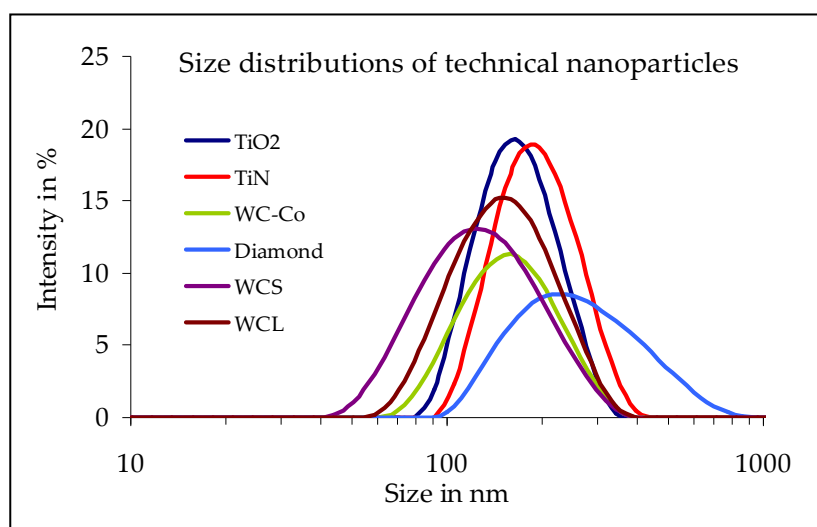


Figure 4. Size distribution curves of technical nanoparticles used in this project measured by dynamic light scattering. Data was obtained and kindly provided by the Fraunhofer Institute of Ceramic Technologies and Systems (IKTS).

Cell culture models

In order to represent possible routes of entry into organisms, several cell lines were chosen for toxicological analyses of nanoparticles. Humans, exposed occupationally, via consumer products or the ambient air, get in contact with nanoparticles via skin, lung or intestine. The research of this thesis was therefore focussed on nanoparticle effects on human skin (HaCaT), lung (A549) and colon (CaCo-2) cells. In cooperation with the project partners I also used peripheral blood mononuclear cells (PMBC), the monocyte cell line THP1 and the rat oligodendrocyte cell line OLN93 for particle uptake studies. The rainbow trout (*Onchorhynchus mykiss*) gill cell line, RTgill-W1, was used as a suitable model to study the impact of engineered nanoparticles on an environmentally relevant aquatic organism. By using the different cell cultures, this thesis focussed on three different endpoints, namely the particle uptake into cells, the cell viability indicating acute toxic effects and global gene expression indicating sub-acute effects and modes of action. Table 2 summarises the cell types used in this thesis. Details about the sources and treatments of the cells are explained in detail in the respective chapters.

Table 2. Cell types chosen for the studies of the thesis.

Cells	Cell type / origin	Endpoints studied
HaCaT	Permanent human skin keratinocytes	Particle uptake, acute toxicity, gene expression
A549	Permanent human lung epithelial cells	Particle uptake, acute toxicity
CaCo-2	Permanent human colon epithelial cells	Particle uptake, acute toxicity
THP1	Permanent human monocytic cells	Particle uptake
PBMC	Primary human peripheral monocytic cells	Particle uptake
OLN93	Permanent rat brain oligodendroglial cells	Particle uptake
RTgill-W1	Permanent rainbow trout gill cells	Particle uptake, acute toxicity

Detection of nanoparticles within cells

Morphological properties of nanoparticles as well as the internalisation of them into cells can be observed with light- and electron microscopy.

Light microscopy was chosen to observe particle internalisation and accumulation within cells over time and co-localisations of particles with fluorescently stained cellular compartments.

Electron microscopy can indicate the sub-cellular localisation of particles and allows a size determination of nanoparticles within a single cell. If coupled with an energy dispersive X-ray detector (EDX), the elemental composition of incorporated particles can be determined. Furthermore, artefacts resulting from sample preparation can be excluded with EDX. The electron microscopy analyses of the different samples prepared during my research were performed by scientists of the Max-Bergmann Centre for Biomaterials (TU Dresden).

Since the measurement of particle uptake into cells in a quantitative manner is difficult with microscopic methods, flow cytometry analyses were performed. Particles within cells change the cellular granularity (firstly shown by Stringer et al. 1995), which can be measured with flow cytometry. Effects of endo- or phagocytosis inhibitors, that may influence particle internalisation, can be quantified with this method as well. In the research presented here, the inhibitory effect of Cytochalasin D (an inhibitor of the cytoskeleton) on particle internalisation by different cell types was investigated.

Qualitative alterations of cellular morphology and vitality are detectable with microscopy and flow cytometry approaches. In addition, two types of particles (WC_L and WC-Co) were chosen for the quantitative assessment of acute and sub-acute toxicological effects, focussing on cell viability and gene expression alone and in comparison to dissolved cobalt ions.

Toxicological endpoints

Cell viability: Acute toxicological effects of engineered nanoparticles on human and fish cells were determined by applying two different fluorescent dyes indicating metabolic activity (AlamarBlue) and membrane integrity (CFDA,AM) of the cells (Schirmer et al. 1997). Furthermore, the effects of leached cobalt ions were considered by the implementation of comparative experiments with cobalt chloride.

Gene expression: In order to identify how nanoparticles may interfere with cells, global gene expression studies were carried out by means of microarray technology. So called “-omics” approaches have been increasingly used in toxicology in the last years. Toxicogenomics, defined as “the study of the relationship between the structure and activity of the genome (the cellular complement of genes) and the adverse biological effects of exogenous agents” (Aardema & MacGregor 2002), is a promising approach to

investigate global toxicological responses and identify modes of action of toxicants. Nevertheless, gene expression profiling is dependent on gene annotation status and therefore more meaningful the more is known about the genes and their functions in an organism. Such data are often limited for environmental organisms. Therefore, human cells were chosen for these experiments. To overcome divergences of the different existing databases, data were analysed by using a combination of different databases and statistical methods. Moreover, microarray data were confirmed by an independent standard method (Polymerase Chain Reaction (PCR)).

Further details to all methods applied are given in the respective chapters of this thesis.

Structure of the thesis

The research of this thesis is described in four chapters that collectively address the objectives and questions guiding my Ph.D. research. Each chapter represents one manuscript accepted or published in an internationally well recognised journal of toxicology, genomics or nanoparticle research. The sixth chapter provides an overall summary, main conclusions and future perspectives.

As described above, particle preparation and characterisation were essential for the toxicological studies and were provided by project partners. Moreover, electron microscopy evaluation, and toxicological studies with brain cells were performed by project partners. In order to reach the aims of the project, strong cooperation and a combined view on the results were necessary and meaningful. On this background, my contributions to the joint publications are explained in detail in the end of the thesis (Page 144).

The first question: “Are different engineered nanoparticles able to enter several types of vertebrate cells?” is addressed in chapter 2. In this study, particle uptake was investigated by several methods with the aim to compare particle uptake and distribution patterns in cell types, and to analyse co-localisation of particles with fluorescently stained cell compartments. Furthermore, the influential effects of particle properties and an inhibitor of actin, and therewith the cytoskeleton (Cytochalasin D), are described in chapter 2.

All types of particles investigated in this study were able to enter all investigated cell types. To investigate their toxicological impact, two types of nanoparticles, namely WC and WC-Co, were chosen for further investigations in this thesis. Thus, chapter 3 presents results addressing the acute toxicity of WC-Co nanoparticles in comparison to WC nanoparticles and/or solvated cobalt ions on mammalian cells *in vitro*. One important outcome in these studies was the stabilising effect of serum albumin on the particle size in suspensions. This is relevant for exposures of cell cultures but also within an organism. Environmental organisms, such as fish, are exposed via the water and particles were found to strongly agglomerate in water without a serum or protein supplement. Therefore, in chapter 4, an investigation into whether particle agglomeration in exposure media influences toxicity and particle uptake in fish cells was performed. Taken together, chapter 3 and 4 helped answer the second key question I addressed in my research: “Do engineered nanoparticles influence the vitality of human and fish cells *in vitro* and what is the role of particle constituents, such as metal ions, in nanoparticle toxicity?”

By studying the impact of WC and WC-Co nanoparticles on cell vitality in chapters 3 and 4 it was consistently found that effects of WC-Co nanoparticles were stronger than effects of equivalent concentrations of WC nanoparticles or cobalt ions, alone or in combination. In order to identify the mechanisms behind this enhanced toxic effect, and to investigate responses on particle internalisation on the gene expression level, whole genome microarrays (transcriptome) analyses were performed. Thus, chapter 5 addresses the third key question of my research: “Is nanoparticle uptake and toxicity detectable on the transcriptomic level and can genome-wide gene expression pattern give evidence for potential modes of action?” Besides the comprehensive toxicogenomic data set for the studied particles, this research presents and discusses new data regarding the mechanisms of cobalt toxicity.

Chapter 6 provides a synopsis of the results of my Ph.D. research in relation to the research questions. I conclude by discussing the scientific findings in the context of standardisation of test methods, transferability of *in vitro* data to *in vivo* situations and by suggesting for future research directions.

Chapter 2

Internalisation of engineered nanoparticles into mammalian cells *in vitro*: influence of cell type and particle properties

accepted for publication in the *Journal of Nanoparticle Research*

Wibke Busch^{1a}, Susanne Bastian², Ulrike Trahorsch^{1b}, Maria Iwe², Dana Kühnel^{1a}, Tobias Meißner³, Armin Springer⁴, Michael Gelinsky⁴, Volkmar Richter³, Chrysanthy Ikonomidou^{2,5}, Annegret Potthoff³, Irina Lehmann^{1b}, Kristin Schirmer⁶

¹UFZ-Helmholtz Centre for Environmental Research, Department ^aBioanalytical Ecotoxicology, ^bEnvironmental Immunology, Permoserstrasse 15, 04318 Leipzig, Germany; ²Department of Pediatric Neurology, University Children's Hospital Carl Gustav Carus, University of Technology Dresden, Fetscherstrasse 74, 01307 Dresden, Germany; ³Fraunhofer Institute for Ceramic Technologies and Systems, Winterbergstrasse 28, 01277 Dresden, Germany; ⁴Institute for Materials Science and Max Bergmann Center of Biomaterials, Technische Universität Dresden, Budapester Strasse 27, 01069 Dresden, Germany; ⁵Department of Neurology and Waisman Center, University of Wisconsin, Madison WI 53792, USA; ⁶Eawag, Swiss Federal Institute of Aquatic Science and Technology, 8600 Dübendorf, Switzerland and ETH Zürich, Institute of Biogeochemistry and Pollutant Dynamics, 8092 Zürich, Switzerland

Abstract

Cellular internalisation of industrial engineered nanoparticles is undesired and a reason for concern. Here we investigated and compared the ability of seven different mammalian cell cultures *in vitro* to incorporate six kinds of engineered nanoparticles, focussing on the role of cell type and particle properties in particle uptake. Uptake was examined using light and electron microscopy coupled with energy dispersive X-ray spectroscopy (EDX) for particle element identification. Flow cytometry was applied for semi-quantitative analyses of particle uptake and for exploring the influence on uptake by the phagocytosis inhibitor Cytochalasin D.

All particles studied were found to enter each kind of cultured cells. Yet, particles were never found within cell nuclei. The presence of the respective particles within the cells was confirmed by EDX. Live-cell imaging revealed the time-dependent process of internalisation of technical nanoparticles, which was exemplified by tungsten carbide particle uptake into the human skin cells, HaCaT. Particles were found to co-localise with lysosomal structures within the cells. The incorporated nanoparticles changed the cellular granularity, as measured by flow cytometry, already after 3 hours of exposure in a particle specific manner. By correlating particle properties with flow cytometry data, only the primary particle size was found to be a weakly influential property for particle uptake. Cytochalasin D, an inhibitor of actin filaments and therewith of phagocytosis, significantly inhibited the internalisation of particle uptake in only two of the seven investigated cell culture. Our study therefore supports the notion that nanoparticles can enter mammalian cells quickly and easily, irrespective of the phagocytic ability of the cells.

Background

Nanoparticle risk assessment is based on toxicological *in vitro* and *in vivo* data and needs to be performed for many different kinds of nanomaterials. These materials differ in their properties, as chemicals do, according to their projected applications. Whereas nanoparticles are modified for medical applications to promote entry into cells, engineered nanoparticles for industrial applications are not designed to do so. Since nanoparticles are close or similar in size to biological entities, such as proteins, DNA, or viruses, concerns about the nanoparticles' ability of entering cells and distributing within organisms undesirably are justified. The potential entry of technical nanoparticles into mammalian cells is therefore of special relevance for occupational health.

Several studies have reported toxicological effects of particles upon internalisation by cells (Xia et al. 2006, Gojova et al. 2007, Bastian et al. 2009, Bhattacharya et al. 2009, Papis et al. 2009). Most effects found so far are related to reactive oxygen species, dissolved ions, or mixtures of unknown components (e.g. diesel exhaust particles). However, understanding the ability of nanoparticles to enter different kinds of cells is important even in the absence of short-term toxicological effects because particle accumulation, transfer between tissues and mixture effects with chemicals (e.g. drugs, xenobiotics) or biological molecules (e.g. DNA, proteins) may have long-term consequences.

To date, particle incorporation is mostly attributed to phagocytic cells, such as monocytes and macrophages; however, particle uptake by non-phagocytic cells has been reported as well, especially for nanoparticles (Stearns et al. 2001, Chen & von Mikecz 2005, Geiser et al. 2005, Chithrani et al. 2006, Long et al. 2006). While large particles are thought to be taken up by phagocytosis, an actin filament-dependent process, smaller particles seem to be internalised by other endocytic pathways with as of yet no apparent strict size threshold. Rejman and colleagues found no uptake of 1000 nm fluorescent microspheres into non-phagocytic cells, whereas the internalisation of 500 nm and smaller microspheres via different endocytic paths was observed (Rejman et al. 2004). On the contrary, Gratton and colleagues demonstrated that particles of 2 and 3 μm were internalised into HeLa cells by different endocytotic pathways (Gratton et al. 2008). We previously analysed the ability of a rainbow trout (*Onchorhynchus mykiss*) gill cell line (RTgill-W1) to internalise and respond to tungsten carbide (WC) and tungsten carbide cobalt (WC-Co) nanoparticles

and found incorporation into the cells irrespective of particle agglomeration state and media composition (Kühnel et al. 2009). These studies indicated that nanoparticles can generally be internalised by cells which are not known to perform phagocytosis.

Since *in vitro* studies so far mostly focussed on effects and uptake of a special kind of nanoparticle on one population or culture of cells, our approach was to compare several technical nanoparticles regarding their internalisation ability into different mammalian cell cultures. Whether the cell type or particle properties influence the particle uptake was one of the major questions. Therefore we chose cells of different origin to model exposed organs (based on permanent and primary as well as phagocytic and non-phagocytic cells). Our focus was on technical nanoparticles which are under development for industrial large scale production. Most of the chosen nanoparticles find application in the field of producing hard metals, also called cemented carbides. We investigated six types of engineered nanoparticles (small and large tungsten carbide [WC_s, WC_L], tungsten carbide cobalt [WC-Co], titanium nitride [TiN], titanium dioxide [TiO₂], and diamond), and compared their ability to enter the cells. All particles were characterised regarding their physico-chemical properties and their behaviour in aqueous media (Bastian et al. 2009, Meißner et al. 2009, Meißner et al. 2010, Potthoff et al. 2009). Particle internalisation was confirmed in different ways, including element analysis as part of the electron microscopic characterisation and measurement of changes in side scatter values in flow cytometry analyses, as suggested for semi-quantitative determination of particle uptake by Stringer and colleagues (Stringer et al. 1995). Finally, Cytochalasin D (CytoD), an inhibitor of actin polymerisation and therewith the function of the cytoskeleton, helped to decipher the involvement of phagocytosis in nanoparticle uptake.

Materials and Methods

Sources and initial characterisation of nanoparticles

Six types of engineered nanoparticles which are of industrial and therewith of occupational relevance were selected for this study. Tungsten carbide (WC) based particles are widely used in hard metal industries for the production of hard metals and tools. Titanium nitride (TiN) is an extremely hard ceramic material, often used as a coating on titanium alloys, steel, carbide, and aluminium components to improve the substrate's surface properties. Metal oxides, such as titanium dioxide (TiO₂), are frequently used in consumer products, especially as pigments or emery substances in, e.g., sunscreens, toothpaste or paints. Finally, diamond nanoparticles are mainly used as polishing agents for industrial applications. The following nanoparticles, which represent these groups of industrially relevant particles, were investigated in this study: Two types of tungsten carbide nanoparticles with different primary particle size (WC_L, WC_S), tungsten carbide cobalt (WC-Co; 10 mass% cobalt content), titanium nitride (TiN), titanium dioxide (TiO₂ P25, Degussa Evonik GmbH, Essen, Germany) and Diamond (MBM 0-1/2, Diamond Innovations, Dreieich, Germany). WC_L was prepared by a chemical process involving carbothermal reduction and carburisation of WO₃, and disaggregated and mixed, respectively, by means of a ball mill. In contrast, WC_S is a powder material manufactured from coarse WC powder by plasma reactor treatment. WC-Co is a mixture of WC_L and a cobalt powder. Detailed information of preparation and physicochemical characterisation of WC_L and WC-Co are already described elsewhere (Bastian et al. 2009). TiN powder was manufactured by chemical vapor reaction of titanium tetrachloride with ammonia and hydrogen (Naß et al. 1994). TiO₂ and diamond were taken as-received.

The specific surface area of the nanopowders was determined according to Brunauer-Emmet-Teller (BET) using a Micromeritics ASAP 2010 Analyser (Accelerated Surface Area and Porosimetry System, Micromeritics GmbH, Mönchengladbach, Germany) and nitrogen. Phase composition was measured using an XRD7 diffractometer (Seifert-FPM, Freiberg, Germany). Morphology and particle size were verified by scanning electron microscopy using a Zeiss LEO FEG (Carl Zeiss SMT AG, Oberkochen, Germany).

Preparation and characterisation of particle suspensions

All particle suspensions were prepared in pure water (resistivity $\geq 18 \text{ M}\Omega\cdot\text{cm}$; Wilhelm Werner GmbH, Leverkusen, Germany). For WC-Co, WCs, TiN and TiO₂, the addition of sodium polyphosphate (Graham's salt; Merck, KGaA, Darmstadt, Germany) was necessary to obtain electrostatic stabilisation of the particles (0.03% (wt/v) for the tungsten based and 0.05% (wt/v) for the titanium based particles). Graham's salt is an often-used dispersant that is non toxic in the applied concentrations. Diamond particles were suspended in 10^{-4} M KOH to achieve stabilisation of the suspension. The suspensions were treated by probe sonication (UDS 751; Topas GmbH, Dresden, Germany) for deagglomeration. Particle suspensions were sterilised by autoclaving and treated for 15 min in an ultrasonic bath (Merck Eurolab, Darmstadt, Germany) prior to treatment of cells to ensure optimal dispersal. After preparation as well as after autoclaving, we quantified particle size and zeta potential. Zeta potentials were determined by measuring the electrophoretic mobility of the suspended particles (Zetasizer Nano ZS, Malvern Instruments Ltd, Worcestershire, UK). The electrophoretic mobility has been calculated into the zeta potential using the Smoluchowski equation. Particle size and the polydispersity index (PDI) were determined by means of dynamic light scattering using again a Zetasizer Nano ZS.

Cell culture

In order to compare the behaviour of several kinds of cells regarding the uptake of nanoparticles we choose cell cultures of different origin. The selected cell cultures represent possible primary or secondary exposed organs, e.g. skin, lung, blood system, and brain. Thereby we chose well established permanent cell lines, such as the human keratinocytes - HaCaT, the lung epithelial cells - A549, the monocyte cell line - THP1, and the rat oligodendroglial cell line - OLN93. Since especially functions of differentiated brain cells are hardly achievable with permanent cell lines, we also used freshly isolated rat astroglial cultures and separated microglia and astrocytes for our experiments. Moreover, since phagocytic cells are supposed to internalise particles, we included another kind of freshly isolated cells, namely human peripheral blood mononuclear cells (PBMC). These cells consist of two cell populations, lymphocytes and monocytes. The monocyte population is responsible for uptake and digestion of endogenous or foreign

particulate material via phagocytosis in the human body. Having included PBMC allowed us to compare the internalisation of nanoparticles between the primary (PBMC) and the permanent (THP1) monocytes.

The handling of all cell cultures, as well as the isolation of the primary cells, was performed according to standard protocols and is explained in detail in the supplemental material (Additional file 1; S1_materials_methods.pdf).

Exposure of cells to particles

Cells were counted using a hemocytometer. Cells were seeded in 24 well plates (TPP) in a volume of 500 μ l (for primary rat brain cells) or in 6 well plates in a volume of 2 ml (for all other cell types) at a density of approximately 1×10^5 cells/ml, and allowed to attach for 24 h before addition of particle suspensions. Numbers of seeded cells varied slightly dependent on exposure time or measured endpoint, but were always the same for biological replicates. Details of cell numbers seeded per experiment are given in the supplemental material (Additional file 1). All exposures were carried out in complete cell culture medium containing 10% foetal bovine serum (FBS). We had previously shown that the nanoparticles formed stable aggregates in the presence of bovine serum albumin (BSA) or serum in the exposure suspensions (Bastian et al. 2009, Meißner et al. 2009, Meißner et al. 2010).

Dosing was achieved by adding 200 μ l (6 well) or 50 μ l (24 well) of the respective particle dilution to 1800 μ l (6 well) or 450 μ l (24 well) of complete cell culture medium to reach final nanoparticle concentrations of 20 and/or 30 μ g/ml, the latter being the highest achievable concentration based on limitations in the preparation of particle suspensions. All experiments were repeated for a minimum of four times. Controls of the water or water with supplements used to prepare the particle suspensions were included as appropriate in all experiments. Cells were treated with nanoparticles for 1h up to 3d.

Treatment of cells with Cytochalasin D

For uptake inhibition experiments, all cell cultures were pre-treated with Cytochalasin D (CytoD) (Applichem, Darmstadt, Germany) for 1 h before starting particle exposure. The cell culture medium was changed to the respective media with or without CytoD, using non toxic concentrations for every cell type as determined in range finding

experiments using cell viability indicator dyes. These concentrations were 5 μM for A549, HaCaT, OLN93 cells, primary astrocytes and microglial cells; and 2 μM for PBMC and THP1 cells.

Flow cytometry

After exposure to nanoparticles for 3 and 24 h (with and without CytoD), cells were washed with PBS, carefully detached with Accutase (PAA Laboratories) and again washed two times with PBS. After re-suspending in 200 μl PBS with 10% FBS, cells were measured directly using a flow cytometer (FACS Calibur, Becton Dickinson, Franklin Lakes, USA). The median side scatter values (SSC) were analysed as a marker for granularity, which increases with particle uptake. For each measurement we counted viable 10^4 cells. Since particle exposure itself affected cell viability in some cases at the highest applied concentrations (30 $\mu\text{g}/\text{ml}$), the gates in flow cytometry data analyses were set to analyse viable cells only.

Cell viability

Cell viability was assessed in independent experiments using standard protocols with fluorescence (alamarBlue, CFDA,AM) or absorbance (MTT) indicator dyes and a GENios Plus fluorescence reader (Tecan, Grödig, Austria). At the highest applied particle concentration (30 $\mu\text{g}/\text{ml}$), TiN and WC-Co nanoparticles caused toxicity in some cell types of up to 15%, based on alamarBlue and as described in Bastian et al. 2009. In THP1 and PBMC cells, cell viability was found to decline as much as 60% upon exposure to, respectively, WC-Co and WC_s nanoparticles, relying on MTT (3-(4,5-dimethylthiazol-2-yl)-2,5-diphenyltetrazolium bromide).

Electron microscopy

Characterisation of nanoparticle morphology and localisation after incubation was performed with scanning electron microscopy (SEM) and scanning transmission electron microscopy (STEM). SEM was assessed as previously described (Bastian et al. 2009). Briefly, cells were fixed with 2% (v/v) glutaraldehyde (Serva, Heidelberg, Germany) at room temperature, post fixed with 1% (v/v) osmium tetroxide (Roth, Karlsruhe, Germany), dehydrated in a graded series of acetone (including a staining step with

1% (v/v) uranyl acetate), and embedded in epoxy resin according to Spurr (1969). Prior to X-ray spectroscopy (EDX), samples were fixed in 2% (v/v) glutaraldehyde, dehydrated, and embedded in epoxy resin as above. Samples were cut on a Leica EM UC6 ultramicrotome (Leica, Vienna, Austria), equipped with a diamond knife (Diatome, Biel, Switzerland), carbon coated, and analysed using a Philips XL 30 ESEM (Philips, Eindhoven, Netherlands) in SEM mode. For energy dispersive X-ray microanalysis (EDX), we used an EDAX detecting unit and EDAX software (version 3.0; EDAX Inc., Mahwah, NJ, USA).

For STEM investigations, harvested cells were fixed with 2% glutaraldehyde at room temperature, post fixed with 1% osmium tetroxide, dehydrated in a graduated series of acetone (including a staining step with 1% uranylacetate) and embedded in epoxy resin (Spurr 1969). Ultra thin sections (about 100 nm to 300 nm) of samples were prepared on a Leica EM UC6 ultra microtome with a Diatome diamond knife, mounted on carbon coated copper grids, and analysed in a Philips ESEM XL 30 equipped with a STEM-detector system. For EDX analysis, epoxy resin embedded samples were prepared as described for SEM-analyses (see above). Ultra thin sections of the samples were analysed in a Philips ESEM XL 30. EDX-analysis and elemental mapping was done with an EDAX detecting unit and EDAX software.

Light microscopy (Movie)

HaCaT cells were plated at a density of 4×10^5 cells/well in a final volume of 2 ml in a 6 well plate (TPP) and allowed to attach for 24 h before addition of particle suspension. Dosing was achieved by adding 200 μ l of the WCL particle suspension to 1.8 ml of complete cell culture medium to reach the final concentration of 30 μ g/ml for WCL nanoparticles. Starting at that time point, photographs were taken every 10 min during a time period of 2 days using an inverse microscope (Leica DMI 4000B, magnification 200x) with a heated stand (37°C). The pictures are shown as a time flow movie, which is provided as supplemental material (Additional file 2; S2_HaCaT_WCL_2d.mpeg).

LysoTracker staining and microscopy

For LysoTracker staining, HaCaT and OLN93 cells were seeded into 6 well plates (Falcon/ Becton Dickinson, Heidelberg, Germany) at a density of 10^5 cells/well in a total

volume of 2 ml and were allowed to attach for 24 h. The medium was then replaced with particle containing medium. After an exposure time of 3 d, the exposure medium was removed and cells were incubated in 50 nM LysoTracker Red (Invitrogen/Molecular Probes, Karlsruhe, Germany) in growth medium using a total volume of 2 ml/well for 2 h. In order to visualise the position of cell nuclei, cells were counterstained with 1 μ M Hoechst 33342 (Invitrogen/Molecular Probes, Karlsruhe, Germany) for the last 5 min of the incubation time. The loading solution was replaced with fresh medium and cells were observed using a fluorescent microscope (Leica DMI 4000 B, Wetzlar, Germany) equipped with the appropriate filter sets. LysoTracker Red exhibits red fluorescence (excitation: 577 nm, emission: 590 nm). Hoechst is excited at 350 nm, and emits at a maximum of around 461 nm. Micrographs were recorded using the Leica LSM software package LAS-AF 1.8.0 build 1346.

Statistics and Graphs

FACS data were analysed using CELLQUEST software (Becton Dickinson, Heidelberg, Germany) and the FlowJo Software (version 7.2.2; Tree Star Inc., Ashland, OR, USA). Side scatter values were converted to percent of control and are presented as mean \pm SE. Statistical differences were analysed with Student's T-Test (treatment vs. control; or particle exposed cells without CytoD vs. particle exposed cells with CytoD) using Microsoft Excel (Version 2002). Values of $p < 0.05$ were considered statistically significant. Graphs were generated with GraphPad Prism software (GraphPad Prism version 4.00 for Windows, GraphPad Software, San Diego California USA, www.graphpad.com).

Results

In this study we investigated interactions between a set of different cells and different nanoparticles focussing on the particle uptake. We aimed to compare the uptake behaviour of several cell cultures using particles of diverse sizes and materials. For this purpose we exposed permanent cell lines of potential exposed organs (human lung [A549] and skin cells [HaCaT]; human blood monocytes [THP1] and rat brain oligodendroglial cells [OLN93] as well as freshly isolated primary blood and brain cells (human peripheral blood mononuclear cells [PBMC], rat astrocytes and microglial cells) to technical nanoparticles with a primary particle size range from 10 (WCs) to 73 (Diamond) nm. Stable aggregates or agglomerates of these particles within physiological media ranged in size (average hydrodynamic diameter, x_{DLS}) from 115 (WCs) to 250 (Diamond) nm. Electron micrographs of all powders and physical and chemical properties of the particles are shown in Figure 1 and Table 1.

Table 1. Summary of physical parameters of the investigated particles.

Particles	crystalline phase	BET (m ² /g)	x_{BET} * (nm)	x_{DLS} (nm)	Zeta potential (mV)
TiO ₂	anatase / rutil 80% / 20%	55.9	27	170	-50 [#]
TiN	titanium nitride	42.0	26	160	-50 [#]
WC _s	tungsten subcarbide	43.2	9	115	-45 [#]
WC _L	tungsten carbide	6.9	56	145	-35 [~]
WC-Co	tungsten carbide + cobalt	6.6	62	145	-50 [#]
Diamond	diamond	23.3	73	250	-40 ⁺

Note: Polydispersity index of the investigated particles was below 0.2 (on a scale of 0 to 1) in all cases, indicating small particles size distributions; * values were calculated assuming the theoretical density of the powders; particles were suspended in ~water or water with [#]Graham's salt or ⁺10⁻⁴ M KOH.

Particles are taken up by all cells

By means of light microscopy we observed particle sedimentation to the bottom of cell culture vessels within the first hour of exposure. Over time, particle agglomerates became visible within all cells, forming a typical pattern around the nucleus (see also Figure 2).

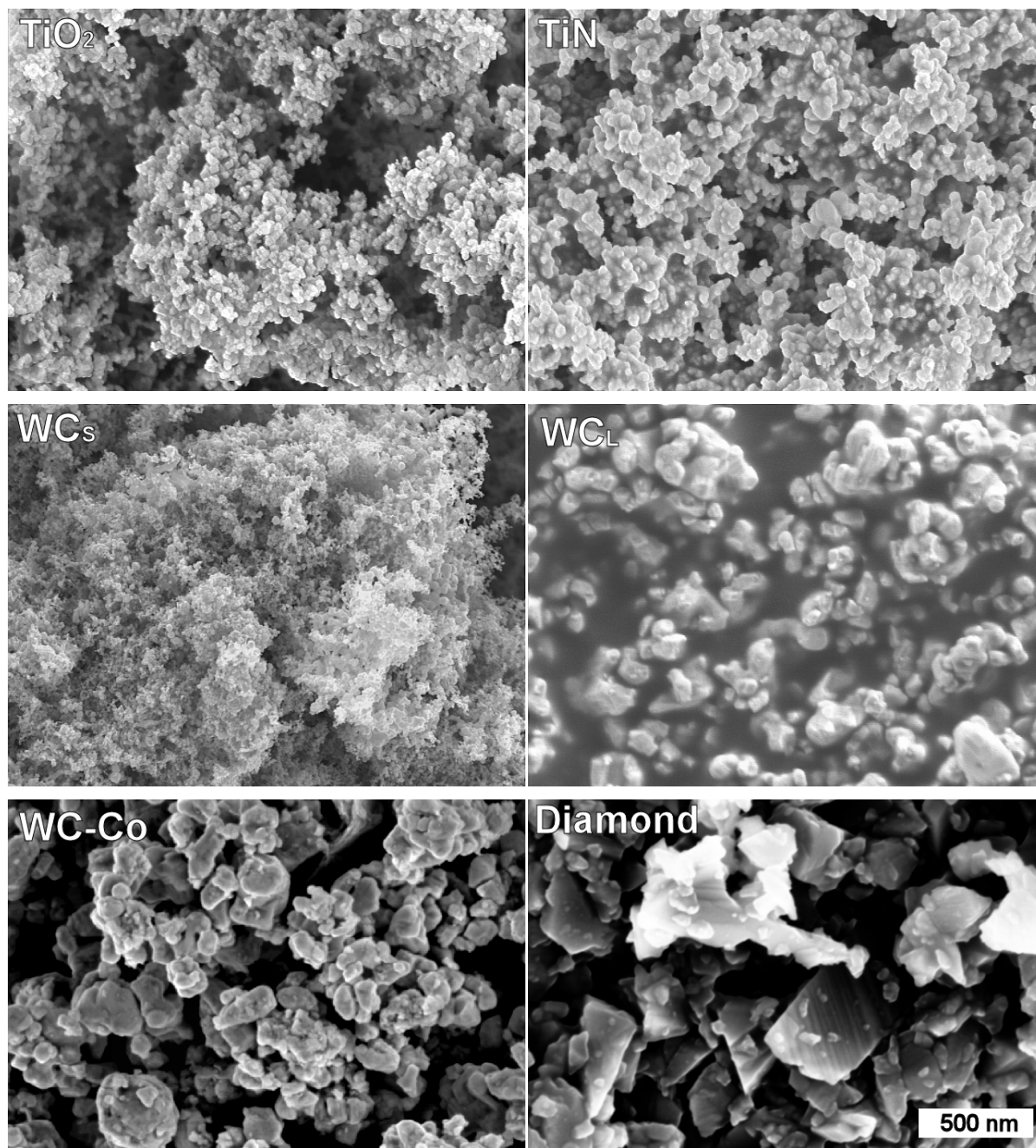


Figure 1. SEM images of TiO₂, TiN, WC_s, WC_L, WC-Co and Diamond. (magnification: 50,000x)

To visualise particle uptake over time in more detail, we photographed HaCaT cells every ten minutes upon treatment with WC_L nanoparticles for two days. The HaCaT cells were found to be robust and well sustain cultivation outside the incubator for up to 48 h without additional buffering or humidity and were therefore chosen for this experiment. About three hours after particle addition, cells performed visible movements leading to incorporation of particles. Areas around the cells were apparently devoid of particles after two days and dark areas appeared inside the cells. It was also seen that some larger particle agglomerates were not taken up by the cells and remained in the media. Particle

uptake had no obvious influence on cell division; it was further observable after particle incorporation. (Movie is provided as supplemental material – Additional file 2; S2_HaCaT_WCL_2d.mpeg).

All particles were found within the cytoplasm as demonstrated by STEM (shown exemplarily in Figures 4 and 6, and (Bastian et al. 2009)). Corresponding to the light microscopy results, different particles built similar patterns within the cells. To confirm the respective nanoparticles within the cells, we performed EDX analyses and found the corresponding elements of the applied nanoparticles. In case of diamond, EDX analyses were not possible because of the high carbon background. Therefore the identification of individual nanoparticles or agglomerates in or on cells had to rely on morphologic characteristics of the diamond nanoparticles.

Particles co-localise with lysosomal structures

In order to shed light on the localisation of particles within cells, we used a fluorescent dye (LysoTracker Red) to stain lysosomal structures of particle exposed and control cells, focussing on a subset of cell lines, namely HaCaT, OLN93 and A549 cells. Figure 2 exemplarily shows that dark particle spots did co-localise with lysotracker positive structures appearing in HaCaT and OLN93 cells after 3 days of exposure to WC-Co and TiN particles, respectively. This indicates a deposition of particles in the lysosomal compartments. This co-localisation was observed in A549 cells as well and was similar for the other types of nanoparticles (data not shown).

Particle uptake changes cellular granularity

Incorporated nanoparticles change the Side Scatter signal (SSC) standing for the granularity of cells in flow cytometry analyses. We found that these changes differ significantly between cell types and particles. Strongest uptake of nanoparticles was found within the monocyte population of primary PBMC. These cells showed a strong time dependent increase in the SSC signal, exemplarily shown for the WCL particles in Figure 3. Interestingly, the SSC signal for lymphocytes, a secondary cell type within the primary culture, was not influenced by particles. Indeed, scanning electron microscopy identified WCL particles exclusively in monocytes but not in lymphocytes after 24 hours of exposure (Figure 4).

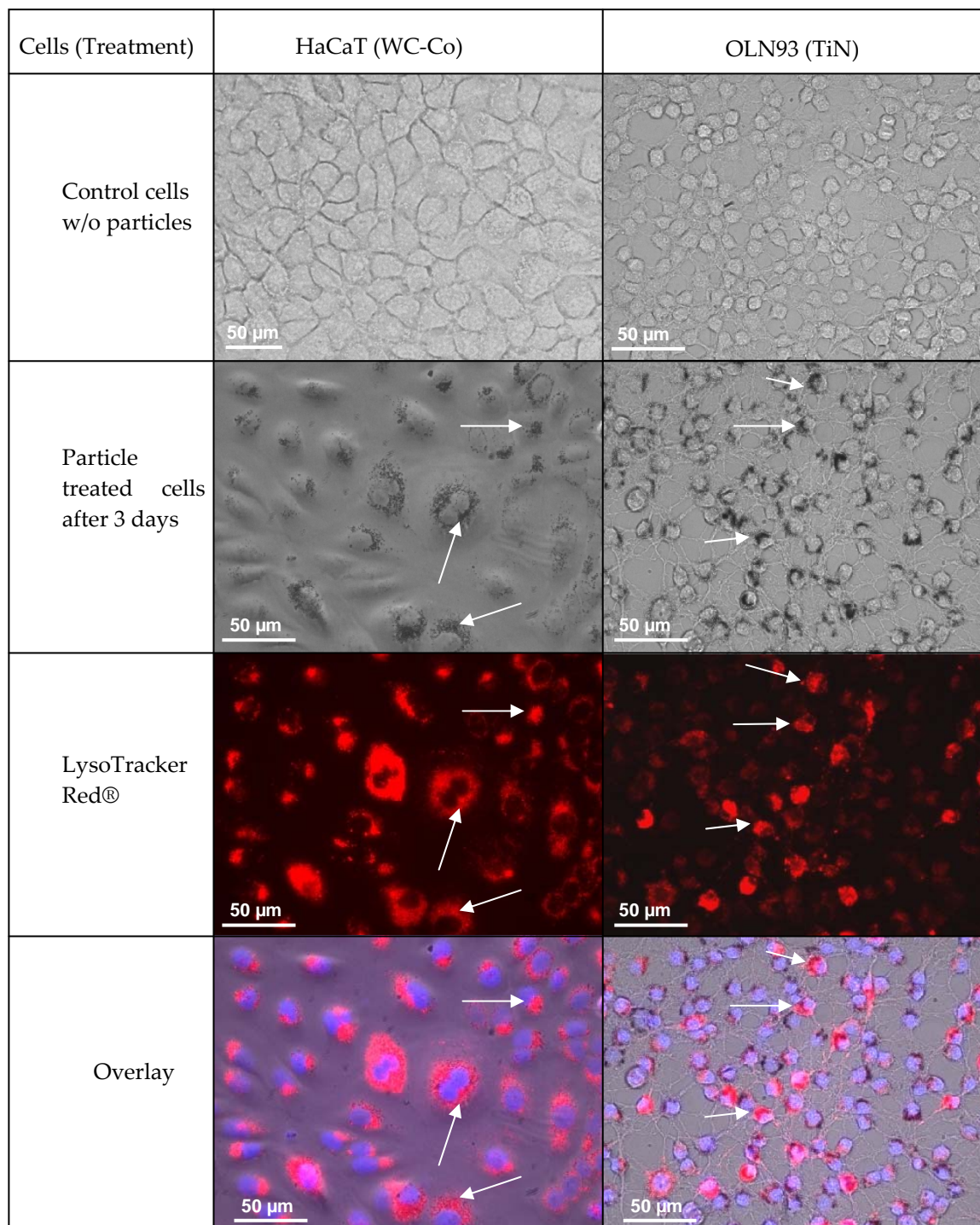


Figure 2. Light and fluorescent microscopy images of HaCaT and OLN93 cells exposed to WC-Co and TiN nanoparticles for 3 days. Cells were stained with the fluorescent dyes LysoTracker Red® (lysosome marker) and Hoechst 33342 (staining of cell nuclei). Particle agglomerates form specific patterns around the cell nuclei visible in transmission light pictures. Staining of cells with LysoTracker Red® indicates the distribution of lysosomes which co-localise with the particle patterns as demonstrated in the overlay. (magnification: 400x)

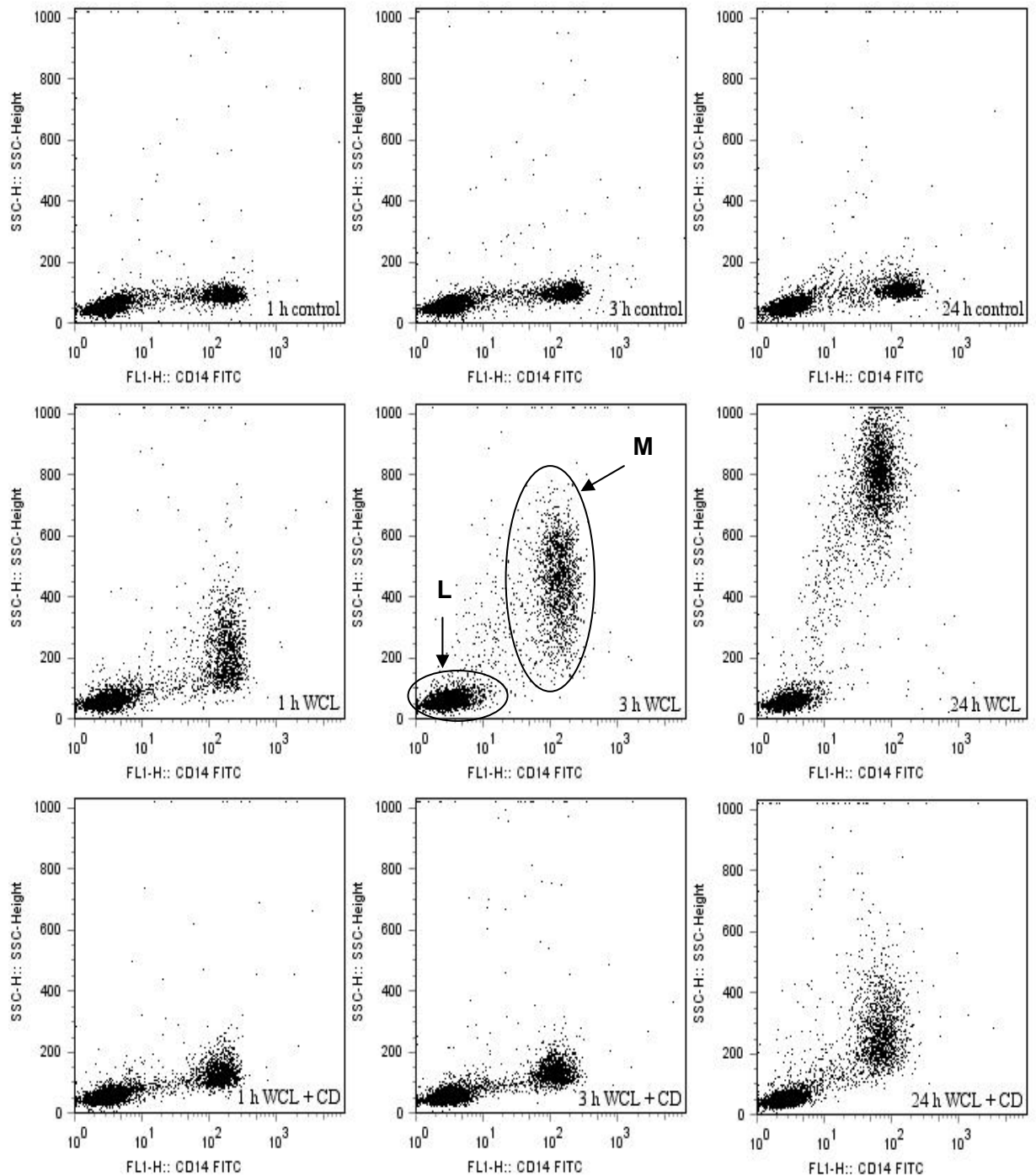


Figure 3. Uptake of WCL nanoparticles by PBMC cells after 1, 3 and 24 hours of exposure to 30 $\mu\text{g/ml}$ WCL. PBMC consist of two cell type populations, monocytes (M) and lymphocytes (L) (exemplarily marked in the middle graph). SSC values of the monocyte cell population increased in a time dependent manner (middle panel) compared to untreated control cells (upper panel). The uptake is inhibited when cells are pre-treated with CytoD (2 μM) (lower panel). No differences of the SSC signals were detected for the lymphocytes, the second cell population in the primary culture, for any of the treatments.

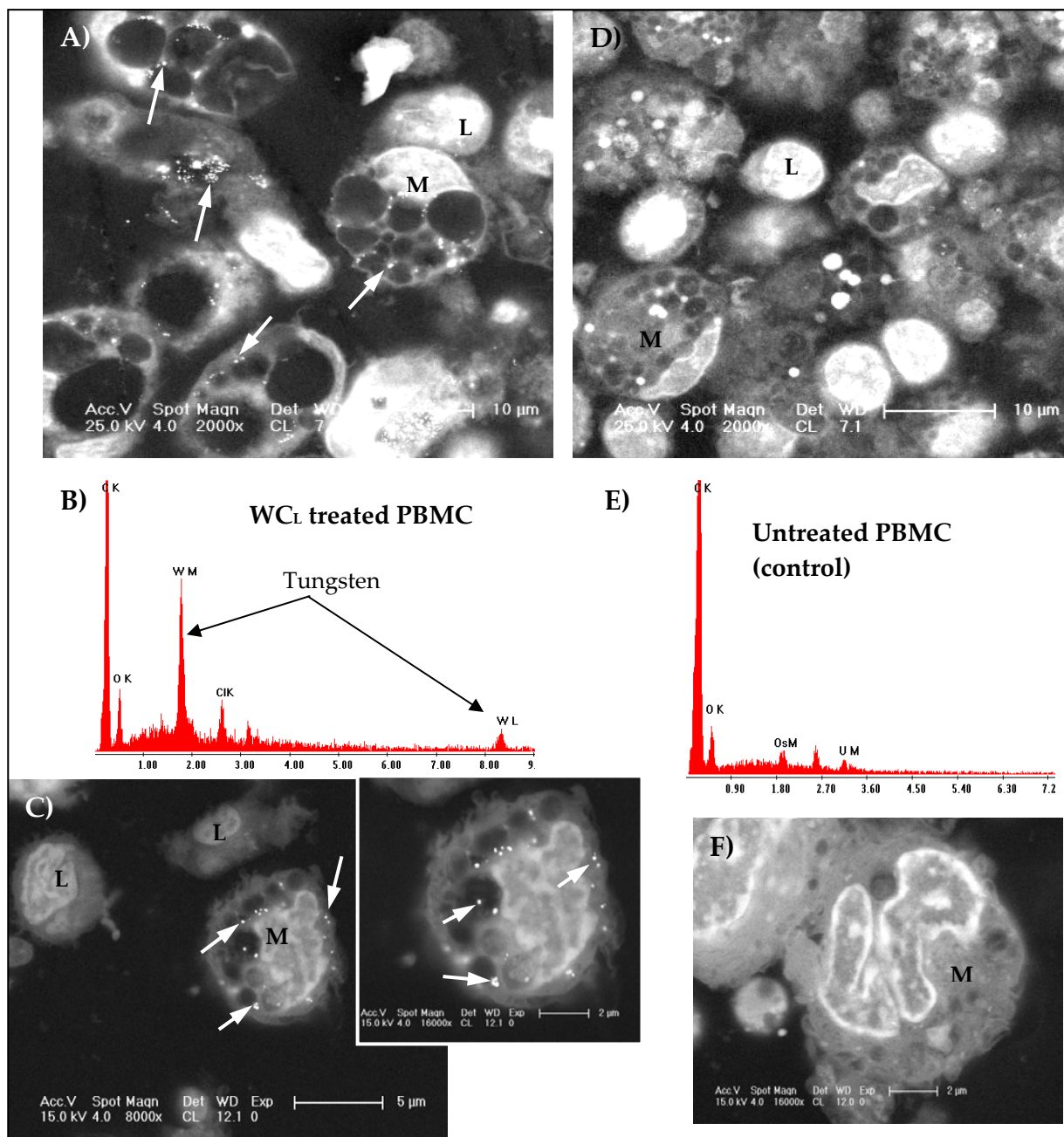


Figure 4. Scanning electron micrographs of embedded PBMC cells after 24 hours of incubation with 30 $\mu\text{g/ml}$ WCL nanoparticles (A, C) and with particle free medium (control, D, F). Heavy elements (e.g., tungsten) appear as light areas (arrows), which are concentrated within the monocytes [M] but were not found within lymphocytes [L] (C). The EDX spectrum of these light spots shows two prominent peaks with the characteristic energy for X-ray quanta originating from the W-M α (WM) and W-L α (WL) atomic shells, respectively (B). No WC was detected in untreated PBMC (E). Other peaks represent further elements in the measured area and are due to compounds of the embedding media (ClK, chloride K α ; OK, oxygen K α), coating (C K α , carbon K α), or staining (OsM, osmium M α and UM, uranium M α) (B, E). Additionally, an intense enlargement of vesicles in monocytes was observed after particle exposure.

Uptake of nanoparticles was likewise observed in all other cell types (and was statistically significant compared to respective controls), but was much less compared to the primary monocytes. This is illustrated again for WCL particles in Figure 5A. The SSC

signal increased about 6-fold for primary monocytes and about 2-fold for all other cell types compared to the respective untreated cells. Surprisingly, the values of the monocyte cell line, THP1, which is assumed to have phagocytic activity (Reyes et al. 1999), were dissimilar to primary monocytes and rather in the range of the other cell types. Exposures to the same mass concentration of WC_s particles (WC with a 6-fold smaller primary particle size, but almost similar size of particle aggregates; Table 1) led to a much lower increase of the SSC signals in all cell types (Figure 5B).

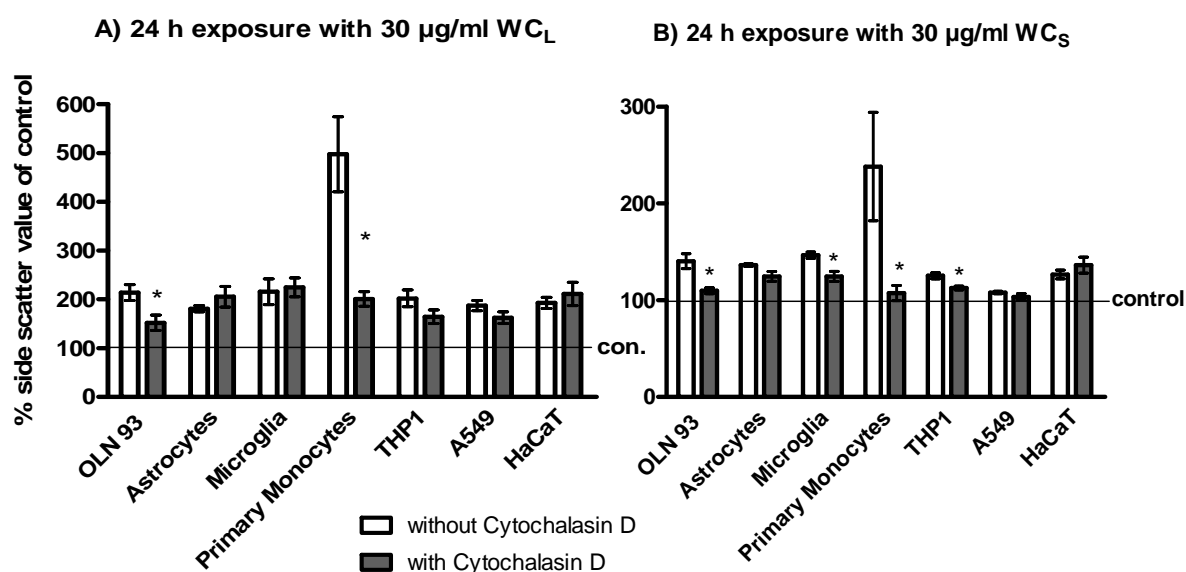


Figure 5. Changes of cellular granularity (measured as SSC) are shown for the different cell types exposed to 30 µg/ml of A) WC_L and B) WC_S nanoparticles for 24 hours without and with CytoD pre-incubation. Bars represent means ± SE as percent of the respective control (n ≥ 4). SSC values were significantly different from control (cells without particles) as analysed with Student's T-Test for all treatments with the exception of A549 cells treated with WC_s and CytoD (p < 0.05); significance of CytoD inhibition is indicated in the graph by the asterisk (*p < 0.05) and was analysed by Student's T-Test (particle exposed cells without CytoD vs. particle exposed cells with CytoD).

The SSC signals generally increased with particle mass concentration for all types of particles (data not shown). However, for some exposure times and mass concentrations, SSC signals differed and did so more between particle types than between cells (with the exception of primary monocytes). To demonstrate these differences, we exemplarily show the results for the OLN93 cell line after 3 h of exposure to 20 µg/ml of particles (Figure 6). A slight increase of cellular granularity was found for WC_s and TiN particles; TiO₂, WC_L and WC-Co caused almost equal increases in SSC signals; and Diamond particles induced the strongest changes of the granularity (Figure 6). This pattern was maintained overall

after 24 h of exposure with the exception of TiO₂, which exhibited changes in SSC signals closer to Diamond than to WC_L and WC-Co particles at this time point (see also Figure 9).

Cytochalasin D (CytoD) indicates involvement of actin filaments in particle uptake for only a few of the investigated cell cultures

We used CytoD to determine whether the destabilisation of actin filaments, which are essential for phagocytosis, influences the ability of cells to incorporate the nanoparticles and found that an inhibition of uptake is dependent on the cell type. Strongest inhibitory effects with CytoD were observed for primary monocytes (Figure 3, bottom row of graphs). Nevertheless, uptake of WC_L particles was significantly inhibited in OLN93 cells as well (Figure 5A). As with the WC_L particles, the SSC signals of WCs treated cells were inhibited significantly by CytoD in primary monocytes. Slight inhibitory effects were observed for OLN93, THP1 and microglia cells (Figure 5B). A significant inhibitory effect of CytoD on particle internalisation was never found for astrocytes, A549, and HaCaT cells.

The inhibitory effect of CytoD on OLN93 cells was observed already after 3 hours of exposure and is demonstrated for all investigated particles in Figure 7A. Pre-incubation of OLN93 cells with CytoD reduced the changes of the SSC signals for all particles by more than 10 % although these changes were statistically significant only for the treatments with WC-Co and diamond particles. Interestingly, SSC signals of primary astrocytes increased particle type dependent in a similar manner as for OLN93 but CytoD had no impact on particle uptake into astrocytes (Figure 7B).

By scanning electron microscopy coupled with element analysis we confirmed the differences in the inhibitory effect of CytoD using independent samples. Figure 8 shows WC_L particles within OLN93 cells and primary astrocytes after 3 hours of exposure. As found with the flow cytometry analyses, qualitative analyses of several (randomly chosen) pictures revealed fewer WC_L particles within OLN93 cells pre-treated with CytoD compared to OLN93 cells without inhibitor pre-incubation. Again, uptake of WC_L particles appeared to be inhibited by CytoD only in OLN93 cells but not in astrocytes: similar amounts of WC_L particles were found in several pictures of astrocytes with and without CytoD pre-incubation. This is again in concurrence with data from cytometric analyses.

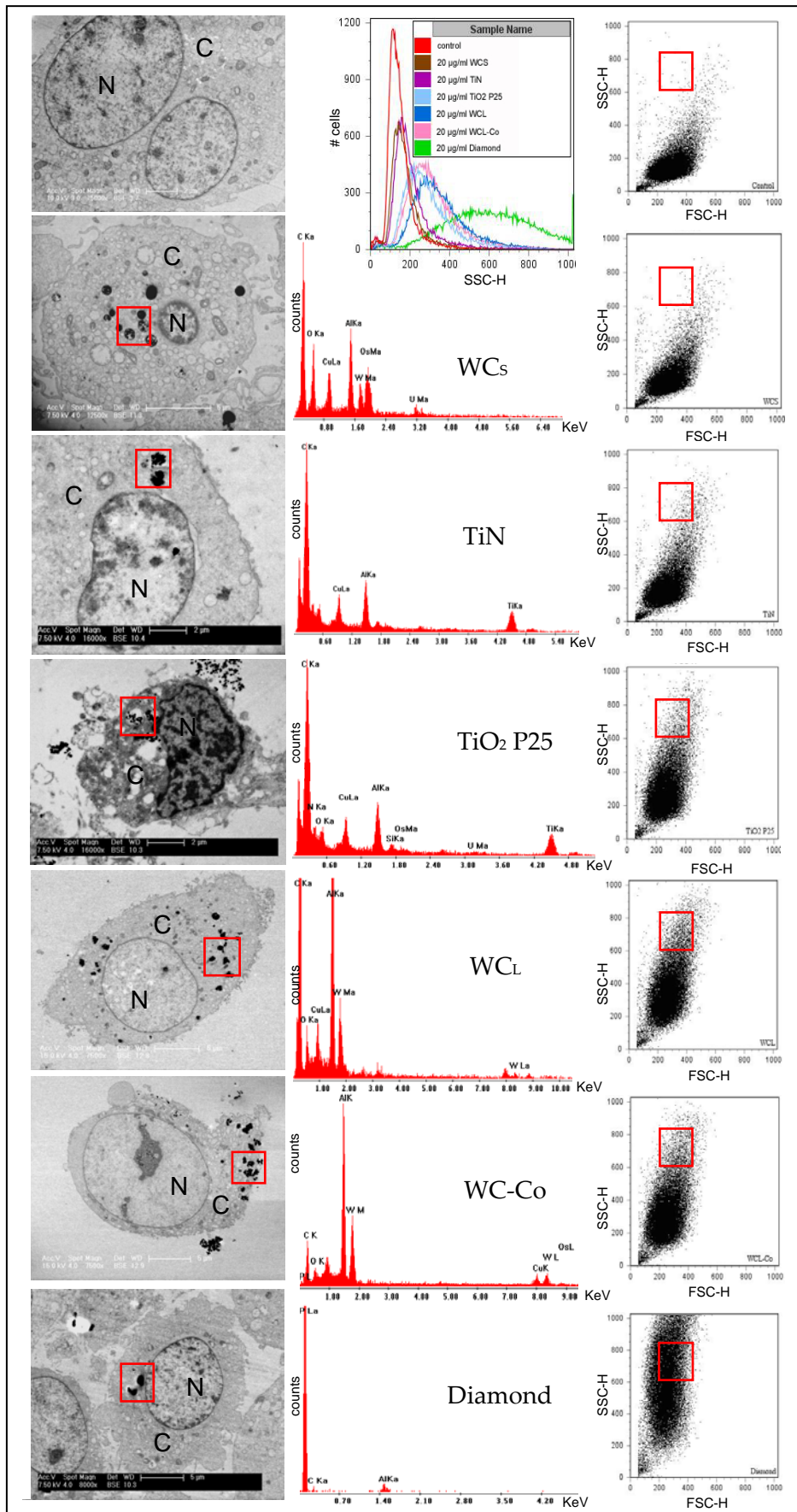


Figure 6. STEM investigations coupled with EDX analyses revealed all types of nanoparticles within the oligodendrocyte cell line OLN93 already after 3 hours of exposure (20 µg/ml for each particle type). The top left micrograph shows a control cell without particles, the micrographs organised in the column below show incorporated nanoparticles within the cytoplasm (C); no particles were found in the nuclei of cells (N). EDX analysis was performed for each sample for a respective area (red rectangle). The spectra, shown in the middle column, indicate the elements found within such an area. Graphs of the right column show the original data from flow cytometry analyses and reveal different SSC values after the exposure with the same concentration (20 µg/ml) of different nanoparticles. Differences of SSC value distributions over the cell population depending on the particle type are summarized in the top middle graph.

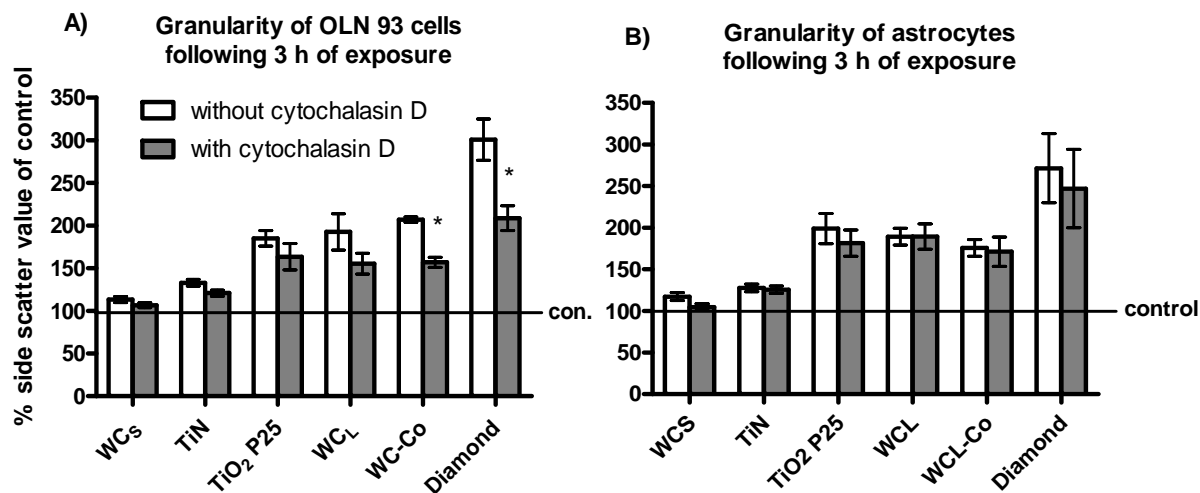


Figure 7. OLN93 cells (A) and primary astrocytes (B) were treated with different nanoparticles (20 $\mu\text{g}/\text{ml}$) with and without CytoD pre-incubation. The bars represent the changes of cellular granularity (measured as SSC values) after 3 hours as mean percent of control (Mean \pm SE, $n = 4$). SSC values were significantly different from control (cells without particles) as analysed with Student's T-Test for all treatments with exception of OLN93 treated with WCs ($p < 0.05$); significance of CytoD inhibition is indicated in the graph by the asterisk ($*p < 0.05$) and was analysed by Student's T-Test (particle exposed cells without CytoD vs. particle exposed cells with CytoD).

Role of particle properties in uptake by cells

By comparing changes in cellular granularity between different cell and particle types it became obvious that differences were greater between the different particles than between the cell cultures. In order to analyse which particle properties are responsible for these particle specific changes of SSC values at same particle concentrations, we tried to correlate several physical particle characteristics (surface area, mass, particle number, primary and aggregate particle size, charge, and material density, Figure 9A) with relative SSC outcomes by multiple regression approaches. For these analyses, we added results of another particle type (magnetite) that was investigated in an earlier study (Hildebrand et al. 2009) and merged the mean SSC values for each particle type over the four different cell cultures (A549, HaCaT, OLN93, and astrocytes) (Figure 9B). As mentioned above, the smallest SSC values were expressed with WCs and the largest with diamond particles. Cellular granularity increased after 24 h in cells exposed to magnetite, TiO₂ and diamond compared to the values after 3 h. Statistical significance was only achieved with TiO₂. However, by comparing particle properties with SSC values we found none of the properties to directly correlate with SSC values, with one exception. After 3 h of exposure, we found a trend towards increasing SSC values with increasing primary particle size

(XBET) (Figure 9C). Yet, this trend was no longer detectable after 24 h, since especially TiO_2 caused much higher values of SSC intensities after 24 h.

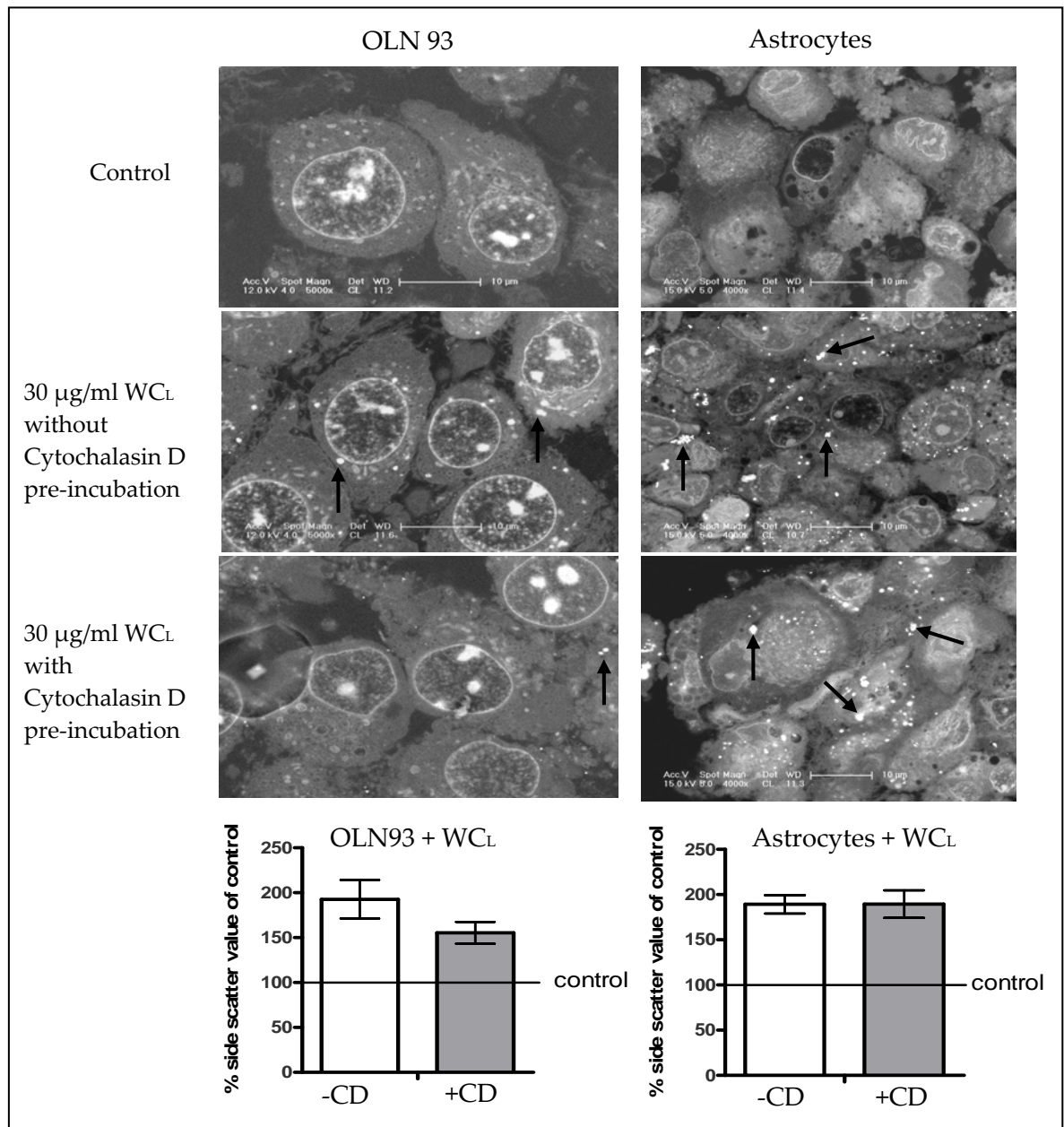


Figure 8. SEM of OLN93 cells (left panel) and primary astrocytes (right panel) exposed to 30 µg/ml WCL nanoparticles for 3 hours with and without CytoD pre-incubation. CytoD treatment reduced particle number in OLN93 cells but not in astrocytes. Graphs show corresponding changes of the SSC values after identical treatments (percent of control; Means \pm SE, n=4).

Particle properties

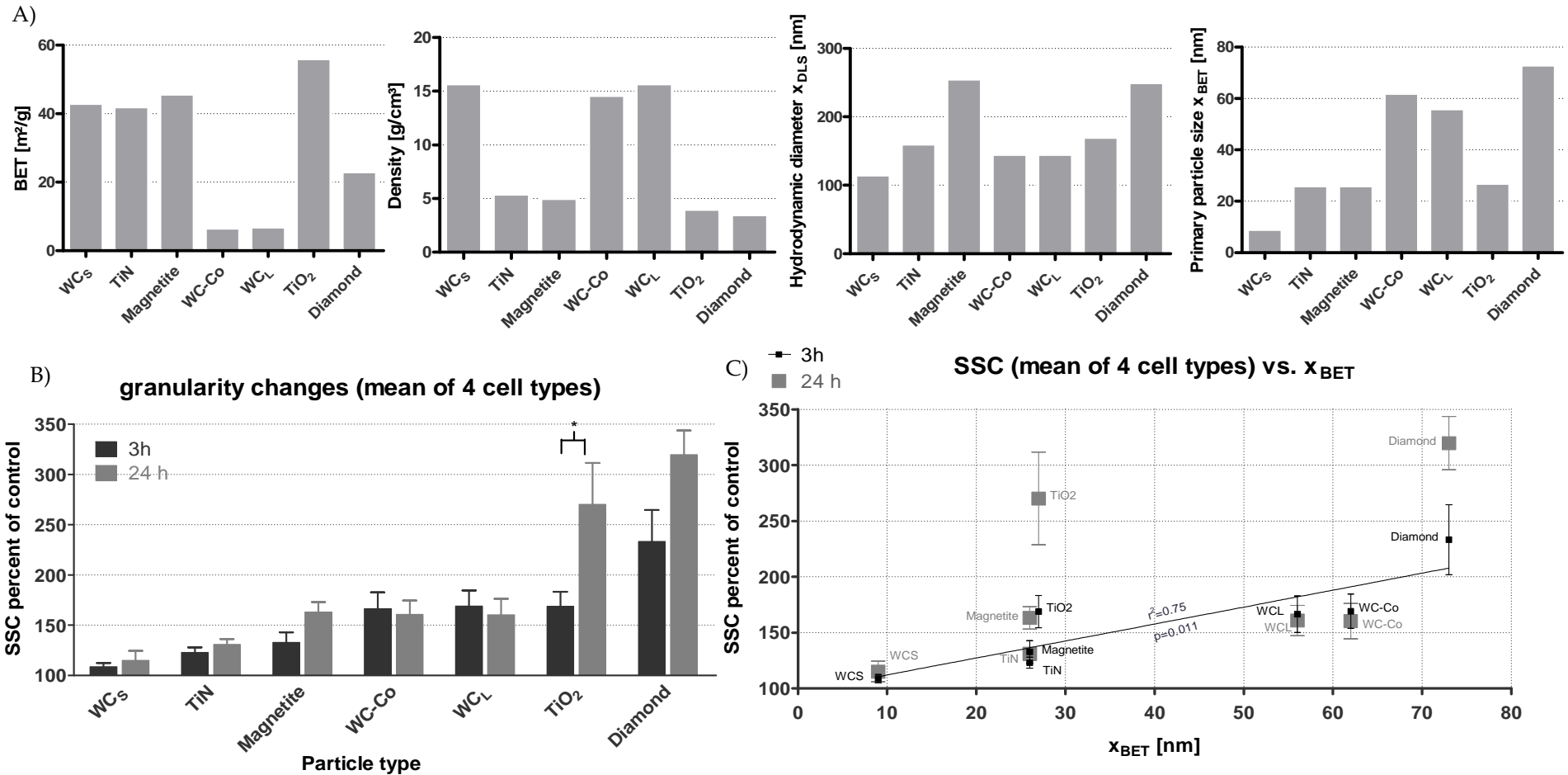


Figure 9. Particle properties (A) were correlated to measured particle type dependent changes of cellular granularity, taking the mean SSC values of four cell types (HaCaT, OLN93, A549, Astrocytes) after 3 and 24 h of exposure to the different nanoparticles (mean \pm SE, $n \geq 4$ for each cell type) into account (B). A statistically significant difference between SSC values after 3 and 24 hours of exposure was found only for TiO₂ particles (* $p < 0.05$, Student's T-Test). By comparing particle properties with SSC values only the primary particle size (xBET) showed a weak correlation with SSC values after 3 hours of exposure (C). After 24 hours of exposure, a direct correlation of SSC values with any of the particle properties could not be identified.

Discussion

Our study showed that all nanoparticles were taken up by cells within the first hours of exposure, irrespective of the particle or cell type. In agreement with earlier studies, we found that uptake positively correlated with particle concentration (Stringer et al. 1995, Bao et al. 2007, Gojova et al. 2007, Habertzettl et al. 2007). All particles in our study had a negative (anionic) surface charge but otherwise varied with respect to particle size and composition. Uptake was confirmed in several ways, including elemental analysis for the different particle types in cell probes. Overall, we found that the particle type had a greater impact on particle internalisation, as judged by changes of cellular granularity, than the cell type. However, differences between the cell cultures were detected by the use of an actin filament inhibitor, indicating the involvement of different mechanisms of particle uptake in the different cell types.

Electron microscopy studies revealed the intracellular localisation of nanoparticles in the cytoplasm; given the detection limits of our system, we never found particles within the nuclei of cells. This observation is reminiscent of our previous work on WC/WC-Co nanoparticle in various vertebrate cells (Bastian et al. 2009, Kühnel et al. 2009). Higher resolution frequently showed particles to be enclosed in an intracellular membrane. Since these regions co-localised with vesicles indicated by fluorescent tracker as lysosomes, we postulate that the majority of particles resides in lysosomal structures. This observation confirms results presented by Harush-Frenkel and colleagues, who showed that anionic particles ended up in lysosomal structures, whereas cationic particles were translocated to the basolateral plasma membrane (Harush-Frenkel et al. 2008). Patterns of particles and stained lysosomes in our study were similar to patterns found by Zhang and Monteiro-Riviere, who investigated several proteins and compartments relevant for endocytotic processes and found strong overlay of fluorescent quantum dots only with the lysosome markers CD63 and Lamp1 (Zhang & Monteiro-Riviere 2009).

The general pattern of particle distribution within cells, independent of particle and cell type, points towards a common determinant of particle uptake. One likely explanation is the particle stabilising effect of serum albumin, as previously reported for ceramic/metal and carbon-based nanoparticles (Deguchi et al. 2007, Bastian et al. 2009, Meißner et al. 2009). In further support of this, Yumoto and colleagues found that albumin

co-localised with lysosomes in lung alveolar epithelial cells and microscopic patterns were similar to those observed by us (Yumoto et al. 2006). Cedervall and colleagues demonstrated strong binding of human serum albumin to nanoparticles and calculated an amount of about 620 albumin proteins binding at the surface of a 70 nm particle (Cedervall et al. 2007). In recent studies of our own, we calculated that the albumin content in our serum supplemented media was always higher than the potential binding ability of the particles in the concentrations applied (Meißner et al. 2010). Binding to nanoparticles of other serum proteins, such as fibrinogen and apolipoproteins, has also been reported (Cedervall et al. 2007, Lundqvist et al. 2008). Kreuter and colleagues demonstrated that medically used apolipoprotein-coated nanoparticles were able to penetrate the blood brain barrier via low density lipoprotein (LDL) receptor mediated endocytosis (Kreuter et al. 2002). It thus seems that particle-bound serum proteins are not only relevant to internal exposure and systemic distribution in organisms but influence cellular uptake and subsequent cell-internal translocation as well.

The observed co-localisation of the different particles with lysosomal structures in all cells points towards endocytosis as mechanism of particle uptake. Despite this general observation, quantification of cellular granularity by flow cytometry, measured as changes in side scatter (SSC), allowed differences in uptake to be identified that were related either to cell or particle type.

With regard to cell type, primary monocytes, which are “professional” phagocytic cells, were most active in particle internalisation as demonstrated by high SSC values. All other cells responded similarly to identical particle preparations and showed significantly lower SSC signals, including cells of the monocyte cell line, THP1. Primary monocytes also differed from all other investigated cells in that particle internalisation led to the formation of large intracellular vesicles. Such vesicles are typical for phagocytosis but may themselves have contributed to increased SSC signals in a fashion unproportional to particle uptake. Primary monocytes also responded most sensitively to exposure to Cytochalasin D (CytoD), an inhibitor of actin filaments, although CytoD also significantly inhibited nanoparticle uptake in the oligodendrocyte cell line, OLN93. Brain cells are generally able to perform phagocytosis, although this is reported more frequently for microglia and astrocytes (Thomas 1992, Roldan et al. 1997, Chang et al. 2000), the latter of which showed no impact by CytoD in this study. Actin filaments are known to be

essential for phagocytosis but have been implied to play a role in other endocytic processes as well (Kaksonen et al. 2006). We therefore conclude that particle internalisation by phagocytosis was likely the main route of uptake in primary monocytes and possibly oligodendrocytes, and that other known endocytic mechanisms must have been involved in particle uptake by the other cells.

Endocytic pathways involved in nanoparticle uptake have been investigated in several studies with non-phagocytic cells (Rejman et al. 2004, Gratton et al. 2008, Harush-Frenkel et al. 2008, Oh et al. 2009, Zhang & Monteiro-Riviere 2009). All these studies evidently showed that cells use more than one pathway to internalise particles, for example by means of clathrin-mediated or caveolae-mediated endocytosis. Zhang and Monteiro-Riviere demonstrated that endosome and lysosome disrupting agents inhibited the internalisation of quantum dots into human epithelial keratinocytes, whereas CytoD had no inhibitory effects (Zhang & Monteiro-Riviere 2009). They confirmed a specific pathway of uptake for quantum dots via lipid raft dependent and GPCR (G-protein-coupled-receptor) pathway regulated LDL/scavenger receptors. Whether similar mechanisms were involved in non-phagocytic uptake in the keratinocytes and the other cell types studied here is as yet unknown. However, two other factors need to be considered for non-phagocytic particle uptake. First, in the *in vitro* experiments, particles are added to the media on top of the cells and therefore gravitational forces may also play a role in particle uptake. Second, as discussed above, proteins and lipids bound to the particle surfaces may impact on the route of particle uptake. Albumin, for example, is proposed to be transported through cells via caveolae mediated endo- and transcytosis (Schubert et al. 2001, Razani et al. 2002). However, whether a protein-particle complex can be internalised the same way as proteins is yet unclear; certainly the nanoparticle-protein complex is much larger than a single protein.

With regard to particle type, the smallest changes of the SSC values compared to control cells were consistently found for WCs and the highest values for diamond particles with comparable relative SSC values for each type of particle in either cell type, except for primary monocytes (see above). With respect to these findings, we conclude that cellular granularity after particle incorporation in non-phagocytic cells is much more influenced by the particle characteristics than by cell type. However, only primary particle size, X_{BET} , showed a weak correlation with early (3 h) particle uptake as quantified by SSC.

Similar observations were made by Limbach and colleagues who showed particle size to be the dominant factor in determining the uptake of ceria nanoparticles into human lung cells (Limbach et al. 2005). The result of a weak correlation only with primary particle size indicates that physical and/or chemical particle characteristics, not accounted for in the current study, contribute to particle uptake and the associated changes in cellular granularity. Granularity of cells is measured as intensity of the right angle scattered light and is brought about by intracellular organelles (e.g. mitochondria, nuclei) or particles that divert the incoming light in a typical pattern. It follows that, optical properties, such as reflection, refraction and absorption (Johnsen & Widder 1999), which also depend on the nanoparticles' surface and quantum effects, may influence light scattering and intensity of the SSC measurements. In support of this, TiN always resulted in much lower SSC values than TiO₂ despite a roughly similar density and particle size. TiO₂ nanoparticles are industrially used because of their white colour and the resulting optical properties (strong reflection, low absorption; absorption coefficient = 2.8 μm^{-1} for the respective wavelength of the FACS system (488 nm); <http://refractiveindex.info>). By contrast, TiN is a dark powder with a much higher light absorption capacity indicated by an absorption coefficient of 34.3 μm^{-1} . All other particles of the study had a dark colour, except for diamond that was grey. Thus, while changes in SSC can clearly indicate particle uptake, additional parameters and methods, such as optical properties and total element quantification by inductively coupled plasma mass spectroscopy, need to be used to link particle properties with uptake and changes in cellular granularity. Combining these approaches and applying them to a set of particles with an even broader range of particle properties to quantitatively predict particle uptake into cells will, however, be a major challenge.

In this study we unequivocally demonstrate that different types of engineered nanoparticles enter several kinds of mammalian cells. Even if found non-toxic, as demonstrated by cell viability measurements for, e.g. WC_L but not for WC-Co (Bastian et al. 2009, Busch et al. 2010, Kühnel et al. 2009), it is still unknown how cells live and deal with incorporated nanoparticles. Particles in cells may act as carriers for endogenous and exogenous substances (Baun et al. 2008, Stoeger et al. 2009), as catalysts for chemical reactions or may cause immunological responses based on recognition of the nanoparticle as a foreign entity (Ashwood et al. 2007, Kanno et al. 2007). Past experiences with several

kinds of lung diseases caused by fibres and industrial dusts, often appearing long time after exposure, support concerns about engineered nanoparticles (Maynard & Kuempel 2005). Therefore, the long-term fate of technical nanoparticles in cells *in vitro* and *in vivo* needs to be identified. Considering the ability of technical nanoparticles to enter various kinds of cells, in conjunction with our currently limited knowledge regarding the intracellular nanoparticle fate, occupational and consumer exposure should be minimised.

Toxicity of tungsten carbide and cobalt-doped tungsten carbide nanoparticles in mammalian cells *in vitro*

Environmental Health Perspectives 2009, **117**(4): 530-536

Susanne Bastian^{1*}, Wibke Busch^{2*}, Dana Kühnel^{2*}, Armin Springer^{3*}, Tobias Meißner^{4*}, Roland Holke^{4*}, Stefan Scholz², Maria Iwe¹, Wolfgang Pompe³, Michael Gelinsky³, Annegret Potthoff⁴, Volkmar Richter^{4**}, Chrysanthy Ikonomidou^{1**} and Kristin Schirmer^{2,5**}

¹Department of Pediatric Neurology, University Children's Hospital Carl Gustav Carus, University of Technology Dresden, Dresden, Germany; ²Department of Cell Toxicology, UFZ-Helmholtz Centre for Environmental Research, Leipzig, Germany; ³Max Bergmann Center of Biomaterials, Institute of Materials Science, University of Technology Dresden, Dresden, Germany; ⁴Fraunhofer Institute for Ceramic Technologies and Systems, Dresden, Germany; ⁵Eawag, Swiss Federal Institute of Aquatic Science and Technology, Dübendorf, Switzerland

*equally contributed first authors, **equally contributed last authors

Abstract

Background: Tungsten carbide nanoparticles are being explored for their use in the manufacture of hard metals. To develop nanoparticles for broad applications, potential risks to human health and the environment should be evaluated and taken into consideration.

Objective: We aimed to assess the toxicity of well-characterized tungsten carbide (WC) and cobalt-doped tungsten carbide (WC-Co) nanoparticle suspensions in an array of mammalian cells.

Methods: We examined acute toxicity of WC and of WC-Co (10 % weight content Co) nanoparticles in different human cell lines (lung, skin, and colon) as well as in rat neuronal and glial cells (i.e., primary neuronal and astroglial cultures and the oligodendrocyte precursor cell line OLN-93). Furthermore, using electron microscopy, we assessed whether nanoparticles can be taken up by living cells. We chose these *in vitro* systems in order to evaluate for potential toxicity of the nanoparticles in different mammalian organs (i.e., lung, skin, intestine, and brain).

Results: Chemical–physical characterization confirmed that WC as well as WC-Co nanoparticles with a mean particle size of 145 nm form stable suspensions in serum-containing cell culture media. WC nanoparticles were not acutely toxic to the studied cell lines. However, cytotoxicity became apparent when particles were doped with Co. The most sensitive were astrocytes and colon epithelial cells. Cytotoxicity of WC-Co nanoparticles was higher than expected based on the ionic Co content of the particles. Analysis by electron microscopy demonstrated presence of WC nanoparticles within mammalian cells.

Conclusions: Our findings demonstrate that doping of WC nanoparticles with Co markedly increases their cytotoxic effect and that the presence of WC-Co in particulate form is essential to elicit this combinatorial effect.

Background

Nanotoxicology is an emerging field of research at the intersection of material science, medicine, and toxicology. The ultimate characteristic of nanomaterials is their size, which can modify the physicochemical properties of the material, enable increased uptake and interaction with biological tissues, and generate adverse biological effects in living cells that would not be possible with the same material in larger or soluble form. Smaller particle size leads to increased surface area and allows for a greater proportion of atoms or molecules to be displayed on the surface. Clinical and experimental studies indicate that a small size, a large surface area, and the ability to generate reactive oxygen species (ROS) contribute to the potential of nanoparticles to induce cell injury (Colvin 2003, Oberdörster et al. 2005, Nel et al. 2006).

Most toxicology data for engineered nanomaterials are derived from inhalation studies concentrating on lung injury and assessment of inflammatory parameters. Uptake of metal oxide nanoparticles in lung cells has been demonstrated *in vivo* as well as in different cell culture systems (Stearns et al. 2001, Limbach et al. 2005, Geiser et al. 2008). Toxic effects in human lung cells depend on particle composition and size and related reactivity (Limbach et al. 2005, Brunner et al. 2006, Duffin et al. 2007, Limbach et al. 2007). So-called nanoeffects, meaning differing effects of nanomaterials compared with bulk materials of the same chemical composition, have been observed, with nanomaterials being more toxic in regard to reduction of cell viability or induction of oxidative stress and inflammatory mediators (Zhang et al. 2000, Zhang et al. 2003, Wörle-Knirsch et al. 2007). Tungsten carbide (WC) nanoparticles are now being considered for the manufacture of hard metals to achieve extreme hardness and wear resistance, and mixing with cobalt is thought to improve toughness and strength of the material. In the past, occupational exposure to Co-containing dust in production facilities, which generally falls in the 1–20 μm size range (Stefaniak et al. 2009), has been associated with bronchial asthma, fibrosing alveolitis, and lung cancer (Lison 1996, Moulin et al. 1998). Tungsten carbide–Co (WC-Co) hard metal is now classified by the International Agency for Research on Cancer (IARC) as probably carcinogenic to humans, based on limited evidence in humans and sufficient evidence in experimental animals (International Agency for Research on Cancer 2006). Experimental work has shown a higher mutagenic

potential of the WC-Co mixture compared with its individual components (Van Goethem et al. 1997), a finding that has been attributed to increased production of ROS. WC-Co exposure of peripheral blood mononucleated cells has been shown to trigger apoptosis of these cells via a caspase-9-dependent pathway (Lombaert et al. 2004) and to generally up-regulate apoptotic and stress/defense response pathways (Lombaert et al. 2008). Ultrastructural analysis revealed that WC particles are incorporated into numerous vacuoles, whereas WC-Co particles lead to lysis of the cells, and no structural alterations due to Co particles could be demonstrated (Lison & Lauwerys 1990). Extensive studies on genotoxicity and mutagenicity have been conducted after a series of epidemiologic studies showed that hard-metal workers exposed to airborne WC and Co dust in occupational settings have increased mortality from lung cancer (Moulin et al. 1998).

Little information exists regarding effects of nanoparticles on other potentially exposed organs (i.e., skin, intestine, and the nervous system); although systemic circulation and distribution of inhaled or injected nanoparticles to different organs have been reported (Nemmar et al. 2001, Takenaka et al. 2001, Kreyling et al. 2002, Nemmar et al. 2002). Nanoparticles may translocate to the central nervous system via the olfactory nerve (Oberdörster et al. 2004). A few neurotoxicologic studies have shown that titanium dioxide nanoparticles accumulate in microglial cells, causing increased ROS production, mitochondrial swelling, and membrane disruption (Long et al. 2006). Pisanic and colleagues reported reduction of neurite outgrowth and formation of intercellular connections after exposure of neurons to iron oxide nanoparticles (Pisanic et al. 2007).

In this study, we evaluated acute toxicity of WC and WC-Co nanoparticles in *in vitro* systems (i.e., human epithelial and rat neuronal and glial cells). Here we report the physicochemical characterization of WC and WC-Co nanoparticles in cell culture media and describe their intracellular distribution and cytotoxicity profile.

Materials and Methods

Particles, Preparation

WC and WC-Co particles (10 % weight content of Co) were prepared by a chemical process and deaggregated and mixed, respectively, by means of a ball mill. We milled the nearly pure WC powder and Co powder in a hard-metal-lined ball mill using hard metal balls [see Supplemental Material, "Particle preparation and characterization," and Supplementary Material, Table 1 and Figure 1 (<http://www.ehponline.org/members/2008/0800121/suppl.pdf>)].

From both types of particles, we prepared suspensions of 100 µg/mL in pure water (resistivity ≥ 18 MΩ·cm; Wilhelm Werner GmbH, Leverkusen, Germany). For WC, water was sufficient to prepare electrostatically stable particle suspensions. For WC-Co, the addition of 0.01 % (wt/v) sodium polyphosphate solution (Graham's salt; CAS no. 10361-03-25; Merck, KGaA, Darmstadt, Germany) was necessary to obtain electrostatic stabilization of the particles, apparently due to the presence of Co. Graham's salt is an often-used dispersant that is nontoxic in the applied concentrations. The suspensions were treated in an ultrasonic bath (RK 255 H; Bandelin, Berlin, Germany) for deagglomeration. After preparation, we quantified particle size and zeta potential. Time-dependent measurements in physiologic media (cell culture media or buffers) were performed by stirring a mixture of 90 % (v/v) media and 10 % (v/v) nanoparticle suspension in a beaker. The resulting suspensions were filled in a square cuvette for measurements. In parallel, studies were carried out in phosphate-buffered saline (PBS; Biochrom, Berlin, Germany) with or without bovine serum albumin (BSA; bovine fraction V, CAS no. 9048-46-8; Merck), which was dissolved in PBS before adding the particle suspension. We also performed experiments in Hank's buffered salt solution (HBSS; Biochrom) or Dulbecco's modified Eagle's medium (DMEM; PAA Laboratories, Pasching, Austria) with or without 5 % or 10 % (v/v) fetal bovine serum (FBS; Invitrogen, Karlsruhe, Germany).

Physicochemical characterization

We determined the N₂-BET specific surface area (BET; Brunauer, Emmet, Teller, after the developers of the basic calculations) of WC and WC-Co powders using an ASAP 2010

accelerated surface area and porosimetry analyzer (Micromeritics GmbH, Mönchengladbach, Germany). We determined the particle size distribution using dynamic light scattering (ZetaSizer Nano ZS; Malvern Instruments Ltd., Worcestershire, UK). We analyzed the mean particle size, x_{PCS} , and the polydispersity index (PDI), which are described in DIN ISO 13321 (2004-10). We calculated the zeta potential from the Smoluchowski equation by measuring the electrophoretic mobility (ZetaSizer Nano ZS). These measurements were taken before and after autoclaving and yielded similar results. Therefore, we chose to sterilize the particle suspensions by autoclaving before exposure of cells. Solubility experiments were performed by centrifuging the nanoparticle suspensions at $15,000 \times g$ (Sigma 4K15; Sigma Laborzentrifugen GmbH, Osterode am Harz, Germany). We then used clear supernatant to determine the tungsten and Co concentration using inductively coupled plasma–optical emission spectroscopy (Ultima; HORIBA Jobin Yvon, Unterhaching, Germany).

Preparation of Co and tungsten salt solutions

We prepared cobalt chloride (CoCl_2 ; Fluka/Sigma-Aldrich, Seelze, Germany) and sodium tungstate dihydrate solutions (Sigma) in distilled water at concentrations of 10 mM or 20 mM. Stock solutions were sterilized by autoclaving. We obtained all concentrations used in cell assays by serial dilution of the stock solutions with cell culture grade water (PAA Laboratories) under sterile conditions. Solutions were stored at 4 °C.

Cell culture, Cell lines

We used the following cell lines: CaCo-2 human colon adenocarcinoma cells (HTB-37; American Type Culture Collection (ATCC), Rockville, MD, USA), HaCaT human keratinocyte cells (CLS Cell Lines Service, Eppelheim, Germany) (Boukamp et al. 1988), A549 human lung carcinoma cells (CCL-185; ATCC), and OLN-93 oligodendroglial precursor cells (provided by the Department of Neonatology, Charité, Berlin, Germany).

Primary neuronal and astroglial cell cultures. Neuronal cell cultures were prepared from cortices of Wistar rat fetuses on gestation day 18 according to Fedoroff and Richardson (Fedoroff & Richardson 1997). Detailed descriptions of the routine maintenance of all applied cell cultures is available in the Supplemental Material [“Cell

culture and assessment of cell viability" (<http://www.ehponline.org/members/2008/0800121/suppl.pdf>).

Exposure of cells to particles

The CaCo-2, HaCaT, and A549 cells were plated at a density of 5×10^4 cells/well in a final volume of 500 μ L in 24-well plates (Techno Plastic Products AG, Trasadingen, Switzerland) and allowed to attach for 24 hr before addition of particle suspensions. We then added 50 μ L of the respective dilution of the particle suspension to 450 μ L complete cell culture medium to reach final concentrations of 7.5, 15, and 30 μ g/mL for WC nanoparticles and 8.25, 16.5, and 33 μ g/mL for WC-Co nanoparticles. The water used to prepare the particle suspension (with or without Graham's salt) was included as a control (vehicle).

We exposed cells to nanoparticle-containing solutions or vehicle control for 1 hr to 3 days. For exposure of cells with CoCl₂ or sodium tungstate dihydrate, we added a maximal volume of 10 % (v/v) salt solution to cell culture medium to reach the desired final concentrations. For co-exposure of CoCl₂ and WC, we added 5 % (v/v) CoCl₂ and 5 % (v/v) of WC suspension to the cell culture medium to reach the same final concentrations of CoCl₂ and 15 μ g/mL WC.

We plated OLN-93 cells (1×10^4 cells/mL) and primary cells (5×10^4 cells/mL) in 96-multiwell plates in a final volume of 100 μ L (Greiner Bio-One, Frickenhausen, Germany) and allowed them to attach for at least 24 hr before adding particle suspension. We added particle dilutions as described above, and cells were exposed for 3 days.

Electron microscopy

For scanning electron microscopy (SEM) of cells, harvested cells were fixed with 2 % (v/v) glutaraldehyde (Serva, Heidelberg, Germany) at room temperature, postfixed with 1 % (v/v) osmium tetroxide (Roth, Karlsruhe, Germany), dehydrated in a graded series of acetone [including a staining step with 1 % (v/v) uranyl acetate], and embedded in epoxy resin according to Spurr (Spurr 1969). To avoid interference of the uranyl acetate and osmium tetroxide during energy-dispersive X-ray spectroscopy (EDX), we did not stain respective samples with the heavy metals; these samples were fixed in 2 % (v/v) glutaraldehyde, dehydrated, and embedded in epoxy resin as above. Samples were cut on

a Leica EM UC6 ultramicrotome (Leica, Vienna, Austria), equipped with a diamond knife (Diatome, Biel, Switzerland), carbon coated, and analyzed using a Philips XL 30 ESEM (Philips, Eindhoven, Netherlands). For EDX analyses, we used an EDAX detecting unit and EDAX software (version 3.0; EDAX Inc., Mahwah, NJ, USA).

Assessment of cell viability, Light microscopy

Before termination of exposure, we observed cells by light microscopy using an inverse microscope.

Assays for cell viability

We determined cell viability using fluorescent indicator dyes that measure cellular metabolic activity [AlamarBlue (Biosource, Nivelles, Belgium) and Cell Counting Kit 8 (CCK-8; Dojindo Laboratories, Kumamoto, Japan)] and cell membrane integrity [5-carboxyfluorescein diacetate, acetoxymethyl ester (CFDA-AM) (Molecular Probes, Eugene, OR, USA)]. We followed procedures described by Schirmer et al. (Schirmer et al. 1997) for AlamarBlue/CFDA-AM and the supplier's protocol for CCK-8. Details of the procedures are provided in the Supplementary Material ["Cell culture and assessment of cell viability" (<http://www.ehponline.org/members/2008/0800121/suppl.pdf>)].

Statistics

Exposure experiments with cells were performed in quadruplicate wells in three independent tests. We analyzed statistical differences using one-way analysis of variance (ANOVA) followed by Dunnett's posttest (treatments vs. control), Tukey's posttest (treatment vs. treatment), or two-way ANOVA followed by Bonferroni posttest using GraphPad Prism software (GraphPad Prism version 4.00 for Windows; GraphPad Software, Inc., San Diego, CA, USA). We considered p-values < 0.05 to be statistically significant. Fluorescence/absorbance units obtained in the cell viability assays were converted to percent of control and are presented as mean \pm SD.

Results

Particles, Initial characteristics

The obtained BET specific surface area was 6.9 m²/g for WC and 6.6 m²/g for WC-Co. We expected the similarity in BET because WC-Co consists of 90 % weight WC powder and both were milled under equal conditions. The particle size distribution and the morphology also were nearly the same, which we confirmed by two independent methods: SEM and dynamic light scattering. The mean particle size, x_{PCS} , which formed the initial value for studying the time dependence of agglomeration, was 145 ± 5 nm in both cases. The PDIs of 0.2 indicated a rather broad size range. We calculated the particle size range to be between 50 and 300 nm [see Supplemental Material, Figure 2 (<http://www.ehponline.org/members/2008/0800121/suppl.pdf>)].

The measured zeta potentials were approximately –35 mV for WC in water and –50 mV for WC-Co in sodium polyphosphate stabilized suspension. The high absolute values of the zeta potentials ensure a stable suspension in both cases because of the strength of the electrostatic repulsion force. Table 1 summarizes the physical parameters of both materials.

Table 1. Physical properties of investigated nanoparticles.

Substance	BET (m ² /g) ^a	x_{PCS} (nm) ^b	PDI	Zeta potential (mV)
WC	6.9	145 ± 5	0.2	–35
WC-Co	6.6	145 ± 5	0.2	–50

^aSpecific surface area. ^bMean particle size.

Dispersion stability in physiologic media

WC and WC-Co particles undergo agglomeration after addition to a protein-free physiologic medium. We studied the influence of different physiologic media (PBS, HBSS, DMEM) on agglomeration but found no differences. Likewise, we found no significant difference in the agglomeration behavior between WC and WC-Co particles. The absolute value of the zeta potential decreased after addition of the particles to PBS, HBSS, or DMEM. Zeta potentials for WC and WC-Co were between –20 and –23 mV.

In contrast to protein-free media, experiments with the protein albumin (BSA) in PBS showed no agglomeration of WC and WC-Co particles. Measured zeta potentials of the BSA-coated particles were about –11 mV. Although this small absolute value stands for a

low electrostatic repulsion force, a steric component of the protein appears to lead to a stabilizing effect. To go one step further, we performed these investigations in DMEM or HBSS with 5 % or 10 % (v/v) serum to have the same conditions as in the cell culture experiments. There, we achieved the same stabilization effect for both serum concentrations. As already described for WC/WC-Co in PBS with BSA, the zeta potential of the particles in DMEM or HBSS with FBS was -11 mV. Figure 1 shows examples of the behavior of the particles in DMEM and PBS.

We determined the tendency of the particles to dissolve after we allowed the stock suspensions to stand for 1 week. For WC, 6 % of the tungsten dissolved. For WC-Co, 15 % of the tungsten and 76 % of the Co dissolved. This level of dissolution of Co^{2+} from WC-Co is similar to that reported by Lombaert and colleagues for microsized WC-Co (Lombaert et al. 2004).

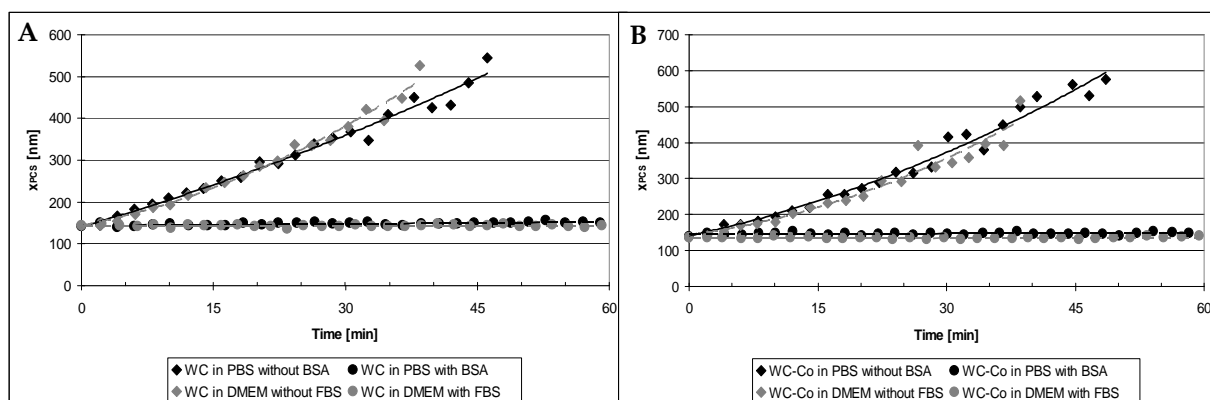
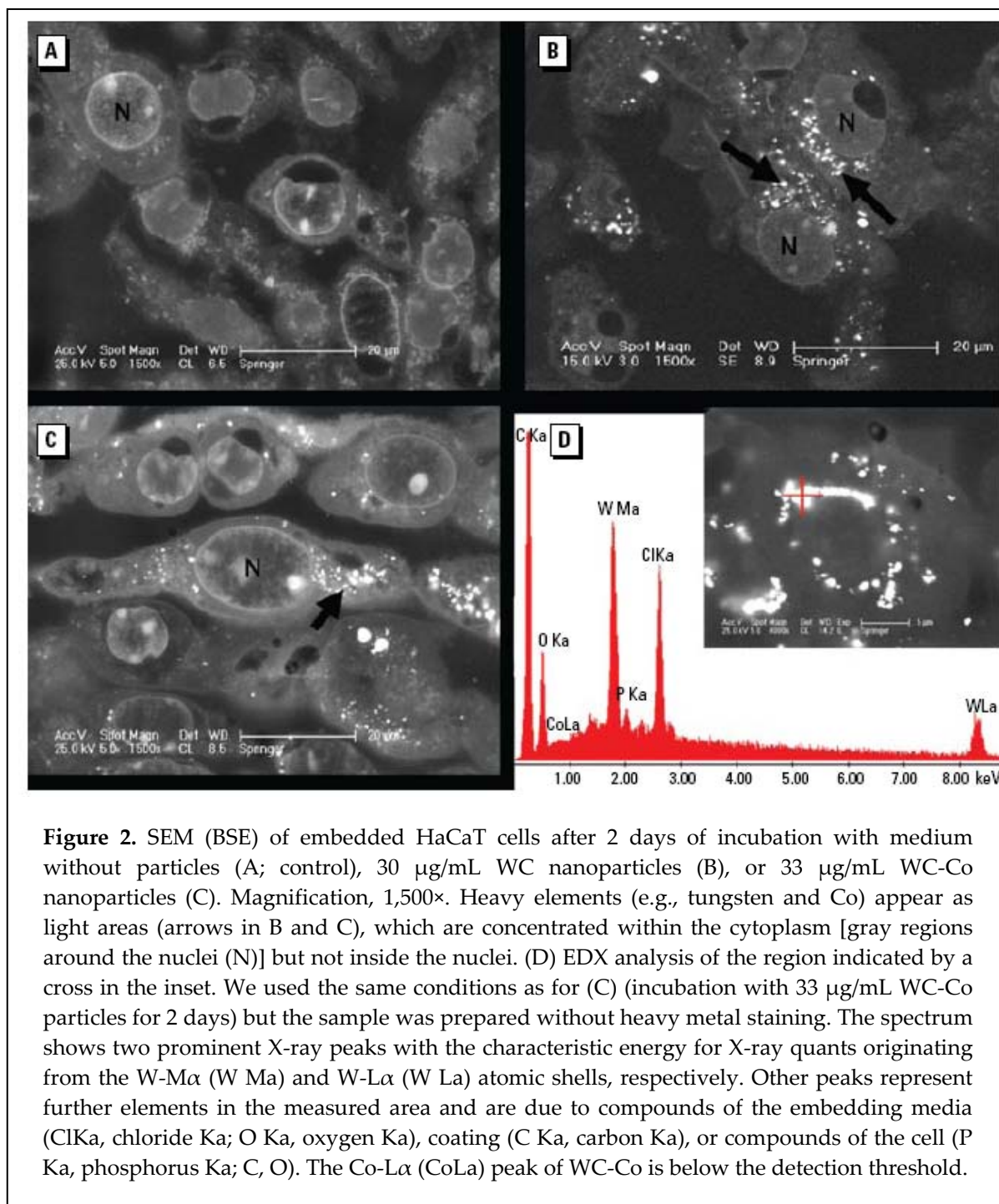


Figure 1. Effect of BSA in PBS and 5 % (v/v) FBS in DMEM on the stability of the WC (A) and WC-Co (B) particles ($10 \mu\text{g}/\text{mL}$) compared to protein-free PBS and DMEM. We found identical results for WC and WC-Co in HBSS (data not shown).

Uptake of particles by cells

To investigate whether WC or WC-Co nanoparticles are able to enter cells, we incubated HaCaT cells for 2 days with $30 \mu\text{g}/\text{mL}$ WC or $33 \mu\text{g}/\text{mL}$ WC-Co particles, respectively (Figure 2). Examination by SEM [back-scattered electron detector (BSE)] of epoxy-resin-embedded samples showed that particles and/or agglomerates with strong BSE signals were detectable in cells treated with WC particles (Figure 2B) and WC-Co particles (Figure 2C) but not in the control group (Figure 2A).



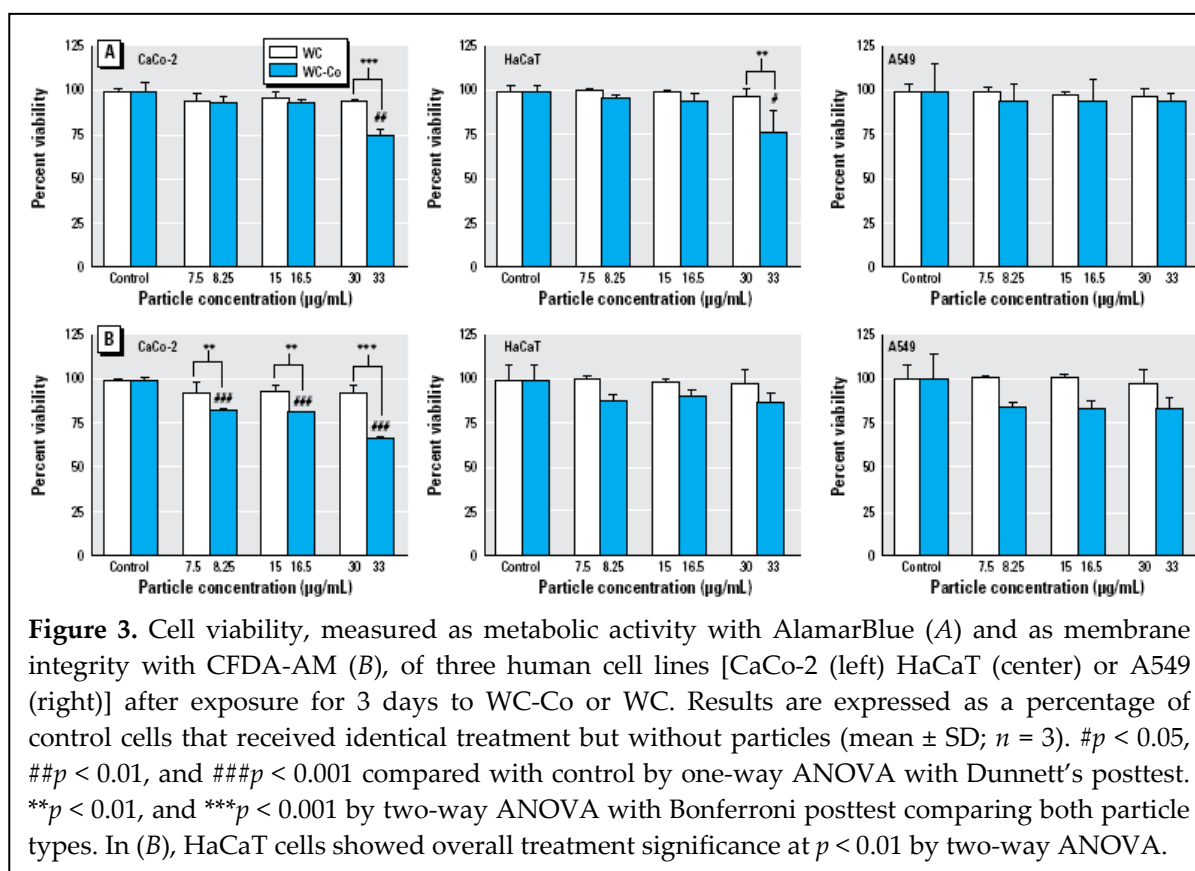
Furthermore, the BSE signals of the particles/agglomerates are visible within the cells, but no agglomerates or particles were detectable inside the nucleus. Additional elemental analysis with EDX of one of the strong BSE signals caused by particles/agglomerates revealed an X-ray energy peak that exclusively belonged to tungsten, thereby indicating WC (or WC-Co; Figure 2D). These observations clearly confirm that nano-sized WC and WC-Co particles (or agglomerates) are able to enter cells. We likewise observed this for a

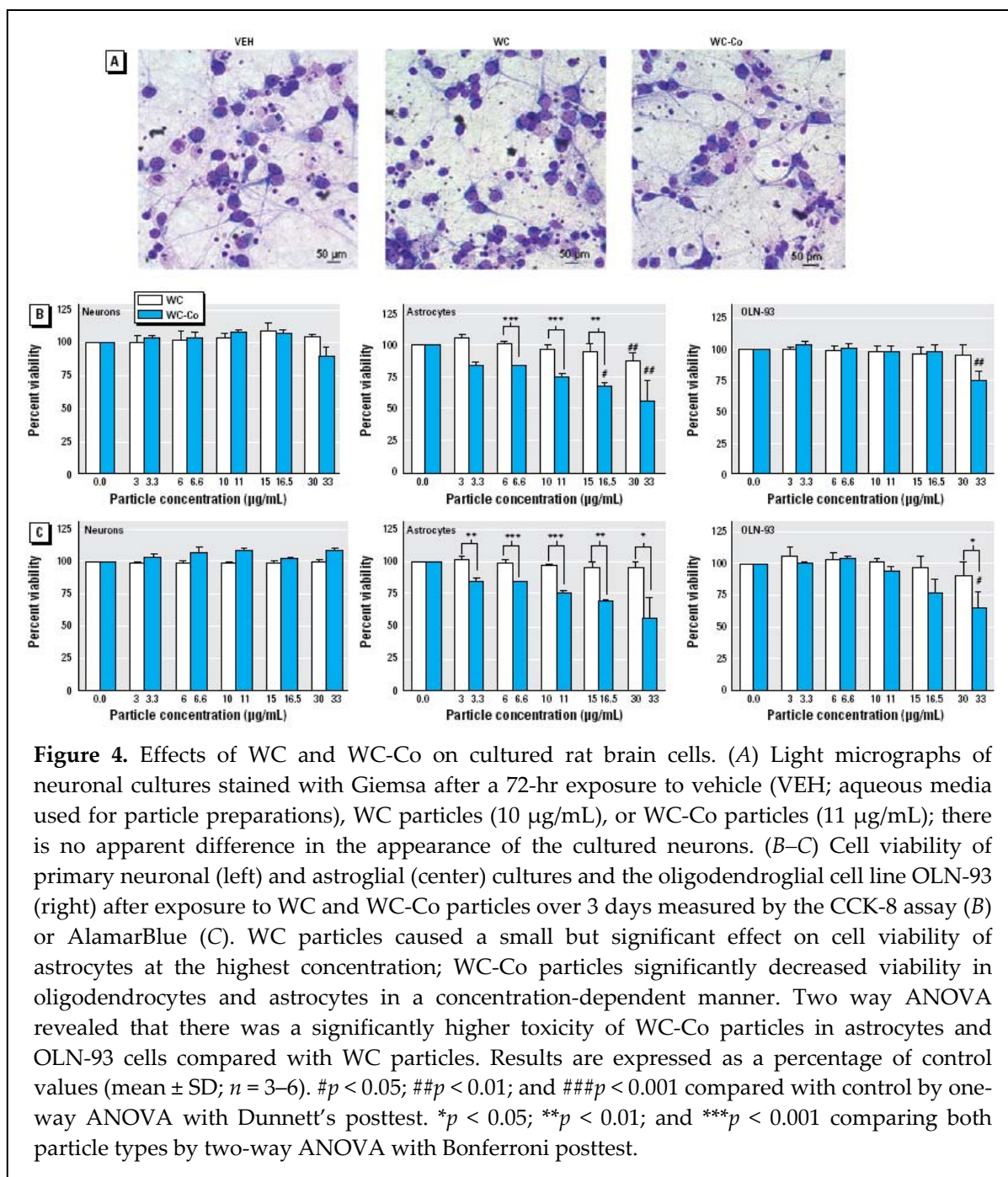
series of other cells, including lung cells (A549) and oligodendrocytes (OLN-93; data not shown).

Impact on cell viability

Particles

WC nanoparticles did not yield a toxic response up to 30 $\mu\text{g}/\text{mL}$ after 3 days of exposure in either of the human epithelial cell lines, the OLN-93 cell line, or the primary rat neuronal and astroglial cells (Figures 3 and 4). Exposure of the cell cultures to WC-Co elicited slight to substantial toxicity, with the order of sensitivity being primary astrocytes > intestinal cells (CaCo-2) > oligodendrocytes (OLN-93) > skin cells (HaCaT) > lung cells (A549) > primary neuronal cells (Figures 3 and 4). Comparison of the sensitivity of each cell line to WC and WC-Co particles over the tested concentration range by means of two-way ANOVA revealed that the addition of Co significantly increased toxicity of the particles for intestinal and skin epithelial cells as well as gliotoxicity (toxicity to astrocytes and oligodendrocytes).

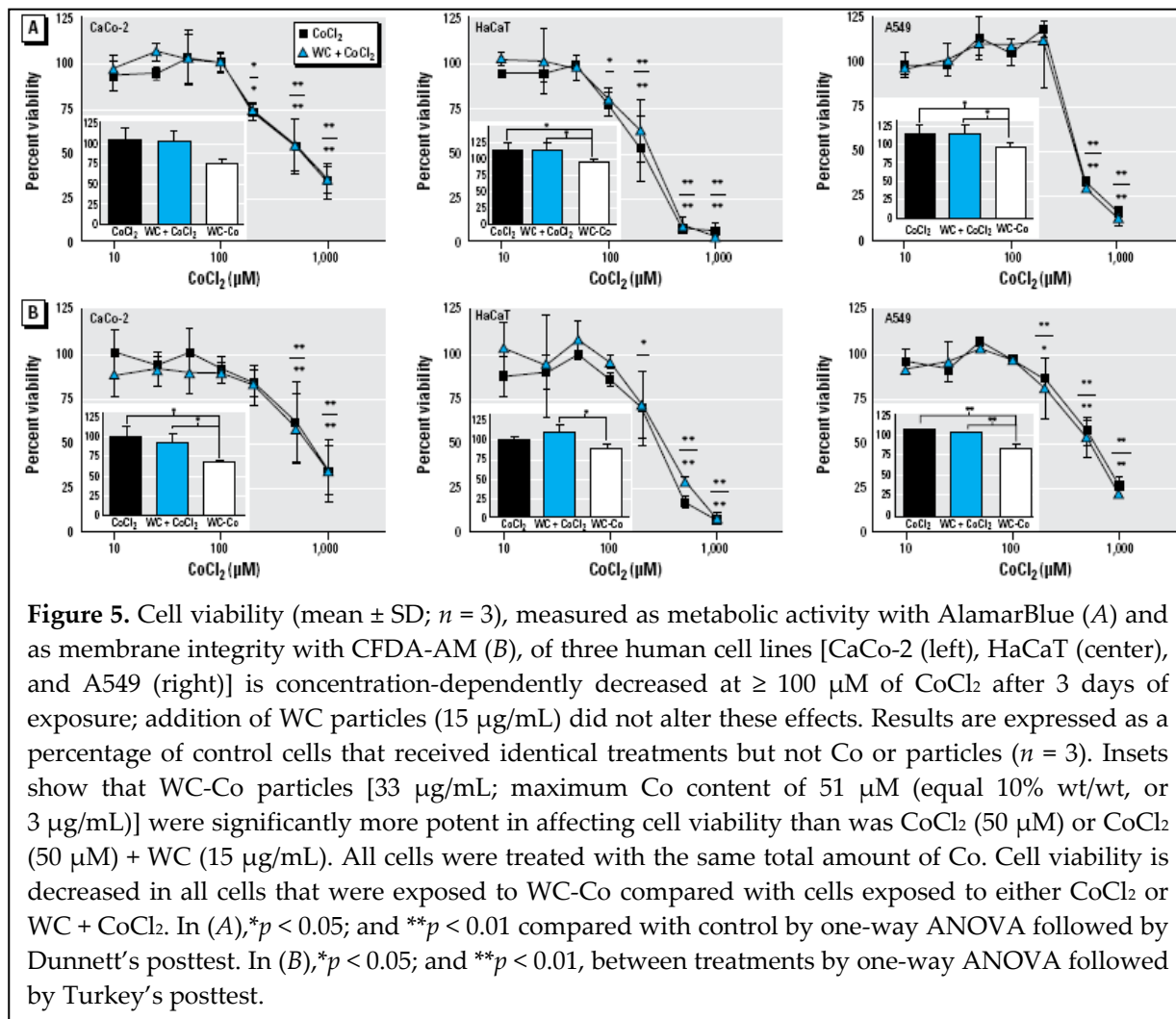




Role of Co ions in toxicity

To investigate whether the Co fraction of WC-Co alone accounts for the toxic effects, we performed experiments using CoCl₂. We found decreased viability of cells treated with CoCl₂ starting from a concentration of 100 µM for the human cell lines (Figure 5). For comparison, the maximum Co concentration in the highest tested WC-Co particle concentration (33 µg/mL) is 51 µM. When cells were exposed to this Co concentration together with WC particles, we likewise did not observe toxicity (Figure 5, insets). We

concluded that the Co fraction in the WC-Co particles alone could not account for the toxicity observed after treatment with WC-Co and that it is the combination of the particulate WC with Co that causes the cytotoxic effect (Figure 5, insets). We obtained similar results for the oligodendroglial cell line OLN-93 (data not shown).



Role of tungsten ions in toxicity

We tested tungsten salt ($\text{Na}_2\text{WO}_4 \cdot 2\text{H}_2\text{O}$) for its toxicity in OLN-93 cells and in astrocytes. We found no cytotoxicity of tungstate at the concentrations of 14 , 28 , and $42 \mu\text{M}$, which correspond to 9% , 18% , and 28% dissolved tungsten. Cytotoxicity became apparent only at tungsten salt concentrations $> 250 \mu\text{M}$, which exceeds the level of tungsten present in any of the particle exposure experiments [for an example, see Supplemental Material, Figure 3 (<http://www.ehponline.org/members/2008/0800121/suppl.pdf>)].

Discussion

Here we show that WC-Co nanoparticles can be toxic to mammalian epithelial, neuronal, and glial cells, whereas we detected no significant acute toxicity of WC nanoparticles in our test systems. Chemical–physical characterization confirmed that WC as well as WC-Co nanoparticles with an average diameter of 145 nm form a stable suspension in buffers that contain albumin and in cell culture media that contain serum. Cytotoxicity seen with WC-Co nanoparticles was higher than expected based on ionic Co content, indicating a qualitative cytotoxic effect of nano-sized particulate matter. Analysis by electron microscopy demonstrated the presence of WC nanoparticles within exposed mammalian cells.

Most of the chemical and physical parameters of WC and WC-Co nanoparticles are similar. Initial physical properties (χ_{PCS} , PDI, BET) and the behavior in the physiologic media are identical. Both nanoparticles show similar agglomeration kinetics in all tested physiologic media. Furthermore, agglomeration of the nanoparticles can be inhibited in the presence of BSA or FBS. Obviously, the protein BSA adsorbs on the particle surface and stabilizes the suspension (Cedervall et al. 2007, Schulze et al. 2008). This result is comparable with stabilization of fullerene (C60) nanoparticles in PBS induced by human serum albumin (Deguchi et al. 2007). This stabilizing effect seems to apply to chemically different nanoparticles. Whereas fullerene is a special carbon modification, WC is a nonoxide ceramic.

Ultrastructural analysis by electron microscopy revealed the presence of WC particles within exposed cells. The examination of the epoxy-resin–embedded samples with different SEM methods (BSE detector signal, EDX analysis) enabled us to identify both the position and the chemical composition of the particles within the cells. The absence of the peak for Co in the EDX spectra may be explained by the low amount [only 10 % (wt/wt) Co in WC-Co] and its tendency to dissolve. The lack of a Co peak may also be an example of possible artifacts that result from the extensive washing steps within the embedding procedure, which can reduce the EDX signal of Co below the detection threshold of the EDX detector. Nevertheless, the observations clearly confirm that nano-sized WC and WC-Co particles (or agglomerates thereof) are able to enter the cells. According to our findings, WC and WC-Co particles do not penetrate the nuclear membrane, because we

detected no nanoparticles within the nuclei. It is, however, possible that particles with a size below the resolution of the SEM (therefore undetectable) can pass through the nuclear membrane. So far, we are not able to propose a mechanism for uptake of nano-sized WC or WC-Co particles or agglomerates based on the SEM and EDX data shown here. Endocytosis is a possibility. Stearns et al. (2001) documented this mechanism for uptake of ultrafine titanium dioxide particles by A549 lung cells. In contrast to the studies by Lison and Lauwerys (1990), who observed uptake of micro-sized (1–4 μm) WC and WC-Co particles by mouse peritoneal and rat alveolar macrophages, the mammalian cells used here and by Stearns et al. (2001) are not primarily phagocytic cells.

Nano-sized WC-Co particles, but not Co or tungsten ions at concentrations equivalent to the particulate form, or WC nanoparticles alone, led to acute toxicity in most of the cell cultures studied. The fact that the enhanced toxicity occurred only for WC-Co nanoparticles and not for WC particles with added Co^{2+} underlines the role of the particulate form for the expression of toxicity. An enhanced cytotoxicity of WC-Co was first reported by Lison and Lauwerys (1990) based on micro-sized dust in macrophage cells and was likewise shown to depend on the particulate form of the WC-Co mixture (Lison & Lauwerys 1992). In light of the genotoxic and carcinogenic potential of Co-containing hard metal particles and free Co^{2+} ions (Lison et al. 2001, Beyersmann & Hartwig 2008), and the current efforts to improve material designs based on WC-Co nanostructures, further studies are warranted to investigate whether nano-level WC-Co particles elicit size-specific toxic effects.

The mechanism behind the increase in toxicity for nano-sized WC-Co particles is not yet understood, but experiments with hard metal alloys suggested that the association of Co and carbide particles represents a specific toxic entity that produces large amounts of ROS. When both materials in particulate form are in close contact, electrons are transferred from Co to the surface of WC. This process leads to the production of activated (reduced) oxygen, and subsequently, oxidized Co (Co^{2+}) passes into solution (Lison et al. 1995, Gries & Prakash 2007). The additional toxic effect of WC-Co may then be due to a combination of two known mechanisms of Co toxicity: cell damage induced by ROS derived from metallic Co (Hoet et al. 2002), and subsequent inhibition of DNA repair mechanisms by the Co^{2+} ions generated in this process (Kasten et al. 1997). In the rat, acute lung toxicity of a mixture of WC and Co was more pronounced than toxicity of

individual components. The amount of excreted Co was higher in WC-Co-exposed animals compared with an equivalent amount of Co. This may be due to an increased bio-availability of Co from WC-Co (Lasfargues et al. 1992).

For nano-sized particles, however, an additional mechanism proposed by Limbach and colleagues may be relevant (Limbach et al. 2007). They suggested a “Trojan horse”-like uptake of toxic ion with the metallic nanoparticle acting as carrier. In cases of toxic ions, the particle helps to cross the cell membrane barrier, thereby enhancing toxicity of the material because the damaging agent is delivered directly into the cell. This mechanism is likely to be involved with WC-Co-mediated toxicity, because a 3-fold higher Co uptake from the WC-Co mixture compared with Co metal powder alone could be demonstrated (Lison & Lauwerys 1990).

In the *in vitro* experiments, we observed that acute toxicity of WC-Co nanoparticles differed depending on the cell culture systems. Most sensitive were astrocytes and colon epithelial cells. Oligodendrocytes, human keratinocytes, and lung epithelial cells showed decreased viability at the highest concentration of WC-Co applied. Interestingly, neurons were resistant to acute application of WC or WC-Co nanoparticles. Little is known so far about the differential sensitivity of the cell lines, for example, with regard to oxidative stress. However, the CaCo-2 cell line appeared more vulnerable to oxidative stress and DNA damage due to a cyanobacterial toxin than were a human astrocytoma and a human B-lymphoblastoid cell line (Zegura et al. 2008). Differences in sensitivity of brain cells to oxidative stress have also been reported. Feeney and colleagues used organotypic hippocampal slices to study toxicity of hydrogen peroxide and found that astrocytes were more sensitive to oxidative stress than were neurons (Feeney et al. 2008). In addition, Dringen and colleagues compared peroxide metabolism in cultured brain cells (astrocytes, oligodendrocytes, microglia, and neurons) and found that cultured oligodendrocytes disposed of the peroxide quicker than did the other neural and glial cell cultures (Dringen et al. 2005). These findings suggest that different brain cells show variable efficiency in dealing with oxidative stress, with the observed susceptibilities conforming with the results of our study, which demonstrate that astrocytes are the most vulnerable brain cells to toxicity of WC-Co. These results indicate that vulnerability of different tissues to WC-Co nanoparticles will differ *in vivo*, as well. If WC-Co nanoparticles were to reach all organs to an equal extent, the highest toxicity would be expected within the nervous

system because astrocytes were most vulnerable. Although neurons were not susceptible to acute toxicity of WC-Co nanoparticles, ongoing studies suggest that neurons react with increased production of ROS (data not shown). Thus, although we did not observe acute neuronal loss, it is possible that chronic exposure of neurons, which are nondividing, long-living cells, may eventually result in slow degeneration *in vivo*. Also, because astrocytes were very susceptible and because there is close interaction between astrocytes and neurons within the brain, secondary effects in neurons can be expected. Particulate matter has been shown to penetrate into the central nervous system of mammals and cause neurodegeneration (Campbell et al. 2005, Peters et al. 2006).

Conclusions

Additional research is needed to evaluate mechanisms of acute toxicity of Co-doped WC nanoparticles in mammalian cells and evaluate biochemical pathways that account for differences in susceptibility of cell types. Our approach of using multiple cell cultures and cytotoxicity end points has proven valuable in revealing the combinatorial nanoparticle-mediated effects important for hazard assessment. An important next step is to take the exposure concentrations *in vitro* and *in vivo* into account to identify whether the potential target sites described by us are indeed prone to significant nanoparticle exposure. *In vivo* toxicology will thus help address whether systemic toxicity and neurotoxicity may occur after exposure to WC-Co.

Chapter 4

Agglomeration of tungsten carbide nanoparticles in exposure medium does not prevent uptake and toxicity toward a rainbow trout gill cell line

Aquatic Toxicology 2009, **93**: 91–99

Dana Kühnel^a, Wibke Busch^a, Tobias Meißner^b, Armin Springer^c, Annegret Potthoff^b, Volkmar Richter^b, Michael Gelinsky^c, Stefan Scholz^a, Kristin Schirmer^{d,e}

^aDepartment of Bioanalytical Ecotoxicology, Helmholtz-Centre for Environmental Research Leipzig (UFZ), Permoserstr. 15, 04318 Leipzig, Germany; ^bFraunhofer-Institute for Ceramic Technologies and Systems (IKTS), Winterbergstr. 28, 01277 Dresden, Germany; ^cMax Bergmann Centre of Biomaterials, Technical University Dresden, Budapester Strasse 27, 01069 Dresden, Germany; ^dEawag, Swiss Federal Institute of Aquatic Science and Technology, 8600 Dübendorf, Switzerland; ^eETH Zürich, Institute of Biogeochemistry and Pollutant Dynamics, 8092 Zürich, Switzerland

Abstract

Due to their increased production and use, engineered nanoparticles are expected to be released into the aquatic environment where particles may agglomerate. The aim of this study was to explore the role of agglomeration of nanoparticles in the uptake and expression of toxicity in the rainbow trout (*Oncorhynchus mykiss*) gill cell line, RTgill-W1. This cell line was chosen as model because it is known to be amenable to culture in complete as well as greatly simplified exposure media. Nano-sized tungsten carbide (WC) with or without cobalt doping (WC-Co), two materials relevant in the heavy metal industry, were applied as model particles. These particles were suspended in culture media with decreasing complexity from L15 with 10 % fetal bovine serum (FBS) to L15 to L15/ex, containing only salts, galactose and pyruvate of the complete medium L15. Whereas the serum supplement in L15 retained primary nanoparticle suspensions, agglomerates were formed quickly in L15 and L15/ex. Nevertheless, scanning electron microscopy (SEM) coupled with energy dispersive X-ray (EDX) elemental analysis revealed an uptake of both WC and WC-Co nanoparticles into RTgill-W1 cells irrespective of the state of agglomeration of nanoparticles. The localisation seemed to be restricted to the cytoplasm, as no particles were observed in the nucleus of cells. Moreover, reduction in cell viability between 10 and 50 % compared to controls were observed upon particle exposure in all media although the pattern of impact varied depending on the medium and exposure time. Short-term exposure of cells led to significant cytotoxicity at the highest nominal particle concentrations, irrespective of the particle type or exposure medium. In contrast, long-term exposures led to preferential toxicity in the simplest medium, L15/ex, and an enhanced toxicity by the cobalt-containing WC nanoparticles in all exposure media. The composition of the exposure media also influenced the toxicity of the cobalt ions, which may dissolve from the WC-Co nanoparticles, with cells reacting much more sensitively toward cobalt ions in the absence of FBS. However, the toxicity observed by ionic cobalt alone did not explain the toxicity of the WC-Co nanoparticles, suggesting that the combination of metallic Co and WC is the cause of the increased particle toxicity of WC-Co. Taken together, our findings indicate that minimal exposure media can lead to rapid agglomeration of nanoparticles but that agglomeration does not prevent uptake into cells and the expression of toxicity.

Background

The production of nanomaterials is increasing worldwide. Many applications already contain nanoparticles and new applications are constantly arising. There is a general concern about potential hazards posed by released nanoparticles not only to humans but also to organisms in the environment. One important path of release is into aquatic systems, either during production processes, during transport or by direct or indirect disposal of consumer products upon use (The Royal Society and the Royal Academy of Engineering 2004). Little knowledge thus far exists regarding the concentrations and behaviour of engineered nanoparticles in surface water (Moore 2006, Handy et al. 2008). Behaviour depends on the composition of water constituents. For example, particles may agglomerate and interactions with organic matter or other substances may occur (Baun et al. 2008). Because the behaviour of nanoparticles in the aquatic environment ultimately affects exposure of organisms and thus their potential ecotoxicity, knowledge about behaviour of nanoparticles is an important prerequisite for risk assessment.

Several *in vivo* and *in vitro* studies on the toxicology of nanoparticles with a number of aquatic organisms have been conducted, including studies with focus on fish or isolated fish cells (e.g. (Zhu et al. 2006, Federici et al. 2007, Smith et al. 2007, Griffitt et al. 2008, Vevers & Jha 2008)). It remains unknown; however, to what extent the toxic potential of the nanoparticles is influenced by agglomeration. This uncertainty arises because comparative test systems, where uptake and toxicity can be studied with or without agglomeration of nanoparticles, have not yet been proposed. One hypothesis is that agglomerates are too large to be taken up by organisms or cells. On the other hand, *in vitro* studies often rely on medium containing a high percentage of serum, which has been found to stabilise several different types of nanoparticles as primary particle suspensions (Deguchi et al. 2007, Murdock et al. 2008, Bastian et al. 2009). In order to shed light on the role of agglomeration in the uptake and expression of toxicity of nanoparticles, we decided to employ a fish cell line that is amendable to exposure in media with differing complexity. This cell line was exposed to two well-characterised engineered nanoparticles, tungsten carbide (WC) and tungsten carbide cobalt (WC-Co) (Bastian et al. 2009).

Tungsten carbide-based materials are used in hard metal industries for the production of extremely hard and wear resistant tools. Usage of WC and WC-Co at the nano-size is very attractive because the strength of the resulting tool is increased with smaller initial particle size. Previous studies using μm -sized particles have indicated a lack of toxicity for WC particles and a hazardous potential for cobalt metal particles toward macrophages derived from mammals (Lison & Lauwerys 1992). WC-Co, a combination of both materials, features an enhanced toxicity compared to cobalt alone (Lison & Lauwerys 1990). A similar combinatorial effect has recently been demonstrated for nano-sized tungsten carbide and tungsten carbide cobalt in different mammalian cells (Bastian et al. 2009). The International Agency for Research on Cancer (IARC) has classified cobalt as 'possibly carcinogenic' and tungsten carbide cobalt as 'probably carcinogenic' to humans (International Agency for Research on Cancer 2006). Exposure to these particles mostly occurs via the workplace. For example, an increased risk of lung cancer has been reported for workers exposed to WC-Co dusts ("hard-metal lung") (Moulin et al. 1998). However, levels of airborne cobalt and tungsten carbide can be high, particularly close to production facilities and deposition or release into the aquatic environment may occur. Importantly, this choice of particles allowed us to study the role of agglomeration in exposure and toxicity for chemically and structurally similar, but toxicologically different, nanoparticles.

In a combined approach including particle characterisation, visualisation and quantification of cytotoxic effects we attempted to assess the potential impact of nano-sized WC and WC-Co on fish cells. Fish may be exposed to water-borne nanoparticles via skin, gill and intestine. Gills as respiratory organs of fish represent a first contact site of ambient water and the blood. Gills of rainbow trout and zebrafish were shown to be primary target organs of nanoparticle exposure (Federici et al. 2007, Griffitt et al. 2007). Therefore, the rainbow trout gill cell line, RTgill-W1 (Bols et al. 1994), a frequently used model in environmental toxicology (Bols et al. 2005), was chosen as the *in vitro* model. Further, the RTgill-W1 cell line was particularly valuable for this study because it is known for its ability to withstand exposure to very simple culture media (Schirmer et al. 1997, Dayeh et al. 2002) or even water (Lee et al. 2006, Lee et al. 2009).

Materials and Methods

Preparation and characterisation of particle suspensions

For physico-chemical characterisation, particle suspensions with a concentration of 100 µg/ml were prepared from tungsten carbide (WC) and tungsten carbide cobalt (WC-Co; 10 mass% cobalt content) powders. The preparation and characteristics of the resulting suspensions were previously described in detail (Bastian et al. 2009). Brunauer–Emmett–Teller (BET) specific surface area was 6.9 m²/g for WC and 6.6 m²/g for WC-Co. Particle sizes calculated from BET values, d_{BET} were 56 and 62 nm, respectively. The mean particle size x_{PCS} of dispersed particles was measured by dynamic light scattering (DLS) and was 145±5 nm for both WC and WC-Co (DIN ISO 13321 2004-10). The Zeta potential was -35 mV for WC and -50 mV for WC-Co. Particle size distribution and morphology were similar for both nanomaterials. Dissolution of metal ions from particle suspensions (assessed 1 week after preparation) was 6 % of tungsten for WC and 15 % of tungsten and 76 % of cobalt for WC-Co (Bastian et al. 2009).

Cell culture experiments were based on nanoparticle stock solutions of 300 µg/ml WC (in water) and 330 µg/ml WC-Co (in 0.03 % sodium polyphosphate, see (Bastian et al. 2009)). The latter concentration was chosen to ensure an equal amount of WC in both suspensions. Characterisation of particle suspensions was carried out in L15 (L15, Gibco, Karlsruhe, Germany) with 10 % FBS (FBS, Sigma–Aldrich, Seelze, Germany), L15 and L15/ex (for composition see below). Particle suspensions were sterilised by autoclaving and treated for 10 min with ultrasound (Merck Eurolab, Darmstadt, Germany) prior to treatment of cells to ensure optimal dispersal. Between experiments, autoclaved suspensions were stored at 4 °C for a maximum of 6 weeks.

Preparation of cobalt chloride solutions

Cobalt chloride (Fluka/Sigma–Aldrich, Seelze, Germany) solutions were prepared in distilled water in concentrations of 20 and 10 mM. Stock solutions were sterilised by autoclaving. All concentrations used in cell assays were obtained by serial dilution of the stock solutions with cell culture grade water (PAA Laboratories GmbH, Pasching, Austria) under sterile conditions.

RTgill-W1 cell culture and exposure of cells

The permanent, epithelial-like cell line, RTgill-W1, was established from primary cell cultures of rainbow trout (*Oncorhynchus mykiss*) gills (Bols et al. 1994). RTgill-W1 cultures were cultivated in Leibovitz's L15 medium (L15, Gibco, Karlsruhe, Germany) supplemented with 10 % fetal bovine serum (FBS, Sigma–Aldrich, Seelze, Germany) and 1 % penicillin/streptomycin (Sigma–Aldrich, Seelze, Germany), in 75 cm² flasks (TPP, Trasadingen, Switzerland). Cells were maintained at 19 °C in normal atmosphere and subcultured once a week. Confluent flasks were washed two times with Versene (Invitrogen/Gibco, Germany) and cells detached by trypsin (0.25 % in phosphate-buffered saline, Biowest, Germany). Cells were counted using a hemocytometer and seeded at densities of 6×10⁵ cells/well in a final volume of 2 ml in 6-well plates and 5×10⁴ cells/well in a volume of 0.5 ml in 24- and 48-well plates. Cells were allowed to grow for 24 h prior to exposure in L15 with 10 % FBS. Growth medium was then exchanged and cells were exposed for different time periods (3 h up to 3 days) to nanoparticles, cobalt chloride or to a mixture of WC particles and cobalt chloride at 19 °C in the dark. Experiments to assess cell viability after WC and WC-Co exposure were performed in 24-well plates (TPP, Trasadingen, Switzerland).

For exposures prior to electron microscopy, 6-well plates (Falcon, BD, Heidelberg, Germany) were used. Cell viability assays with cobalt chloride and cobalt chloride combined with WC nanoparticles were done in 48-well plates (Falcon, BD, Heidelberg, Germany). Exposures were performed in complete media L15 with 10 % FBS, L15 without FBS and in L15/ex. L15/ex contains salts, galactose and pyruvate of the L15 medium but no vitamins and amino acids. It was prepared according to Schirmer et al. (1997). For exposure of cells, a volume of 10 % treatment solution (v/v) was added to cell culture medium. For nanoparticles, all concentrations used in cell assays were obtained by dilution of stock suspensions with water or sodium polyphosphate (Merck KGaA, Darmstadt, Germany) buffer to reach final concentrations of 7.5, 15 and 30 µg/ml for WC and 8.25, 16.5 and 33 µg/ml for WC-Co. For cobalt chloride, concentrations of 10, 25, 50, 100, 200, 500, 1000 and 2000 µM (corresponding to 0.6–118 µg/ml) were prepared. Co-exposure of cobalt chloride and WC was done by adding 5 % cobalt chloride solution (v/v) and 5 % 30 µg/ml WC suspensions (v/v) to the cell culture medium to reach final

concentrations of 10, 25, 50, 100, 200, 500, 1000 and 2000 μM cobalt chloride and 15 $\mu\text{g/ml}$ WC. Cobalt chloride stock solutions were stored at 4 °C.

Cell viability assays

To monitor cell viability, two fluorescent indicator dyes were used as previously described (Schirmer et al. 1997). Alamar Blue (Biosource, Belgium) is a non-fluorescent dye which is reduced by cellular oxidoreductases to a fluorescent product, conversion to the fluorescent product indicating cellular metabolic activity. The 5-carboxyfluorescein diacetate acetoxyethyl ester (CFDA-AM, Molecular Probes, USA) indicator dye is an esterase substrate that can be converted by non-specific esterases of living cells from a non-polar, non-fluorescent substance to a polar, fluorescent dye, carboxyfluorescein indicating plasma membrane integrity. To determine the impact of nanoparticles and cobalt on these two parameters, exposed cells were first washed once with phosphate buffered saline (PBS). A mixture of both dyes was prepared by combining 5 % (v/v) of Alamar Blue and 4 μM CFDA-AM in PBS. Aliquots of 500 and 200 μl /well were added to the cells in 24- and 48-well culture plates, respectively. After 30 min of incubation, fluorescence was quantified with the GENios Plus fluorescence reader (Tecan, Crailsheim, Germany). Excitation/emission wavelengths were 530/595 nm for Alamar Blue and 493/541 nm for CFDA-AM.

Electron microscopy

A 2-day exposure of cells prior to preparation for electron microscopy was done as described above. After exposure, cells were washed twice with Versene and scraped off the cell culture surface with a cell scraper (TPP, Trasadingen, Switzerland). The cell suspension was transferred into 1.5 ml tubes (Eppendorf, Hamburg, Germany) and centrifuged at 800 \times g for 3 min. The supernatant was removed and the cell pellet resuspended in 2 % glutaraldehyde (Serva, Heidelberg, Germany) in PBS for fixation. After incubation at 4 °C for 4 h, the glutaraldehyde solution was changed and cells were fixed for a further 24 h. Cells were then washed twice with PBS and stored at 4 °C in PBS until further processing for electron microscopy. For scanning electron microscopy (SEM) investigations of the block face, samples were post-fixed with 1 % osmium tetroxide (Roth, Karlsruhe, Germany), dehydrated in a graduated series of acetone (including a

staining step with 1 % uranylacetate (Plano GmbH, Wetzlar, Germany)) and embedded in epoxy resin according to Spurr (1969). Samples were cut on a Leica EM UC6 ultramicrotome (Leica, Vienna, Austria), equipped with a diamond knife (Diatome, Biel, Switzerland), carbon coated and analysed with a Philips XL 30 ESEM (Philips, Eindhoven, Netherlands). EDX-analysis was done with an energy dispersive analysis of X-rays (EDAX) detecting unit and EDAX software (EDAX INC, Mahwah, USA).

Statistical analyses

Exposure experiments were performed in triplicate or quadruplicate wells in three to five independent tests. Control wells without cells were included to identify a potential interference of nanoparticles with the fluorescence of the indicator dyes. No such effect was found in any of the treatments. Fluorescent units obtained in the cell viability assays were converted to percent viability of control cells and are presented as mean \pm SD. Statistical differences were analysed with one-way ANOVA followed by Dunnett's post-test (treatment vs. control) or Tukey's post-test (treatment vs. treatment) using GraphPad Prism software (GraphPad Prism version 4.00 for Windows, GraphPad Software, San Diego California USA, www.graphpad.com). Graphs were created with GraphPad Prism as well. Values of $p < 0.05$ were considered statistically significant.

Results

Particle behaviour in cell culture media

In order to characterise physical–chemical properties of WC and WC-Co nanoparticles under cell culture conditions, particle size distribution and zeta potential in L15 with 10 % FBS, L15 without FBS and L15/ex were assessed. The WC and WC-Co particles behaved similarly, but media composition significantly influenced particle behaviour (Fig. 1). In complete medium consisting of L15 supplemented with 10 % FBS, WC and WC-Co nanoparticles retained a constant particle size x_{PCS} of 145 ± 5 nm over an observation period of 60 min (Fig. 1). In contrast, WC and WC-Co particles agglomerated after addition to L15 without FBS or the minimal medium L15/ex. Starting from an average size of 145 ± 5 nm both types of particles formed agglomerates within 30 min. The size of agglomerates at this time point was approximately 400 for WC and 350 nm for WC-Co (Fig. 1), after which the measurement in L15 and L15/ex was stopped because particle size distribution became too broad to properly determine the size of single particles and because of resulting sedimentation.

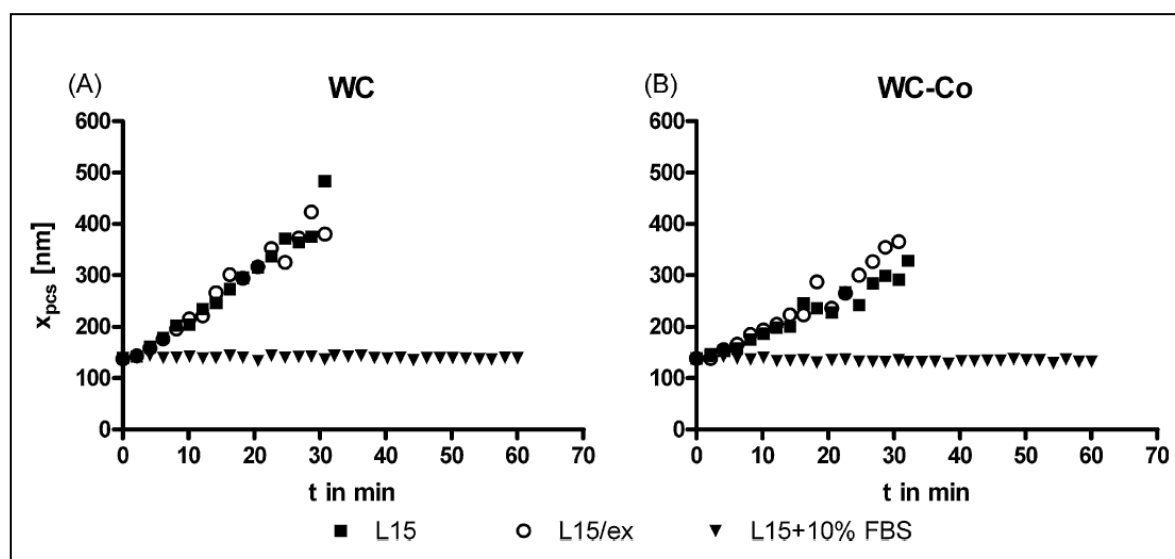


Figure 1. Agglomeration behaviour of tungsten carbide (WC) (A) and tungsten carbide cobalt (WC-Co) (B) nanoparticles in L15 + 10 % FBS (black triangles), L15 (black squares) and L15ex (white circles) depends on the composition of media with the presence of fetal bovine serum (FBS) preventing agglomeration as indicated by a constant particle size of 145 ± 5 nm. After a measurement period of 30 min, nanoparticle size distribution in both L15 and L15/ex broadens and sedimentation of particles occurs. Therefore, measurement in L15 and L15/ex was stopped after 30 min. x_{PCS} was determined by dynamic light scattering (DLS).

Uptake and localisation of particles within cells

Scanning electron microscopy (SEM) in combination with a back scattered electron detector (BSE) revealed particle agglomerates with strong BSE signals in both WC and WC-Co nanoparticles exposed RTgill-W1 cells, but not in the control group without particles. Irrespective of the exposure media, particles and agglomerates were detectable in the cytoplasm but not in the nucleus of exposed cells (examples in Fig. 2). Measurement of particle sizes revealed the presence of large agglomerates with diameters of around 1 μm but also of smaller agglomerates or particles with diameters below 300 nm. Additional elemental analysis of the observed agglomerates by energy dispersive X-ray spectroscopy (EDX) showed an X-ray energy peak belonging exclusively to tungsten (W), thus confirming the presence of WC or WC-Co in the cells (see spectra in Fig. 2B and C). EDX spectra for control cells revealed no peaks for tungsten. These observations clearly confirm that nano-sized WC or WC-Co particles (or agglomerates) were able to enter RTgill-W1 cells and uptake occurred, irrespective of exposure medium and agglomeration status of nanoparticles. In WC-Co nanoparticles exposed cells, no signal could be obtained for cobalt, which was not unexpected because the initial cobalt content in WC-Co is 10 % and a significant portion may dissolve either during cell exposure or preparation of samples for SEM. Additionally, the cobalt signal is merged with the background scatter of the other elements present in the biological sample and is, therefore, not detectable. Analysis of the dry, unsuspended WC-Co powder showed a clear peak for cobalt, indicating that the initial cobalt content of the powder was above the detection limit (data not shown).

Viability of RTgill-W1 cells after exposure to nanoparticles in the different media

Exposure to nanoparticles led to significant reductions of cell viability between 10 and 50 % relative to controls, but the pattern of impact varied depending on exposure media and time. After 3 h of incubation, an impairment of cell viability was observed for both nanomaterials in all exposure media as indicated by a significant reduction of metabolic activity (Alamar Blue) and membrane integrity (CFDA-AM) (Fig. 3). This impairment was consistently observed for the highest exposure concentrations. Dose–response relationships were also found for exposure of cells toward WC particles in L-15, particularly in the absence of FBS.

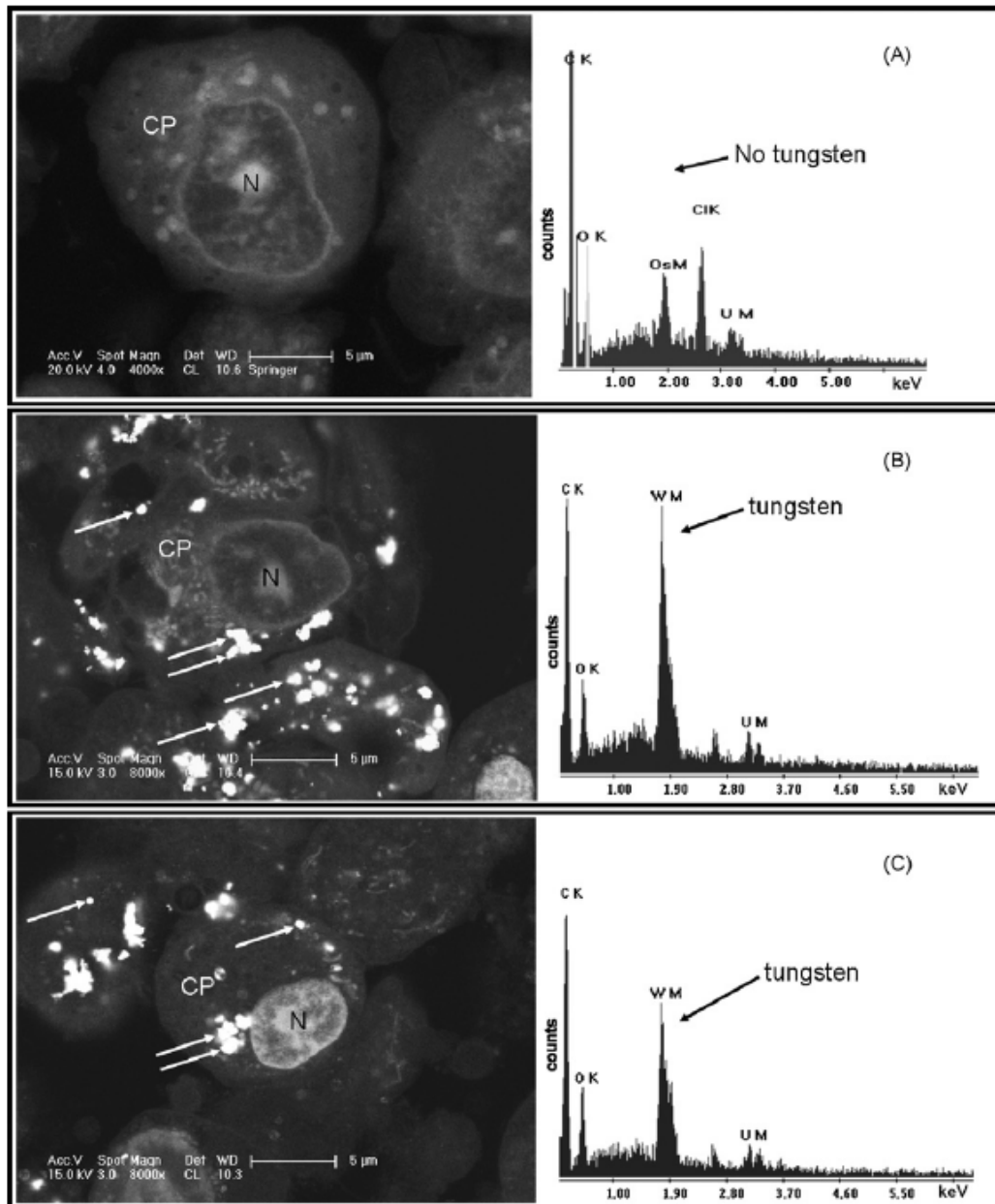


Figure 2. SEM micrographs of sections of embedded RTgill-W1 cells after 2 days of incubation with (A) medium without nanoparticles (control), (B) 30 $\mu\text{g/ml}$ WC nanoparticles in L15 with 10 % FBS and (C) 33 $\mu\text{g/ml}$ WC-Co nanoparticles in L15/ex. On the left-hand side BSE detector pictures at a magnification of 4000x and 8000x, respectively are shown, on the right-hand side the corresponding EDX spectra. Heavy elements like W or Co appear as light areas in BSE detector pictures. Control cells (A) do not contain nanoparticles whereas cells treated with 30 $\mu\text{g/ml}$ WC (B) and 33 $\mu\text{g/ml}$ WC-Co (C) show primary particles as well as particle agglomerates in the cytoplasm (arrows, CP) irrespective of exposure media. No particles were observed in nuclei (N). EDX analysis of intracellular particles demonstrated strong X-ray energy peaks for tungsten (W) (arrows, B, C); control cells (A) do not contain tungsten.

A reduction in cell viability at the highest exposure concentration occurred only in L15 with 10 % FBS when cells were exposed for 3 days (Fig. 4). A reduction was observed for both particle types but was greater for particles containing cobalt. Surprisingly, exposure of cells toward WC particles in L-15 led to some stimulatory effects. U-shaped dose-response curves were seen for WC-Co exposures in L15 and L15/ex, although the effect was not significant in L15. The strongest toxic effect was observed for 16.5 $\mu\text{g/ml}$ WC-Co when applied in L15/ex.

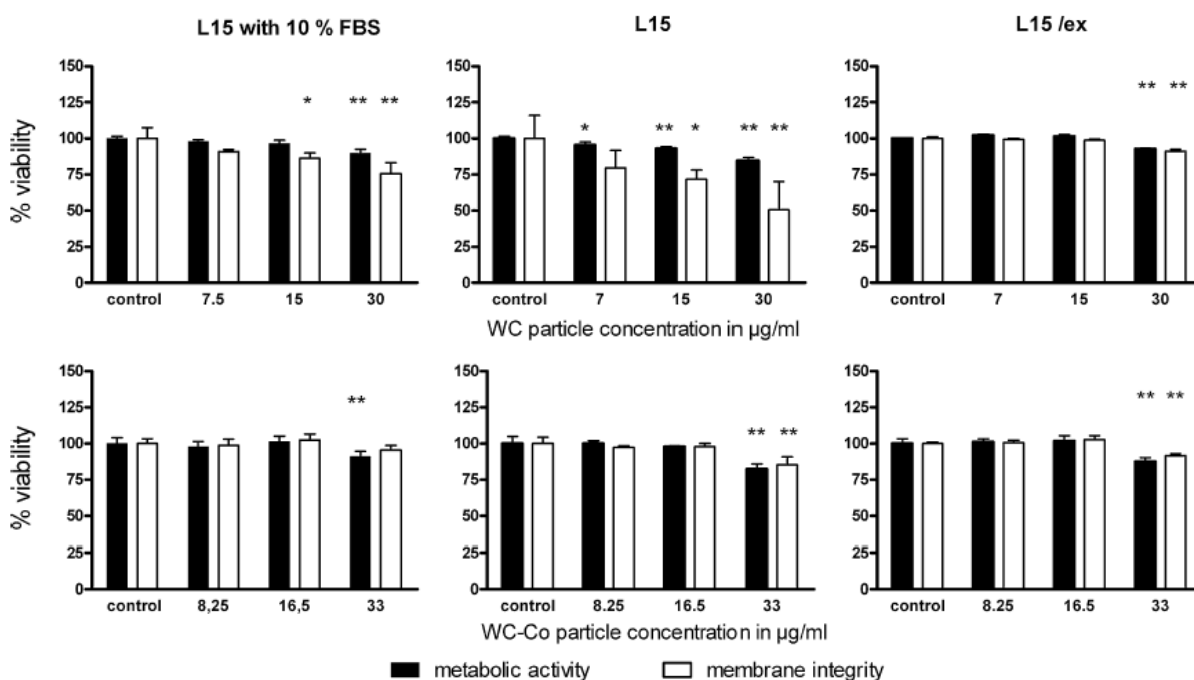


Figure 3. Viability of RTgill-W1 cells upon exposure to WC and WC-Co in L15 with 10 % FBS, L15 and L15/ex for 3 h. Cell viability was measured with Alamar Blue (black bars) and CFDA-AM (white bars). Results are expressed as a percentage of the fluorescence readings in control wells. Each bar represents the mean \pm SD of three to five independent experiments (triplicate or quadruplicate wells per experiment). Significant differences compared to controls are indicated by * $p < 0.05$; ** $p < 0.01$ and were calculated with one-way ANOVA and Dunnett's post-test.

Influence of cobalt ions on viability of RTgill-W1 cells in the different media

From the particle characterisation data it was known that a significant portion of the cobalt contained in WC-Co nanoparticles was dissolved. Hence, cells exposed to WC-Co not only encounter nanoparticles, but also a substantial amount of cobalt ions. Part of the toxic effect of WC-Co particles on RTgill-W1 cells may therefore be due to the presence of dissolved cobalt ions. To address this question, RTgill-W1 cells were incubated in the presence of CoCl_2 for 3 days.

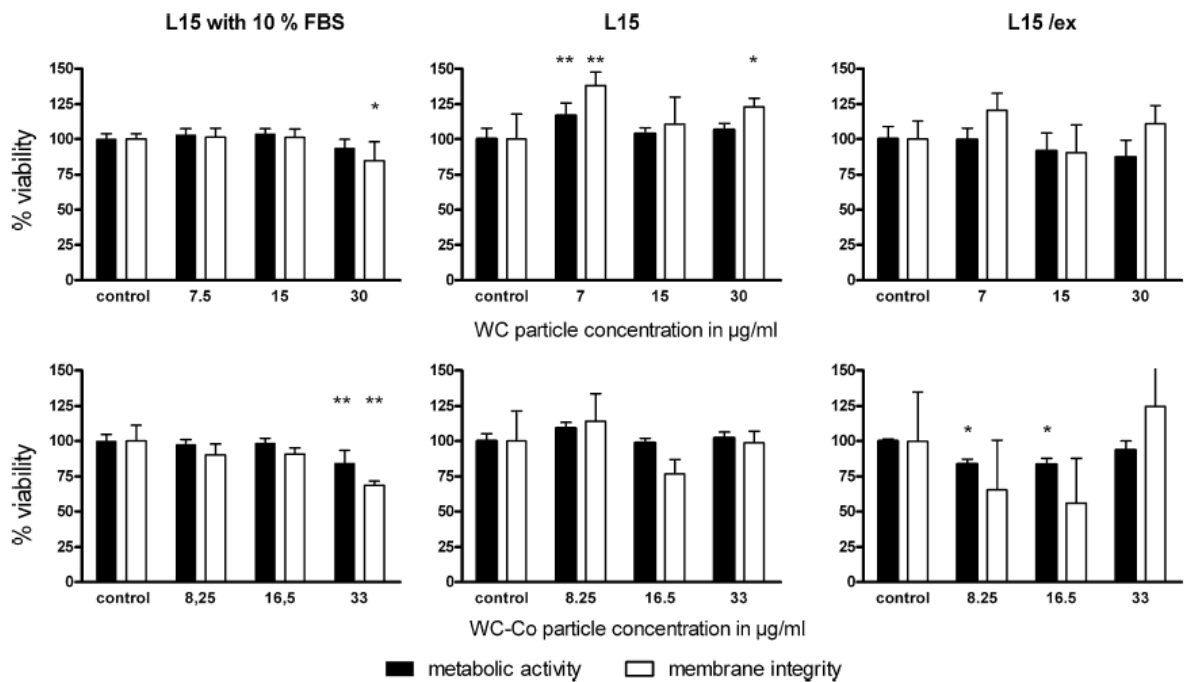


Figure 4. Viability of RTgill-W1 cells upon exposure to WC and WC-Co in L15 with 10 % FBS, L15 and L15/ex for 3 days. Cell viability was measured with Alamar Blue (black bars) and CFDA-AM (white bars). Results are expressed as a percentage of the fluorescence readings in control wells. Each bar represents the mean \pm SD of three to five independent experiments (triplicate or quadruplicate wells per experiment). Significant differences compared to controls are indicated by * $p < 0.05$; ** $p < 0.01$ and were calculated with one-way ANOVA and Dunnett’s post-test.

As illustrated in Fig. 5, cobalt ions led to a significant impact on cell viability in all three exposure media, but much lower cobalt concentrations were able to elicit toxicity in the absence of serum. Yet, in no case did the potential maximum cobalt ion concentration from dissolution of WC-Co particles elicit a significant loss of cell viability (respective concentration, 50 μ M, is marked by circles in Fig. 5).

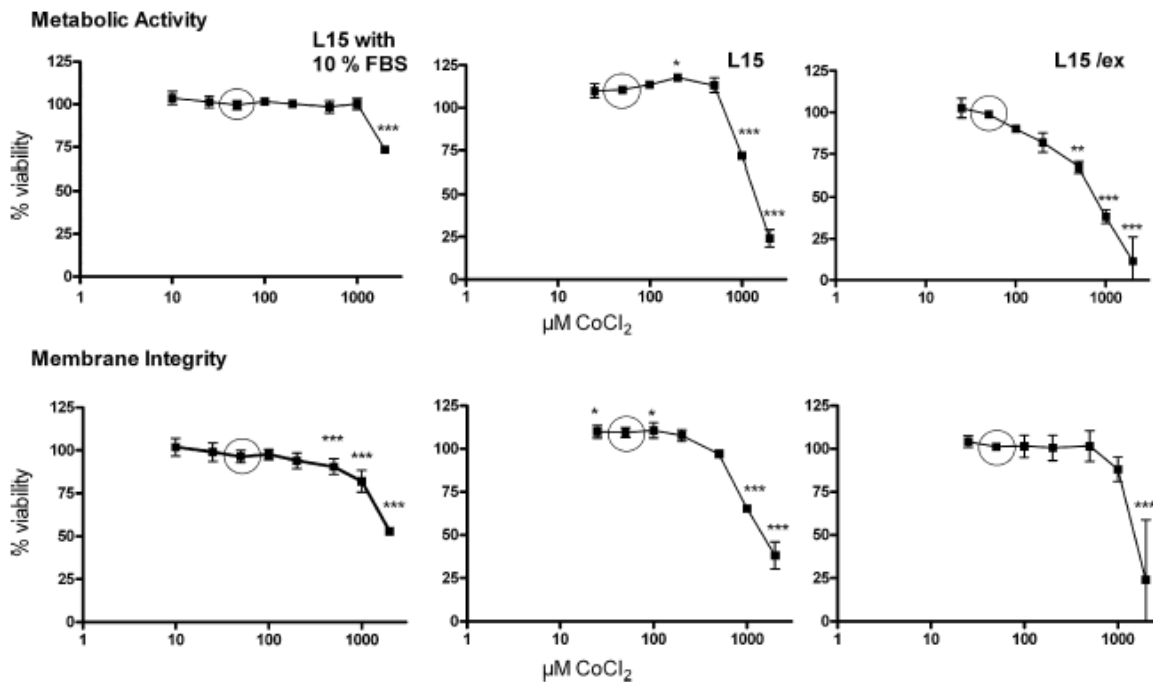


Figure 5. Viability of RTgill-W1 cells upon exposure to CoCl₂ in L15 with 10% FBS, L15 and L15/ex. Cells were exposed for 3 days to 25–2000 µM CoCl₂ (■). Results are expressed as a percentage of the fluorescence readings in control wells. Each data point represents the mean ± SD of four independent experiments (quadruplicate wells per experiment). Circles indicate a cobalt concentration of 50 µM, the amount contained in 33 µg/ml WC-Co nanoparticles. Significant differences were calculated with one-way ANOVA with Dunnett's post-test and are indicated by * $p < 0.05$ and ** $p < 0.01$.

These results led to the assumption that the toxicity found for WC-Co was not due to the cobalt ions dissolved from the particles, but due to the combination of particulate WC and Co. Indeed, this was confirmed by a comparative quantification of the differences in % cell viability after exposure to either cobalt ions, to WC or WC-Co nanoparticles (Fig. 6). Further support came from experiments where cobalt ions were mixed with WC particles, which led to toxicity comparable to that of cobalt ions alone (data not shown). This combinatory effect of metallic cobalt and tungsten carbide in particulate form was observed independent of the exposure medium (Fig. 6).

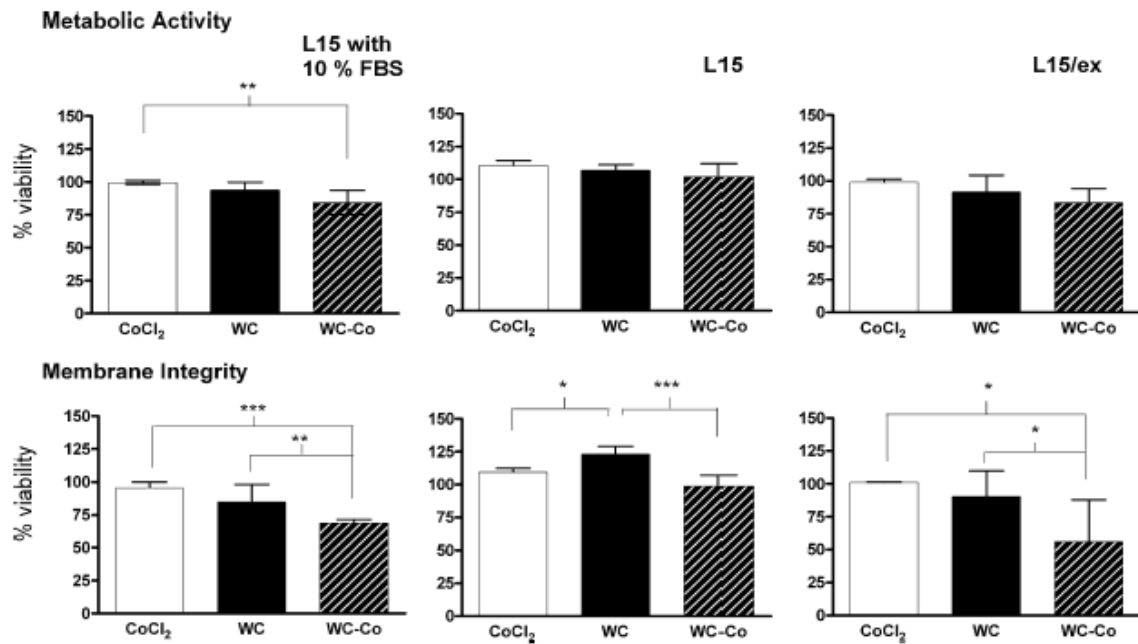


Figure 6. Comparison of the viability of RTgill-W1 cells treated with either 50 μM CoCl_2 (white bars), WC nanoparticles (black bars) or WC-Co nanoparticles (containing approximately 50 μM CoCl_2 ; hatched bars). Exposure to WC-Co nanoparticles reduced the viability of cells whereas 50 μM CoCl_2 did not, indicating an effect exclusively belonging to particle exposure. Compared are doses which showed the strongest effects in the cytotoxicity tests: 30 and 33 $\mu\text{g}/\text{ml}$ WC and WC-Co nanoparticles in L15 with 10 % FBS; 15 and 16.5 $\mu\text{g}/\text{ml}$ WC and WC-Co nanoparticles in L15 and L15/ex. Results are expressed as a percentage of the fluorescence readings in control wells. Each bar represents the mean \pm SD of three to five independent experiments (quadruplicate wells per experiment). Significant differences between treatments are indicated as * $p < 0.05$; ** $p < 0.01$; *** $p < 0.001$ and were calculated with one-way ANOVA and Tukey's post-test.

A summary of the exposure conditions and cell viability test results is provided in Table 1.

Table 1. Overview of exposure conditions and cell viability test results.

Exposure to	Concentration				Impact on cell viability for different exposure conditions ^(a)					
	WC		Co / Co^{2+}		L15 + 10% FBS		L15		L15/ex	
	$\mu\text{g}/\text{ml}$	μM	$\mu\text{g}/\text{ml}$	μM	3 h	3 days	3 h	3 days	3 h	3 days
WC ^b	30	153	-	-	+	-	++	♣	+	-
WC-Co ^b	30	153	3	51	+	++	+	-	+	+++
WC + Co^{2+} ^{b,c}	30	153	3	51	n.a.	-	n.a.	n.a.	n.a.	-

^a Impact on cells qualitatively indicated as follows: (+) significant toxicity at highest exposure concentration; (++) significant toxicity at highest and medium exposure concentrations; (+++) significant toxicity at lowest and medium exposure concentrations; (-) no statistically significant effect; (♣) significant hormetic response, n.a.: not analysed.

^b All concentrations given are the highest concentrations tested.

^c No toxicity observed under any exposure conditions at 3 $\mu\text{g}/\text{ml}$ (or 51 μM) of Co^{2+} alone (see Fig. 5)

Discussion

This study demonstrates that tungsten carbide (WC) and tungsten carbide cobalt (WC-Co) nanoparticles are able to enter cells of the rainbow trout gill cell line, RTgill-W1, regardless of whether cells are exposed in media that prevent (L15 with 10% FBS) or favour (L15; L15/ex) the formation of nanoparticle agglomerates. Short-term exposure of the cells led to significant cytotoxicity at the highest nominal particle concentrations, irrespective of the particle type or medium composition. In contrast, long-term exposures led to preferential toxicity in the simplest medium, L15/ex, and an enhanced toxicity by the cobalt-containing WC nanoparticles. The composition of the exposure media also influenced the toxicity of cobalt ions, which may dissolve from the WC-Co nanoparticles, as cells reacted much more sensitively toward the exposure to cobalt ions in the absence of a serum supplement. Nevertheless, under no condition could ionic cobalt alone explain the toxicity of WC-Co nanoparticles, suggesting that the combination of metallic Co and WC is the cause of the increased particle toxicity of WC-Co observed. This pattern of increased particle toxicity was in turn observed independent of the composition of the exposure medium.

Detailed knowledge on the behaviour of nanoparticles in exposure media is crucial in order to link exposure conditions to observed effects. We, therefore, determined the initial properties and time dependent behaviour of the selected model nanoparticles, WC and WC-Co, in the three exposure media. The size distribution of the particles was constant in L15 with 10% FBS but shifted to larger agglomerates in L15 and L15/ex. Even though L15 and L15/ex differ in complexity, the absence of FBS alone seemed to initiate agglomeration.

This observation is in agreement with previous studies that demonstrated the ability of serum proteins to act as effective dispersing agents of nanoparticles (Deguchi et al. 2007, Bastian et al. 2009). Due to electrosteric stabilisation, the presence of BSA hinders the agglomeration process effectively (Meißner et al. 2009). Specifically, WC and WC-Co particle behaviour was found to be the same as in a variety of buffers and media used for the cultivation of mammalian cell lines, such as, e.g. DMEM and RPMI (Bastian et al. 2009).

The agglomeration status of WC and WC-Co nanoparticles seemed to be secondary for internalisation, as particles were found to enter the cells irrespective of the culture medium. Both the localisation and the chemical composition of particles within the cells were identified. Our observations clearly confirm the intracellular location of nano-sized WC or WC-Co particles and agglomerates in rainbow trout gill cells. No nanoparticles were observed in the cell nuclei. However, we cannot exclude that particles with size below the resolution of the SEM pass the nuclear membrane. Both uptake and distribution within the cells match results obtained for human epithelial and rodent brain cells (Bastian et al. 2009). Hence, an uptake mechanism common to at least vertebrate cells can be assumed. So far, we are not able to propose a mechanism of uptake of nano-sized WC or WC-Co particles or agglomerates based on the SEM and EDX data shown here. An interesting observation is that particles began to settle on cells during exposure experiments, which may be a prerequisite for the uptake process. Phagocytosis is a possible uptake mechanism as demonstrated for uptake of ultra fine TiO₂ particles by A549 lung cells (Stearns et al. 2001), but also non-phagocytic eukaryotic cells are able to internalise particles, as was shown for latex particles in the size range of 50-1000 nm (Rejman et al. 2004). For particles below 200 nm, uptake via clathrin-coated pits was proposed as the primary mechanism. The clarification of the uptake mechanism will be subject to further studies. With regard to environmental exposure, however, the phenomenon of cellular uptake of agglomerated WC and WC-Co nanoparticles is an important observation, as agglomeration of nanomaterials, which is often assumed to occur in surface waters, is unable to prevent uptake into cells. Whether agglomeration impacts on the quantity of internalized nanoparticles cannot, however, be deduced at this point.

In accordance with the similarities in physico-chemical properties and uptake behaviour of the two nanomaterials in all investigated exposure media, several common patterns of cytotoxicity were observed. First, short-term exposures over 3 h led to slight but significant reductions of cell viability at the highest particle concentration. Differences in cell density due to the different exposure media are unlikely to occur at this early time point because cell proliferation of gill cells is slow even in the presence of 10% FBS (Bols et al. 1994). As well, nanoparticles began to settle on cell surfaces, which presumably is a prerequisite of the uptake process. Therefore, the observed reduction in cell viability may

indicate an initial but recoverable stress response to particle exposure. In fact, an early interaction of the particles with the cellular membrane may also explain why CFDA-AM, an indicator of cell membrane integrity, responded more sensitively at this early time point than Alamar Blue, which measures metabolic activity. Second, long-term exposures over 3 days led to enhanced cytotoxicity due to WC-Co particles compared to WC alone. This finding is reminiscent of that observed for the same particle preparations for mammalian cells in serum-containing exposure media (Bastian et al. 2009) and for micro-sized WC-Co, whose toxicity to murine macrophages was also shown to depend on the combination of WC with metallic cobalt (Lison & Lauwerys 1992). As we have previously discussed in detail (Bastian et al. 2009), the mechanisms underlying this toxicity are not yet understood but an increased bioavailability of cobalt ions stemming from the WC-Co particles, or the production of reactive oxygen species as a general phenomenon of the association of solid cobalt and carbide particles, are two possibilities. Our current study with the RTgill-W1 cell line shows that the increased toxicity of WC-Co is independent of the exposure medium and thus the initial nanoparticle agglomeration state. The surface area of the nanoparticles most likely does not change dramatically because of agglomeration. This relatively constant surface area, thus, should not change the reactivity of the particles and should not cause a significant change in toxicity, provided that the agglomerate size does not influence the uptake efficiency.

Despite the similarities for the different exposure media in supporting a cytotoxic response to nanoparticles, some differences were also noted. The first was a dose-dependent decline in cell viability for WC particles after short-term exposure in L15, which was particularly pronounced in L15 without FBS. This observation is difficult to explain, particularly because no differences in toxicity were found for the same time point in either media for WC-Co. WC particles have, thus far, largely been described as inert and we have previously shown that tungsten ions require concentrations higher than present in the particles to exert an effect in mammalian cells (Bastian et al. 2009). The observed effect may be due to the quenching of the interaction between WC particles and specific L15 components in the presence of serum. A specific interaction of L15 with WC particles may have also been observed after 3 days of exposure, where a significant stimulatory, although not consistently dose-dependent, effect was observed. Another difference in the response of cells to nanoparticles was the enhanced sensitivity toward

WC-Co after 3 days in L15/ex. In contrast to L15, L15/ex is devoid of amino acids and vitamins. RTgill-W1 cells maintained in L15/ex are vital but do not proliferate (Schirmer et al. 1997). Therefore, the lack of a fully active cellular machinery, paired with the absence of protection provided e.g. by vitamins, may account for the strong cytotoxic effect of WC-Co in L15/ex. Finally, a pronounced U-shaped dose-response curve was observed for cells exposed for 3 days to WC-Co in L-15/ex. This may, in fact, indicate limited uptake of particles into cells under conditions of very restricted nutrient supply.

The enhanced toxicity toward the fish gill cell line of WC-Co after 3 days of exposure could not be explained by cobalt ions present in the media, despite the significant increase in cobalt ion toxicity with decreasing medium complexity from L15 with 10% to L15 and L15/ex. This observation confirms previous results described for copper toxicity toward RTgill-W1 cells (Dayeh et al. 2005). The inability of cobalt ions in the culture medium to explain WC-Co toxicity is in agreement with the observations made for WC-Co and cobalt ions in mammalian cells (Bastian et al. 2009). Moreover, increased toxicity toward aquatic organisms of nanoparticles compared to metal ion content in the exposure media have recently been reported for silver (Griffitt et al. 2008, Navarro et al. 2008), copper (Griffitt et al. 2007, Griffitt et al. 2008, Karlsson et al. 2008) and selenium (Li et al. 2008a). One hypothesis postulated to explain this phenomenon is that of facilitated transport of metals as particles cross cell membranes (Limbach et al. 2007). Once in the cell, ions may be released and exert toxic effects at far lower concentrations than expected by exposure via external media. In the case of WC-Co, however, such a mechanism might be complicated by specific carbide-metal interactions (Lison et al. 1995, Gries & Prakash 2007).

In conclusion, our study demonstrates that minimal exposure media lead to rapid agglomeration of WC and WC-Co nanoparticles but that agglomeration does not prevent the uptake and toxicity of nanoparticles to a rainbow trout gill cell line. Additional research is needed in order to shed light on the role of cobalt in the expression of toxicity by WC-Co and the mechanisms underlying the modulation of toxicity in minimal and complex culture media. In this respect, the RTgill-W1 cell line could be used to study the uptake and transport through the gill epithelial layer upon exposure to nanoparticle-containing water in a multi-compartment set-up as proposed by Lee et al. (2009). Such an approach would help to clarify the extent to which the results obtained *in vitro* imply a risk for whole organisms exposed in an aquatic environment.

Chapter 5

Tungsten carbide cobalt nanoparticles exert hypoxia-like effects on the gene expression level in human keratinocytes

BMC Genomics 2010, 11: 65

Wibke Busch^a, Dana Kühnel^a, Kristin Schirmer^b, Stefan Scholz^a

^aDepartment of Bioanalytical Ecotoxicology, Helmholtz-Centre for Environmental Research Leipzig (UFZ), Permoserstr. 15, 04318 Leipzig, Germany; ^bEawag, Swiss Federal Institute of Aquatic Science and Technology, 8600 Dübendorf and ETH Zürich, Institute of Biogeochemistry and Pollutant Dynamics, 8092 Zürich, Switzerland

Abstract

Background: Tungsten carbide (WC) and tungsten carbide cobalt (WC-Co) nanoparticles are of occupational health relevance because of the increasing usage in hard metal industries. Earlier studies showed an enhanced toxic potential for WC-Co compared to WC or cobalt ions alone. Therefore, we investigated the impact of these particles, compared to cobalt ions applied as CoCl₂, on the global gene expression level in human keratinocytes (HaCaT) *in vitro*.

Results: WC nanoparticles exerted very little effects on the transcriptomic level after 3 hours and 3 days of exposure. In contrast, WC-Co nanoparticles caused significant transcriptional changes that were similar to those provoked by CoCl₂. However, CoCl₂ exerted even more pronounced changes in the transcription patterns. Gene set enrichment analyses revealed that the differentially expressed genes were related to hypoxia response, carbohydrate metabolism, endocrine pathways, and targets of several transcription factors. The role of the transcription factor HIF1 (hypoxia inducible factor 1) is particularly highlighted and aspects of downstream events as well as the role of other transcription factors related to cobalt toxicity are considered.

Conclusions: This study provides extensive data useful for the understanding of nanoparticle and cobalt toxicity. It shows that WC nanoparticles caused low transcriptional responses while WC-Co nanoparticles are able to exert responses similar to that of free cobalt ions, particularly the induction of hypoxia-like effects via interactions with HIF1 α in human keratinocytes. However, the enhanced toxicity of WC-Co particles compared to CoCl₂ could not be explained by differences in gene transcription.

Background

Engineered nanomaterials are used in large amounts in several industries and an increasing demand, including new types of particles, is anticipated in the future (The Royal Society and the Royal Academy of Engineering 2004). Their physico-chemical properties, i.e. the small size and the high surface to volume ratio are one of the most interesting characteristics, which is useful for many applications in medicine, chemistry, material sciences and physics. However, these physico-chemical characteristics may be associated with undesired health effects not known for, or different from, the bulk materials. Hence, the field of nanotoxicology is emerging to assess possible hazards of nanomaterials. Several reviews have summarised the potential cellular mechanisms of nanoparticles toxicity such as increase in the production of reactive oxygen species (ROS) and induction of inflammatory responses (Nel et al. 2006, Medina et al. 2007, Li et al. 2008b). The cellular responses appear to be dependent on the physical and chemical properties of the particles, such as particle size, dissolution behaviour, surface reactivity and binding ability (Oberdörster et al. 2005, Nel et al. 2006, Warheit 2008).

So far, the majority of *in vivo* and *in vitro* studies in nanotoxicology have focussed on endpoints such as vitality, production of reactive oxygen species, immunological parameters or cell death. However, the elucidation of the mode of action and identification of subacute effects with potential implications for chronic toxicity are difficult to obtain from these studies. Therefore, modern toxicogenomic approaches established already in pharmacology and toxicology (Waring et al. 2002, Andrew et al. 2003, Stierum et al. 2005, Vengellur et al. 2005) could be used to unravel the toxicodynamics of nanomaterials. First studies on the effects of nano- or ultrafine particles on global gene expression patterns revealed compound-specific but no general responses due to the exposure to particles (Gottipolu et al. 2009, Griffitt et al. 2009, Thomson et al. 2009, Waters et al. 2009). Hence, the chemical composition of the particles seems to play a major role for transcriptional responses. Griffitt and colleagues (Griffitt et al. 2009) showed that metal ions (silver and copper) caused similar expression patterns as nanoparticles of the same materials in zebrafish, but the numbers of affected genes were always higher after exposure to the particles. In an *in vitro* study by Waters et al. (2009) it was found that changes in cell viability provoked by silica exhibited a higher correlation

with particle surface area than either particle mass or number in macrophages. The majority of biological processes represented by the differentially expressed genes were nearly identical, irrespective of particle diameter.

A toxicogenomic approach has been used in this study to analyse the mode of action of tungsten carbide (WC) and tungsten carbide cobalt (WC-Co) nanoparticles. These nanoparticles are intended to be increasingly used in hard metal industries for the production of wear resistant and hard tools. The major advantage of using WC and WC-Co nano-scaled instead of micro-scaled particles is the increased hardness of resulting composite materials and therefore a prolonged wear lifespan of tools and other products (Richter & Von Ruthendorf 1999). Cobalt serves as binding agent improving the sintering of hard metals from WC nanoparticles. Therefore, the use of WC-Co particles is favoured in hard metal industries. Potential health implications may be of concern for workers involved in the manufacturing process. Previous studies using μm -sized particles have indicated a lack of toxicity for WC particles but a hazardous potential for cobalt metal particles *in vivo* and *in vitro* (Lasfargues et al. 1992, Lison & Lauwerys 1992, Lasfargues et al. 1995). A mixture of these μm -scaled powders (WC-Co) exhibited an enhanced toxicity if compared to cobalt metal powder alone (Lison & Lauwerys 1990, Lasfargues et al. 1992, Lison & Lauwerys 1992, Lasfargues et al. 1995, Roesems et al. 2000). Our previous research also showed toxicity enhancing effects for nano-sized WC-Co compared to WC or CoCl_2 (Bastian et al. 2009, Kühnel et al. 2009). The increased toxicity was proposed to result from specific interactions of WC and cobalt. Since the International Agency for Research on Cancer (IARC) has classified cobalt as 'possibly carcinogenic' and tungsten carbide cobalt as 'probably carcinogenic' to humans (International Agency for Research on Cancer 2006) research on the elucidation of the mode of action of nano-sized particles of these materials is of high relevance for occupational health.

Ionic cobalt (Co^{2+}) is known to exert hypoxia like responses via stabilising the α subunit of the hypoxia inducible transcription factor (HIF1) (Yuan et al. 2003, Vengellur & LaPres 2004, Kaczmarek et al. 2009). Ubiquitously expressed HIF1 α is degraded via oxygen-dependent prolyl-4-hydroxylation under normoxic conditions (Bruick & McKnight 2001). These degradation processes are blocked by cobalt binding or oxygen deficiency (hypoxia) which results in enriched HIF1 α levels in the cells. HIF1 is a transcription factor that mediates response to hypoxia by regulating the transcription of genes encoding

proteins that play key roles in angiogenesis, glucose and energy metabolism, cell survival and proliferation, iron metabolism, and vascular functions (Semenza 2001, Wenger 2002). Comparative gene expression studies showed HIF1-mediated responses to be similar for hypoxia and CoCl₂ exposure (Vengellur et al. 2005, Olbryt et al. 2006).

Whether metallic cobalt in nanoparticles, particularly in combination with tungsten, provokes specific toxic effects deviating from or exceeding those observed for dissolved ionic cobalt is not finally clarified yet. Lison and co-workers (Lison et al. 1995) described the formation of reactive oxygen species (ROS) after a rapid dissolution of cobalt ions out of WC-Co micrometer sized particles in a cell free system, a phenomenon that could not be found with metal cobalt particles or a combination of WC particles with CoCl₂. Furthermore, another study that evaluated the role of ROS in the interactive toxicity of carbide-cobalt mixtures found no evidence that production of ROS contributed to the toxicity of WC-Co in macrophages (Lison & Lauwerys 1993). Lombaert and co-workers (Lombaert et al. 2008) investigated gene expression in macrophages exposed to micrometer sized WC-Co particles (a mixture of cobalt metal with a median particle size (d_{50}) of 4 μm and WC particles $d_{50} < 1 \mu\text{m}$). They identified differential expression of genes involved in apoptosis regulation, stress response, glucose metabolism, cell signalling, immune response and other pathways. The effects were discussed to be at least partially provoked by dissolved cobalt ions.

In a previous study (Bastian et al. 2009) we have investigated the impact of WC and WC-Co nanoparticles on the vitality of various mammalian cells (lung, skin, colon and oligodendrocyte cell lines; primary neural cell and astroglial cultures). Significant cytotoxic effects were observed for nano-sized WC-Co (33 $\mu\text{g}/\text{ml}$). About 15 % of WC and 76 % of Co were found to be dissolved after 1 week of storage of the stock solution. Interestingly, WC-Co particles (consisting of 30 $\mu\text{g}/\text{ml}$ WC and 3 $\mu\text{g}/\text{ml}$ cobalt) showed a higher toxicity than equivalent concentrations of CoCl₂ (3 $\mu\text{g}/\text{ml}$) indicating that leaching of cobalt alone may not explain the toxic effects. It was also demonstrated that the tungsten based nanoparticles could enter various cell types (Bastian et al. 2009, Kühnel et al. 2009). Based on this study we selected the human skin cell line HaCaT to investigate the effects of WC and WC-Co nanoparticles and cobalt ions on gene expression patterns. Our major goal was to elucidate (1) whether the observed effects indicate specific mode of

actions of WC-Co nanoparticles and/or (2) whether the effects can primarily be explained by dissolved Co.

Materials and Methods

Preparation and characterisation of particle suspensions and cobalt chloride solutions

Particles and exposure conditions used in this study were identical to those in a previous study which also describes details of the particle preparation, characterisation and behaviour in cell culture media (Bastian et al. 2009). Briefly, particle suspensions with a concentration of 100 µg/ml were prepared from tungsten carbide (WC) and tungsten carbide cobalt (WC-Co; 10 mass % cobalt content) powders as described in detail by Bastian et al. (Bastian et al. 2009). Particles exhibited a Brunauer-Emmett-Teller (BET) specific surface area of 6.9 m²/g (WC) and 6.6 m²/g (WC-Co). A mean particle size 56 and 62 nm was calculated from BET values (d_{BET}) for WC and WC-Co, respectively. By dynamic light scattering a mean particle size of 145 ± 5 nm for both WC and WC-Co was estimated (calculated according to DIN ISO 13321 2004-10). Similar ranges of particle size distribution and morphology were measured for both types of particles. Particle size was shown to be stable in cell culture media supplemented with FBS (see also (Bastian et al. 2009)). One week after the preparation of the suspension about 6 % of tungsten from WC and 15 % of tungsten and 76 % of cobalt from WC-Co were found to be dissolved (Bastian et al. 2009).

Exposure of cells to nanoparticles was performed using stock suspensions of 300 µg/ml WC (in water) and 330 µg/ml WC-Co (consisting of 300 µg/ml WC and 30 µg/ml cobalt, in 0.03 % sodium polyphosphate, see Bastian et al. 2009). Particle suspensions were sterilised by autoclaving and treated for 10 min with ultrasound (Merck Eurolab, Darmstadt, Germany) to disperse aggregates before exposure of cells. Previous investigations did not reveal any changes in particle characteristics by autoclaving and re-dispersing (Bastian et al. 2009).

A cobalt chloride (Fluka/Sigma-Aldrich, Seelze, Germany) stock solution of 10 mM was prepared in distilled water, sterilised by autoclaving and diluted with cell culture grade water (PAA Laboratories, Pasching, Austria). All suspensions and solutions were kept at 4°C.

HaCaT cell culture and exposure of cells

The permanent human keratinocyte cell line, HaCaT (purchased from CLS - Cell Lines Service, Eppelheim, Germany) (Boukamp et al. 1988), was maintained in RPMI medium ('Roswell Park Memorial Institute' medium; Biochrom, Karlsruhe, Germany) supplemented with 5 % (v/v) FBS and 1 % (v/v) penicillin/streptomycin. Cells were cultured in monolayers at 37°C in a humidified, 5 % (v/v) CO₂-atmosphere and sub-cultured twice a week in 75 cm² flasks (Techno Plastic Products AG, Trasadingen, Switzerland); passages 30 to 40 were used for experiments. For sub-culturing, cells were washed three times with Versene (Invitrogen/Gibco, Berlin, Germany) and detached by trypsin (0.25 % (v/v) in phosphate-buffered saline (Biowest, Renningen, Germany)).

Cells were counted using a haemocytometer and seeded at densities of 2x10⁵ cells/ml for 3 d of exposure or 5x10⁵ cells/ml for 3 h of exposure, respectively in a final volume of 10 ml per 75 cm² flasks. In order to synchronise proliferation prior to exposure with nanoparticles, cells were allowed to grow for 24 h in RPMI with 5 % FBS and subsequently for 24 h in RPMI without FBS for synchronisation (Khammanit et al. 2008). Subsequently, cells were exposed to 30 µg/ml WC, 33 µg/ml WC-Co (cobalt content was 3 µg/ml), or 3 µg/ml cobalt chloride by mixing RPMI containing 5 % FBS with 10 fold concentrated stock solutions. Exposure was performed in the dark with 5 independent replicates (performed at different days using different cell passage numbers).

Controls were performed with the water used for the preparation of particle suspensions. The WC-Co suspension also contained polyphosphate (0.003 % v/v). However, polyphosphate was not included in controls since the final polyphosphate concentration did not exceed the normal sodium phosphate concentration in cell culture media. Furthermore, no evidences for any effect of low polyphosphate concentrations on cell vitality and function was observed in a previous study (Bastian et al. 2009). As also shown previously (Bastian et al. 2009), nanoparticles did not aggregate during the exposure period if exposure was performed in FBS supplemented cell culture medium.

RNA extraction

Total RNA was extracted from 75 cm² cell culture flasks with 1 ml Trizol reagent (Invitrogen, Karlsruhe, Germany) according to the manufacturer's instructions. RNA samples were additionally purified using the RNeasy Kit (Qiagen, Hilden, Germany),

RNA qualities and quantities were determined with the Experion detection system (Biorad, Munich, Germany).

Microarray experiments

The effect of the different treatments on transcription profiles of HaCaT cells was compared by microarray analysis (whole genome human 44K array, Agilent Technologies, Böblingen, Germany). Therefore, microarray hybridisations were performed for each treatment (control, WC 30 µg/ml, WC-Co 33 µg/ml, CoCl₂ 3 µg/ml; 3h and 3d exposure each) with 5 independent biological replicates. All hybridisations were performed against a common reference RNA (Sterrenburg et al. 2002) consisting of a mixture of equal amounts of RNA from all treatments. Synthesis of cDNA, cRNA and cRNA-labeling was performed with the Agilent Low RNA Input Linear Amplification Kit according to the manufacturer's instructions. cRNA was labelled with Cy3 (controls and treatments) and Cy5 (common reference). Cy3 and Cy5 labelled cRNA were combined and hybridised to the microarray slides in the DNA Microarrays Hybridisation Oven (Agilent Technologies). Slides were scanned with the Agilent DNA Microarray Scanner (Agilent Technologies). Hybridisation and scanning were performed according to standard protocols of the manufacturer.

Microarray data analysis

Dye-normalised fluorescent intensities of individual microarray spots were extracted using the Agilent Feature Extraction software 9.5. Data were further normalised by dividing the Cy3/Cy5 ratio of each treatment by the mean Cy3/Cy5 ratio of the controls. Data were then analysed using the TMEV software version 4.3 (<http://www.tm4.org/>) (Saeed et al. 2003). Genes with significantly altered expression patterns were identified by a modified t-statistic (SAM = significance analysis of microarrays) (Tusher et al. 2001). Multiple comparison of the complete data set was performed using the lowest possible false discovery rate that allows identification of significantly differentially expressed gene (FDR<0.03 %). Further descriptive analysis by hierarchical clustering (TMEV 4.3) and principal component analysis (PCA, JMP 8.0, SAS institute; www.jmp.com) was restricted to the statistically significant genes. Fold changes (FC) of expression levels were calculated using the mean values of each treatment and the mean of the respective

controls. A complete list of FC-values of all significantly differentially expressed genes is included in the supplementary information section of this paper (Additional file 1, <http://www.biomedcentral.com/content/supplementary/1471-2164-11-65-S1.XLS>).

The microarray data have been submitted to the Gene Expression Omnibus database (GEO, series no. GSE16727; <http://www.ncbi.nlm.nih.gov/geo/query/acc.cgi?acc=GSE16727>)

Gene set enrichment and pathway analysis

In order to identify biological pathways and functions associated with the changes in gene expression patterns, transcription profiles were analysed by Gene Set Enrichment Analysis (GSEA) (Mootha et al. 2003, Subramanian et al. 2005) (<http://www.broad.mit.edu/gsea/>). GSEA is based on ranking of the genes according to their statistical significance and comparison of the patterns to sets of predefined genes. These predefined gene sets are provided by the Molecular Signatures Database (MSigDB) and include five different types of databases (C1 to C5). For our analyses we used the databases C2 (gene sets collected from various sources such as online pathway databases, publications in PubMed including microarray studies, and knowledge of domain experts), C3 (transcription factor targets, i.e. genes that share a transcription factor binding site defined in the TRANSFAC database version 7.4, <http://www.gene-regulation.com/>) and C5 (gene sets of the Gene Ontology (GO) database, www.geneontology.org). Further details are explained on the MSigDB homepage (<http://www.broad.mit.edu/gsea/msigdb/index.jsp>). Since GSEA does not allow the analysis of multiple datasets, analysis was performed pair wise comparing each treatment with the control.

Furthermore, pathway analysis was performed by means of the Database for Annotation, Visualisation and Integrated Discovery (DAVID; Huang et al. 2009; <http://david.abcc.ncifcrf.gov/>) using the list of differentially expressed genes identified by SAM (see above).

RT-PCR

cDNA was synthesised from RNA using the RevAid™ First Strand cDNA Synthesis Kit (MBI Fermentas, St. Leon-Rot, Germany) according to the manufacturer's instructions. Primers were designed using the computer program Primer3 (Rozen & Skaletsky 2000) or

Beacon Designer 7 (Premier Biosoft, Palo Alto, USA; www.PremierBiosoft.com) and purchased from Invitrogen. Primer sequences are listed in Table 1.

Target genes and the reference gene RPL41 (Waxman & Wurmbach 2007) were amplified from 1 µl of cDNA using 1 unit of Taq Polymerase (Promega, Mannheim, Germany), 50 mM TRIS-HCl (pH 9.0, Serva, Heidelberg, Germany), 1.5 mM MgCl₂ (Sigma, Steinheim, Germany), 15 mM (NH₄)₂SO₄ (Sigma), 0.1% (v/v) Triton-X 100 (Merck, Darmstadt, Germany), 0.2 mM dNTPs (MBI Fermentas) and 0.6 µM of each primer in a 25 µl reaction volume. The number of cycles was adjusted to obtain amplified DNA during the exponential phase of the reaction. Annealing was performed at 55°C. PCR-fragments were analysed by agarose gel electrophoresis (1.5 % w/v agarose) and ethidium bromide staining (0.005% w/v). mRNA abundance was evaluated by either visual comparison of band intensity or densitometric analysis using the image analysis software ImageJ (Version 1.33u, available at <http://rsb.info.nih.gov/ij/>). Relative gene expression levels were calculated by normalisation of band intensities to the reference gene. These relative gene expression values were converted to percent of the average control values. Statistical differences were analysed after confirmation of normal distribution (Kolmogorov-Smirnov test) with one-way ANOVA followed by Dunnett's post test using GraphPad Prism 4.0 software (GraphPad Software, San Diego California USA, www.graphpad.com). Values of p<0.05 were considered statistically significant.

Table 1. Sequences of primers used for the validation of microarray data by RT-PCR.

Gene Name	GenBank Accession	Forward Primer Sequence	Reverse Primer Sequence
RPL41	NM_021104	AAGATGAGGCAGAGGTCCAA	TCCAGAATGTCACAGGTCCA
LOXL2	NM_002318	AGCTTCTGCTTGGAGGACACA	TGAAGGAACCACCTATGTGGCA
ANGPTL4	NM_139314	GTCTCGCACCTGGAACCC	CTTCGGGCAGGCTTGGCCAC
PFKFB4	NM_004567	TCCCCACGGGAATTGACAC	GAGAGTTGGGCAGTTGGTCAT
BNIP3	NM_004052	ACACCACAAGATACCAACAG	TCTTCATGACGCTCGTGTTCCTC
GAPDH	NM_002046	AGGCTGAGAACGGGAAGC	AGAGGGGCAGAGATGATG
CA9	NM_001216	AACCAGACAGTGATGCTGAG	TGGCATAATGAGCAGGACAGG
MAL	NM_002371	AAACATTGCTGCCGTGGTGT	AGGTTAGACACAGCAAGCTCCC
OLFM4	NM_006418	ATTGGGTGGCGCCATTGAATA	TGGTGTCATAGTACGGGTGGC
ID2	NM_002166	GACCCGATGAGCCTGCTATAC	AATAGTGGGATGCCGAGTCCAG
DSG4	NM_177986	TGAAGATGAAGGTCCGACCAG	GGGTTGCACACATGGATCAGCA
KRT1	NM_006121	AGAATGCCCTCAAGGATGCC	TTCTCCGTAAGGCTGGGACAA
MMP1	NM_002421	AAGAGGCTGGGAAGCCATCA	TCAGTGAGGACAAACTGAGCC

Results

We compared the mode of action of WC and WC-Co nanoparticles and dissolved CoCl₂ in HaCaT cells by recording changes in transcription profiles by microarray analysis. HaCaT cells were exposed to the lowest concentration of WC-Co causing a reduction of cell vitality (33 µg/ml; Bastian et al. 2009) and corresponding concentrations of WC and CoCl₂. RNA isolated after 3h and 3d of exposure from 5 independent biological replicates per treatment was analysed using a commercial human whole genome microarray. Various analyses routines were performed to identify differentially expressed genes, treatment clusters and affected biological pathways.

Identification of differentially expressed genes

SAM analysis of normalised microarray fluorescence intensities for all treatments revealed 1956 significantly differentially expressed genes with about 1146 showing an induction or repression of more than 2fold. The highest number of genes with a significantly altered expression above 2fold was observed after 3d of exposure (Table 2). Among the different treatments, exposure to CoCl₂ provoked the strongest changes in gene expression (373 and 826 genes for 3h and 3d of exposure, respectively) followed by WC-Co (37 and 248, respectively) and WC nanoparticles (28 and 49 respectively). Comparison of the genes affected by the different treatments revealed a considerable overlap of transcription profiles.

Table 2. Number of significant repressed or induced genes >2fold per treatment*.

Treatment	up	down	total	Treatment	Overlapping genes between treatments				
WC3h	26	2	28	WC3h	WC3h				
WCCo3h	13	24	37	WCCo3h	8	WCCo3h			
CoCl3h	242	131	373	CoCl3h	8	17	CoCl3h		
WC3d	18	31	49	WC3d	3	2	11	WC3d	
WCCo3d	141	107	248	WCCo3d	2	8	29	31	WCCo3d
CoCl3d	541	285	826	CoCl3d	8	15	134	19	184

* identified with SAM; the pair wise comparison indicates genes that were differentially expressed in both of the considered treatments

The highest commonalities were observed between the gene expression patterns of CoCl₂ and WC-Co after 3d of exposure (184 genes differentially expressed in both treatments), followed by the exposure to CoCl₂ at 3h and 3d (134 genes) and WC/WC-Co at 3d (31 genes). A list of the genes with the strongest differential expression (>5fold) can be found in Table 3 (provided in the Appendix of this thesis), the complete set of genes is available in the Additional file 1 (<http://www.biomedcentral.com/content/supplementary/1471-2164-11-65-S1.XLS>).

Confirmation of microarray data

In order to verify the microarray results, RT-PCR analysis was conducted using the same set of samples used for the microarrays as well as RNA samples from independent exposure experiments. Twelve genes with significantly differential expression and a minimum of 2fold up- or downregulation were selected for RT-PCR confirmation. However, care was taken that genes with weak (close to 2fold differential expression) and strong changes (up to 23fold) in expression were included (Figure 1). For eight of the selected genes the significant changes of expression could be confirmed (BNIP3, LOXL2, ANGPTL4, CA9, PFKFB4, KRT1, MAL, MMP1). Trends (induction or repression) were conserved between microarray and RT-PCR data for each treatment. The remaining genes (GAPDH, ID2, OLFM4, DSG4) exhibited a high variability and could not be confirmed as statistically significant from controls by RT-PCR.

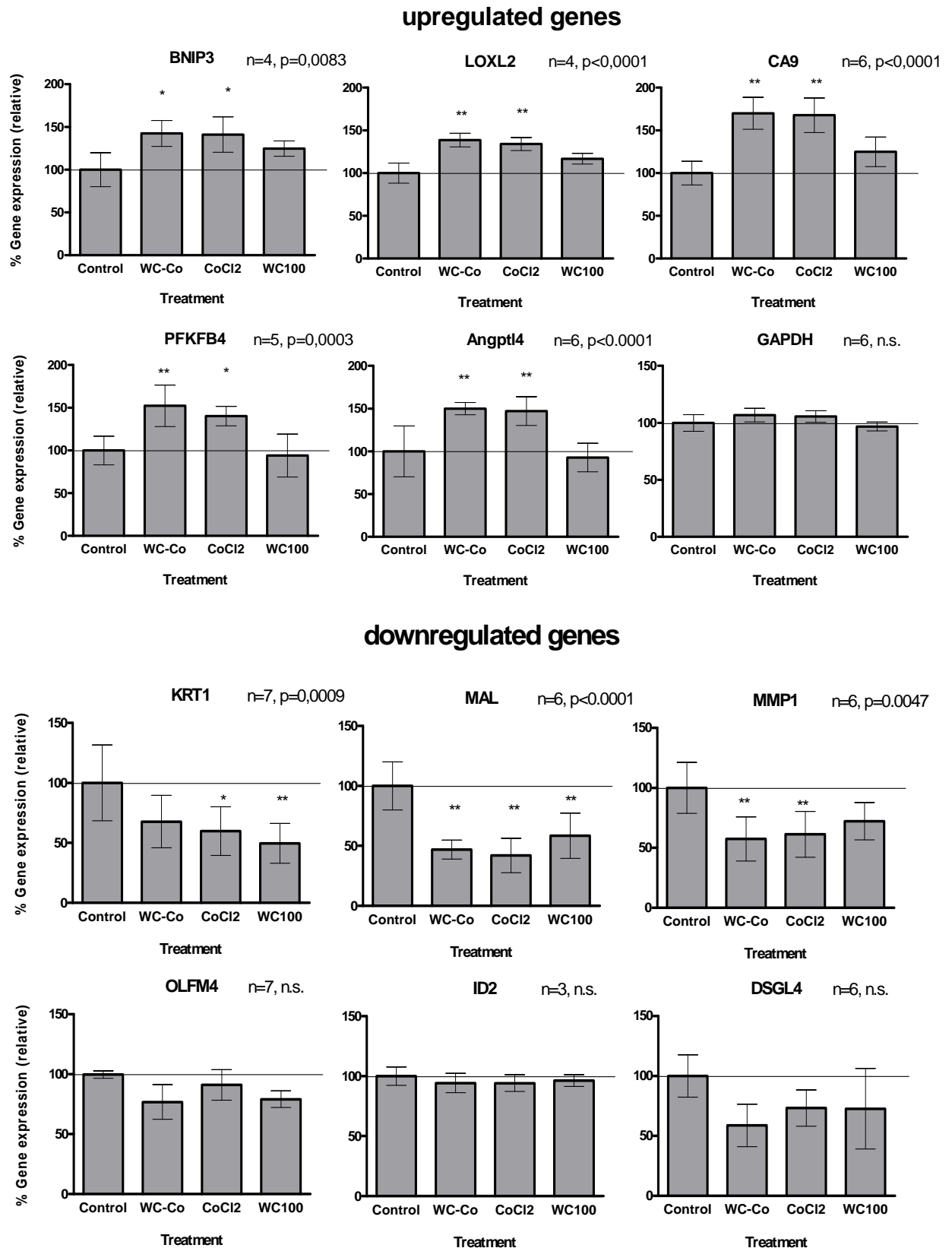


Figure 1. Validation of microarray data by RT-PCR. Relative gene expression of arbitrarily selected genes in HaCaT cells after 3d of exposure to 30 $\mu\text{g/ml}$ WC and 33 $\mu\text{g/ml}$ WC-Co nanoparticles and 3 $\mu\text{g/ml}$ CoCl₂ was analysed by semiquantitative RT-PCR. Selected genes represent genes with significant changes (2 to 23fold) of expression levels in microarrays. Gene expression values were converted to percent of the mean of controls and are presented as mean \pm standard deviation (SD). Statistical differences were analysed with one-way ANOVA followed by Dunnett's post test (treatment vs. control). Values of $p < 0.05$ were considered statistically significant; * $p < 0.05$, ** $p < 0.01$.

PCA and cluster analyses

Two methods of descriptive statistics – PCA (principal component analysis) and HCA (hierarchical cluster analysis) - were applied to identify commonalities or differences between treatments based on the patterns of significantly differentially expressed genes. By PCA analysis about 65 % of the variability in different treatments was represented by the first 3 components. Four clearly separated clusters, i.e. cells treated with CoCl₂ for 3h, the same treatment for 3d, cells treated with WC-Co for 3d and cells treated with WC for 3d were identified (Figure 2). All other treatments, including the controls, were not separated and formed a large cluster with apparently weak gene expression changes if compared to controls. WC-treated cells were less clearly separated from controls. This was indicated by the observation that a clear distinct cluster was only demonstrated for PC axis 2 and 3.

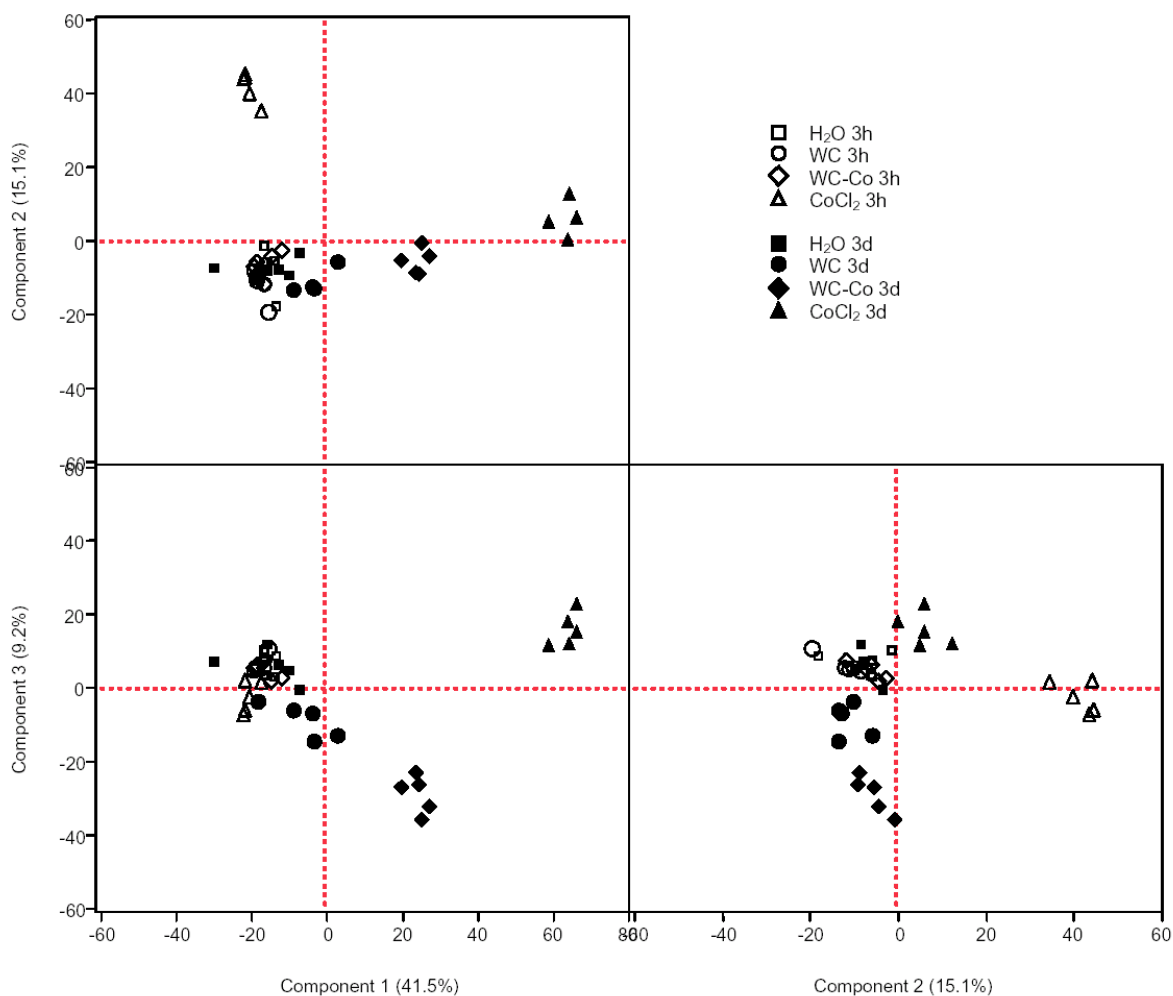


Figure 2. Principle component analyses of differentially expressed genes in HaCaT cells exposed for 3h and 3d to 30 µg/ml WC, 33 µg/ml WC-Co nanoparticles and 3 µg/ml CoCl₂. Each symbol represents a biological replicate.

Similar results were obtained by HCA, which identified 3 treatment clusters. Both CoCl₂ treatments and the 3d exposures of WC-Co formed a distinct cluster. All other treatments (controls, WC3d, WC3h, WC-Co3h) were grouped in one cluster (Additional file 2, <http://www.biomedcentral.com/content/supplementary/1471-2164-11-65-S2.PDF>).

Gene clustering revealed two clusters with strongly induced genes. Genes of these clusters (i.e. LOXL2, BNIP3, CA9, PDK1, ASB2, EGLN3, ANKRD37, PNCK) are coding for proteins with diverse functions, but some of them are known to be direct targets of the transcription factor HIF1 α (see below). For the remaining clusters it was not possible to identify predominating groups of gene ontology. Therefore, gene clusters were not analysed in detail but two types of pathway analysis were used to identify signalling pathways and biological functions associated with the differentially expressed genes.

Gene set enrichment analysis (GSEA) and identification of affected signalling pathways

Pathway analysis was performed by two approaches, with (1) GSEA software (Mootha et al. 2003, Subramanian et al. 2005) using the complete set of gene expression data from the microarray experiments, and (2) the DAVID database (Huang et al. 2009) using the list of more than 2fold differentially expressed genes previously identified with SAM.

GSEA identified communalities with existing gene sets (enrichment) primarily for induced genes. The highest number of affected gene sets was found for the 3d WC-Co treatment. The majority of pathways associated with down-regulated gene sets were found after 3h of exposure with WC-Co. An overview of pathway related gene sets with the highest commonality (based on statistical significance analysis) to the observed patterns of differentially expressed genes is given in Table 4 (provided in the Appendix of this thesis).

Gene sets related to the hypoxia pathway as well as carbohydrate metabolism were induced by WC-Co and CoCl₂ after 3d. A significant association with the induction of the hypoxia gene sets was also observed after 3h of exposure with WC-Co. As indicated by the enrichment of genes for the transcription factor HIF1 α (hypoxia inducible factor 1 alpha), regulation via HIF1 α may play a major role in provoking the observed changes in hypoxia and carbohydrate metabolism genes. Furthermore, GSEA detected an enrichment of genes related to RNA metabolism and processing as well as genes coding for proteins of the nucleus and the nuclear membrane. These gene sets referred mainly to genes down-

regulated after 3h of exposure to WC-Co nanoparticles. Some of the genes with strong differential repression (> 5fold; e.g. MAL, KRT1, GDF15, MMP1; identified by SAM) were not found to be included in these pathways.

DAVID revealed similar results as GSEA. However, small gene sets, for instance a down-regulation of metallothioneins in the 3h CoCl₂ exposure, were additionally identified by DAVID. Furthermore, genes coding for several proteins containing a functional prolyl-4-hydroxylase alpha subunit were highlighted as up-regulated for the 3d of exposure with CoCl₂ and WC-Co.

The complete results of the GSEA and DAVID analyses are provided in the Additional file 3 (<http://www.biomedcentral.com/content/supplementary/1471-2164-11-65-S3.XLS>).

Discussion

The increasing use of nanoparticles may also lead to an increased human exposure and adverse health effects. Occupational exposure is one of the most relevant exposure routes. In order to estimate the potential human health impacts of nanoparticles a precise knowledge on their mechanism of action is indispensable. This knowledge allows, for instance, clarifying whether effects are specifically associated with or enhanced by the nano-sized dimensions or whether the same type of effects as known for corresponding bulk material or dissolved compounds occurs.

In the present paper we focussed on WC and WC-Co nanoparticles which are used in hard metal industries. Dermal uptake, inhalation or accidental oral uptake present possible routes for occupational exposure for these particles. Our previous study has demonstrated their incorporation into various types of cells. Toxicity was low but enhanced for WC-Co compared to pure WC particles (Bastian et al. 2009, Kühnel et al. 2009). A transcriptome analysis of human macrophages exposed to μm -sized WC-Co revealed differential expression of genes known to be affected by cobalt as well (Lombaert et al. 2008), providing first evidence that dissolved cobalt seems to play a role in WC-Co toxicity. However, no direct comparison of transcription patterns provoked by nano-sized WC-Co, WC and dissolved cobalt is available so far. In order to model human skin exposure, the human keratinocyte cell line (HaCaT) was selected as experimental model to perform microarray analyses. A number of statistical methods and database analysis tools were used to compare the data sets and perform a detailed pathway analysis.

Transcriptional changes in WC exposed cells

Identification of significantly altered genes revealed only little changes for the exposure of HaCaT cells to WC. Similar observations were made for WC in larger particle size *in vitro* and *in vivo* (Lison & Lauwerys 1990, 1992). The weak transcriptomic response may be explained by the physicochemical characteristics, since WC nanoparticles were shown to be chemically inert (Bastian et al. 2009). The genes detected as differentially expressed with WC were mostly also affected by WC-Co and CoCl_2 (e.g. EGLN3, CA9, BNIP3, LOXL2, PDK1, KRT1, MMP1).

This might be due to traces of cobalt and other metals in WC nanoparticle preparations that have been reported at low concentrations of about 5×10^{-4} μM (described by Bastian et al. 2009). Some of the genes, however, showed a reciprocal differential expression pattern. For example, while induced by CoCl_2 , a repression was detected for WC and WC-Co nanoparticles, for e.g. *TLL7*, *KIT*, *CHST6*, *NODAL*, *WDR64*, *DES*, *HS6ST3*, *DLX2*, *GPR158*. In order to identify potential effects associated with the dimensions of nanoparticles but not related to the chemical compound, we compared our expression data set with 503 genes that were found to be affected by exposure to amorphous silica nanoparticles (Waters et al. 2009). In this study, transcriptomic profiles of macrophages exposed to amorphous silica particles in two different sizes and different concentrations were recorded. Similar to WC, amorphous silica is known to be chemically inert. Only 29 out of 503 of the silica-sensitive genes were also found to be differentially expressed in our study. Since these genes showed an altered expression with CoCl_2 rather than with WC particles, they may reflect a general unspecific stress response.

Transcriptional changes in WC-Co and CoCl_2 exposed cells

Compared to the effects with WC nanoparticles, more genes were affected by the WC-Co nanoparticles. Most of them were altered by CoCl_2 as well. We found strong overlaps of the expression data of WC-Co and CoCl_2 treated cells, whereas the highest number of genes differentially expressed was found with CoCl_2 . As demonstrated by GSEA analysis, the differentially expressed genes involved in the transcriptional response to WC-Co and CoCl_2 could be associated to various biological functions or signalling pathways which are discussed in detail in the following paragraphs.

Whereas most of the affected genes were induced, a number of genes repressed by WC, WC-Co and CoCl_2 exposure have been found as well (e.g. *MAL*, *OLFM4*, *KRT1*, *CLCA2*, *MMP1*, *IQGAP2*). For most of these genes the mechanisms of transcriptional regulation are not known and special pathways related to this group of genes could not be identified.

The role of HIF1 for differential gene expression in WC-Co and CoCl_2 treated cells

Comparison of the pattern of significant genes and gene set enrichment analyses demonstrated similar responses and signalling pathways for cells exposed to WC-Co and CoCl_2 , e.g. genes involved in the metabolism of glycolysis and gluconeogenesis, cell

adhesion and the response to hypoxia. Under hypoxic conditions, the α subunit of hypoxia inducible factor 1 (HIF1 α) accumulates and induces transcription of diverse target genes. HIF1 α is a transcription factor that is ubiquitously expressed but rapidly degraded under normoxic conditions. Cobalt ions are known to stabilise HIF1 α under normoxic conditions and therefore exert hypoxia-like cellular responses (Yuan et al. 2003, Vengellur & LaPres 2004, Kaczmarek et al. 2009, Moroz et al. 2009). Several genes sorted into gene sets related to hypoxia and other pathways e.g. glycolysis and gluconeogenesis, are primary targets of the transcription factor HIF1. To analyse whether such HIF1 target genes were affected by our treatments we generated a list of HIF1 α target genes (list contained two gene sets from the GSEA C3 TFT database and the “HIF1_Targets” gene set (C2) that was generated after Semenza (2001). When the expression of HIF1 primary targets is compared, WC-Co nanoparticles provoke almost the same pattern of induction or repression as CoCl₂ (Figure 3).

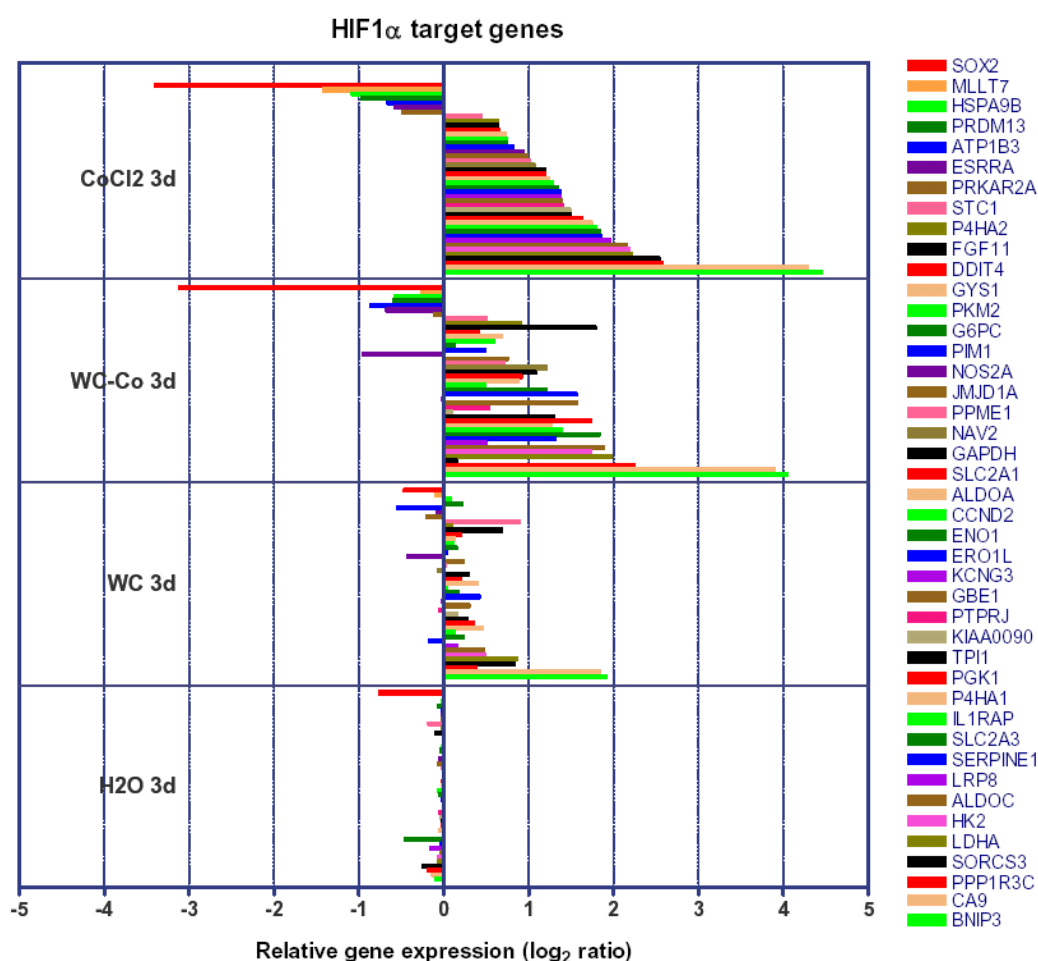


Figure 3. HIF1 α target genes and their expression levels after 3d of exposure of HaCaT cells to 30 μ g/ml WC and 33 μ g/ml WC-Co nanoparticles and 3 μ g/ml CoCl₂. Bars indicate the mean microarray expression levels of 5 biological replicates. This figure represents all affected HIF target genes identified as significantly differentially expressed by SAM without a fold change threshold.

HIF1 as an initial factor for downstream regulation

The list of affected HIF1 targets contained transcription factors that could be involved in the regulation of secondary HIF1 targets. One example is SOX2. SOX2 contains a putative HIF1 promoter binding site and was found to be strongly repressed after 3d of exposure with WC-Co and CoCl₂. SOX2 is known to play a key role in stem cell generation and pluripotency (Kim et al. 2008, Loh et al. 2008, Pei 2009). Greber et al. (2007) studied the transcription profile of embryonic stem cells and embryonic carcinoma cells following a knock down of SOX2. In HaCaT cells exposed to CoCl₂, 97 genes with differential expression (26 repressed, 71 induced genes) showed a similar expression pattern if compared to the SOX2 knock down. None of these genes is known as direct HIF1 targets or exhibit HIF1 binding sites and quite a few of them were mentioned in the context of hypoxia earlier. These genes might be regulated by the SOX2 transcription factor as potential secondary HIF1 targets.

Endothelin 2 (EDN2) is another example for a gene with a putative promoter HIF1 binding site that could be involved in the differential expression of genes in the CoCl₂ treatment. In agreement with the HIF1 promoter binding site, Na et al. (2008) reported the induction of EDN2 after 3 and 6 hours of hypoxic treatment in granulosa cells. Similarly, EDN2 was found to be induced in HaCaT cells exposed to WC-Co and CoCl₂ after 3h. An induction of other genes of the endothelin complex (EDNRB, EDNRA, ECE2) was detected with the same treatments after 3d. The induction of collagen mRNA levels and the repression of the matrix metalloproteinase 1 (MMP1) by the endothelin complex was described by Shi-Wen and colleagues (Shi-Wen et al. 2001). Indeed, an induction of the collagen gene COL5A1 and the repression of the endothelin downstream target MMP1 were detected in HaCaT cells exposed to WC-Co and CoCl₂ for 3d.

In addition to the sets of genes regulated by HIF1, GSEA identified sets of genes that are regulated by other transcription factors. However, similar to HIF1, transcripts of the genes encoding the transcription factors themselves were not found to be differentially expressed. The list (see Additional file 3) contained transcription factors known to be HIF1 α interaction partners – e.g. ARNT (aryl hydrocarbon nuclear translocator, (Jiang et al. 1996)) - or HIF1 supporting factors – e.g. (AP1, (Yamashita et al. 2001); Smad3/4; (Sanchez-Elsner et al. 2002)), but also a number of the enriched gene sets not known to be related to HIF1 or targets of HIF1 (such as BACH2, NEF2, ALX4, PAX3).

By comparing HIF1 target genes with known hypoxia responsive genes it becomes obvious that only part of the hypoxia related genes are known to be direct or indirect targets of HIF1. Nevertheless, the fact that most of the genes and pathways affected with WC-Co and CoCl₂ were also observed in toxicogenomic studies investigating hypoxia (Manalo et al. 2005, Vengellur et al. 2005, Mense et al. 2006) led us to conclude that the stabilisation of HIF1 α via cobalt is an initial step and most of the reactions that are not directly related to HIF1 α might reflect downstream events.

Cobalt ions as co-factor substitute

In CoCl₂ treated cells the YY1 transcription factor was identified as a potential master regulating factor with GSEA. YY1 is a ubiquitous transcription factor with fundamental biological functions. Its role in cancer biology is also intensely discussed (Gordon et al. 2006). An interaction of YY1 with cobalt was not yet described but might be conceivable, because YY1 contains four zinc finger domains. The substitution of zinc ions and other divalent metal ions by Co²⁺ is often discussed to play a role in transcription factor domains, DNA repair mechanisms and calcium metabolism (Kasten et al. 1992, Kopera et al. 2004, Beyersmann & Hartwig 2008). The transcriptional changes of YY1 target genes after the CoCl₂ exposure indicate an induction or enrichment of the YY1 protein but it remains unclear, whether the substitution of zinc ions by Co²⁺ is responsible for that.

In HaCaT cells, a significant depletion of intracellular Zn²⁺ and Mg²⁺ after CoCl₂ exposure was described by Ortega and colleagues (Ortega et al. 2009). A substitution of magnesia ions by Co²⁺ may result in the interruption of ATPases and the energy balance of the cell (Karovic et al. 2007). It is proposed that ion substitution plays a role in uptake mechanisms of cobalt ions into cells, which evidently happens via cation-dependent ionic pumps (Kasten et al. 1992, Ortega et al. 2009). Although we found gene sets related to metal ion or cation ion binding proteins to be affected, we did not detect an enrichment of gene sets connected to the described effects resulting from ion substitution.

Differential expression of protein kinases and phosphatases

It was noticed that in WC-Co and CoCl₂ exposures several kinases and phosphatases exhibited a differential expression. Kinases are a major group of proteins involved in endocytosis (Pelkmans et al. 2005, Doherty & McMahon 2009). In a knock-down study of

Pelkmans and colleagues (Pelkmans et al. 2005) 209 kinases with known important functions in several pathways were identified to be involved in endocytosis. Interestingly, most of the pathways they could link with endocytotic processes were also affected in our study (e.g. mTOR, Wnt, integrin/adhesion, RTKs/RSTKs, GPCR).

Protein tyrosine phosphatases (PTPs) and kinases as well as enzymes of the phosphoinositol-3-kinase family (PI3Ks) seem to play a special role in the response to cobalt. The latter have been described as possible upstream regulators of HIF1 α (Mottet et al. 2003, Tang & Lasky 2003, Jin et al. 2007, Wang et al. 2008b) and have functions in some of the pathways found to be induced (e.g. Insulin-, IGF1-, PPAR α -pathway; based on GSEA analysis). PTPs are known to be signalling molecules that regulate a variety of cellular processes including cell growth, differentiation, mitotic cycle, and oncogenic transformation. Some genes coding for PTPs were not only affected by the cobalt containing treatments but also by WC (PPFIA4, PTPRT, PTPRZ1). Since kinases and phosphatases are also involved in the cellular response to various kinds of environmental stress, their altered expression may be related to a cobalt-induced and/or a particle uptake related stress response.

Oxidative stress and transcriptional response

The production of reactive oxygen species (ROS) and the subsequent induction of oxidative stress are discussed as major modes of action of nanoparticles (Nel et al. 2006, Limbach et al. 2007, Papageorgiou et al. 2007) and was also described to be involved in the cellular response to cobalt ions (Chandel et al. 1998, Zou et al. 2001, Karovic et al. 2007). Nevertheless, genes or gene clusters that are related to oxidative stress responses could not be found within our data set of differentially expressed genes. This was confirmed by a lack of ROS production in HaCaT cells for any of the treatments (manuscript in preparation).

Cobalt ions and WC-Co toxicity

Cobalt is an essential trace element for humans, but becomes toxic at high concentrations. In a previous study, we analysed acute toxicity by measuring cell viability of HaCaT cells after same exposure conditions as performed in this study (Bastian et al. 2009). Altered proliferation or morphological changes of the cells were not observed.

Toxicity of CoCl₂ was indicated by decreasing cell viability at concentration of 100 µM (corresponds to 6 µg/ml) and above. Lower concentrations of CoCl₂ have not been observed to cause acute toxicological reactions in several cells *in vitro*, including in HaCaT cells (Ermolli et al. 2001, Karovic et al. 2007, Bastian et al. 2009). Intense transcriptional changes were observed in this study at concentrations slightly below those causing *in vitro* toxicity. The differentially expressed genes may serve as indicators for potential long term effects and may also be useful for investigations of molecular mechanisms.

WC-Co nanoparticles exhibited an increased toxicity in previous studies performed in different types of cell lines (human and fish) when compared to WC particles and CoCl₂ (Bastian et al. 2009, Kühnel et al. 2009). Viability of HaCaT cells was slightly (15%) decreased after 3 days of exposure. This enhanced toxicity was discussed as either a result of increased cellular cobalt uptake associated with the uptake of WC particles – the so called “Trojan horse” hypothesis (Limbach et al. 2007) – or a result of unknown combinatory effects of WC particles and cobalt. The “trojan horse” theory is supported by studies showing increased toxicity of nanoparticles with leaching ions compared to the ions alone (Li et al. 2008a, Navarro et al. 2008, Xia et al. 2008, Griffitt et al. 2009). However, analysing the global transcriptional response of HaCaT cells to WC-Co nanoparticles and equivalent WC and cobalt treatments, no evidence for either of these theories could be provided. The number of transcriptional changes was more pronounced in CoCl₂ exposed cells, but particularly the regulation of genes resulting from cobalt dependent stabilisation of HIF1 α was similar for both, WC-Co and CoCl₂. The patterns of transcriptional regulation clearly indicate that the majority of the effects were associated with cobalt ions and did not indicate a special type of interaction between WC and cobalt. However, the enhanced toxicity of WC-Co with respect to CoCl₂ appears to be mediated via unknown non-transcriptionally regulated pathways.

Conclusion

Analysis of gene expression patterns in the human keratinocyte cell line HaCaT demonstrated that the transcriptional response to WC-Co nanoparticles is mainly caused by cobalt ions leaching from the particles. While WC nanoparticles alone do only show very weak effects in expression patterns, WC-Co and CoCl₂ exhibited significant transcriptional changes in genes involved in carbohydrate metabolism, hypoxia response, endocrine pathways, cell adhesion and others. The cobalt-sensitive transcription factor HIF1 plays an important role in the regulation of genes involved in these pathways, showing that WC-Co nanoparticles exert hypoxia-like responses similar to CoCl₂. The subacute response to CoCl₂ was analysed and discussed with respect to downstream events of HIF1 and involvement of other transcription factors (e.g. SOX2, YY1) in cobalt toxicity. A simplified scheme of potential major pathways resulting from cobalt reactions within the cell is provided in Figure 4.

However, while detailed analyses of transcriptional regulations clearly indicate that leached cobalt is likely to be the major trigger for gene regulation in cells exposed to WC-Co, the changes in transcription patterns do not explain the enhanced toxicity of WC-Co if compared to equivalent concentrations of WC or CoCl₂. This enhanced toxicity is suggested to be mediated by unknown combinatorial effects of WC and cobalt not reflected primarily at the transcriptional response level. However, support or rejection of this hypothesis requires further investigations.

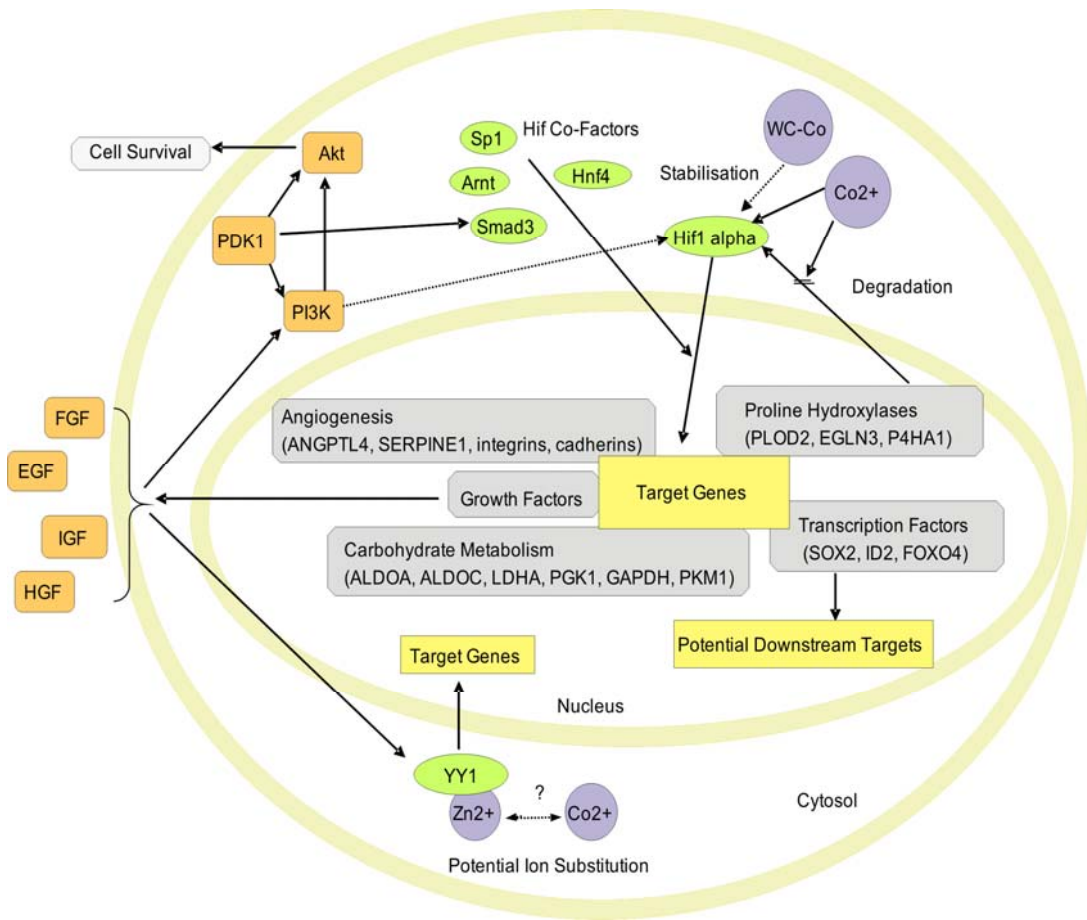


Figure 4. Illustration of the major cellular signalling pathways that were indicated by analyses of the transcriptional responses to WC-Co nanoparticles and cobalt chloride. Arrows indicate known (full lines) or potential (dashed lines) interactions. (Complex Proteins = orange, Transcription Factors = green)

Chapter 6

Summary and Conclusion

Nanotechnology is currently at the forefront of emerging technologies. Engineered nanoparticles are produced for applications that benefit from the properties associated with their small size and high surface to volume ratio. However, occupational and environmental risk assessment is necessary for nanoparticles that may be released during production processes or during use. Therefore, the research in this thesis aimed to elucidate the toxicological potential of technical nanoparticles *in vitro*. Different types of nanoparticles were proven to be able to enter different kinds of isolated cells. Particles were shown to enter cells even if they were present in agglomerated form in the exposure medium. Focussing on tungsten carbide (WC) and tungsten carbide cobalt (WC-Co) nanoparticles because of their particular occupational relevance, a special role of metallic cobalt in conjunction with WC was confirmed for the nano-sized material. Genome-wide analyses of mRNA abundance (gene expression) revealed a transcriptional response that is dominated by cobalt present in the WC-Co particles. Thus, the importance of considering the chemical composition of particles was underlined.

Summary of results

Engineered nanoparticles enter several types of mammalian cells

Toxic effects of nanoparticles may arise either from interactions with the cell surface or by internalisation into the cytoplasm and sub-cellular structures. Thus, at first it was investigated whether engineered nanoparticles are principally able to penetrate mammalian cells. Several cell types and six types of nanoparticles with different properties were considered for this study (Chapter 2). Results of light- and electron microscopy experiments showed that all investigated types of particles were able to enter all of the different cell types. The particles were always found within the cytoplasm but never in cell nuclei. Furthermore, it could be shown that nanoparticles within cells co-localise with lysosomal structures. A relative quantification of particle uptake was established by flow cytometry measurements. Changes of cellular granularity were generally more dependent on the particle than on the cell type; indicating an influence of particle properties either on their internalisation ability or the cellular granularity measurements itself. After short exposure times, a slight correlation was found for the granularity data with the primary particles sizes. However, particle properties which were not considered in the study might influence the cellular granularity measurements as well. Further research is necessary to elucidate these interactions.

Flow cytometry was also used to investigate the impact of the actin- (i.e. a cytoskeleton-) inhibitor Cytochalasin D on the particle incorporation into cells. The ability to incorporate nanoparticles was not affected by the inhibitor in most of the cell types but a reduction of the particle internalisation was found in a few cases. This study illustrated that technical nanoparticles are able to enter all kinds of mammalian cells independent of the cellular phagocytosis ability. However, the underlying mechanisms of incorporation remain to be elucidated. An export of particles out of the cells was not observed *in vitro* in this study, but translocation aspects within and out of whole organisms should be considered for future research projects.

Toxicity of tungsten based nanoparticles

Acute toxicity of technical nanoparticles was assessed with focus on WC (tungsten carbide) and WC-Co (tungsten carbide cobalt) nanoparticles and their impact on human

(Chapter 3) and fish cells (Chapter 4). By physico-chemical characterisation of the particles it was found that serum proteins (especially albumin) bound to the particles. The inclusion of serum proteins in cell culture media had a stabilising effect and prevented agglomeration of particles. Furthermore it was shown that cobalt leached out of WC-Co nanoparticles to some extent. This was considered by implementing comparative experiments with CoCl_2 . Cell viability and membrane integrity of human lung, skin, and colon cells were not affected by WC nanoparticles up to a concentration of 30 $\mu\text{g/ml}$. In contrast, WC-Co nanoparticles were slightly toxic to all cells; the colon cells were the most sensitive type of the human cells. The effects of WC-Co were always stronger than effects of CoCl_2 or WC+ CoCl_2 applied in equivalent concentrations (Chapter 3). An increased toxicity for WC-Co was also found with trout gill cells (Chapter 4). WC and WC-Co nanoparticle were detected within the cytoplasm of the gill cell line; media of different complexity, whose constituents (e.g. proteins) influence the agglomeration of the particles, had no effects on the particle internalisation. However, the toxicological effects of CoCl_2 as well as the nanoparticle effects were found to vary depending on the composition of exposure media (Chapter 4).

Altered gene expression and the role of leached ions

In order to analyse effects of WC and WC-Co nanoparticles in more detail and with the aim to elucidate the modes of action of the enhanced toxicity of WC-Co nanoparticles, global gene expression in human skin cells (HaCaT) was investigated also in comparison to dissolved cobalt ions (Chapter 5). Therefore, whole genome microarrays were used and patterns of the transcriptome were compared between WC, WC-Co or CoCl_2 treated cells. Extensive data and pathway analyses showed that most genes were differentially expressed after the CoCl_2 treatment. Exposure to WC-Co nanoparticles resulted also in a large number of genes with altered expression. By contrast, gene expression patterns of WC treated cells were hardly influenced by the nanoparticles. Most of the genes affected by WC-Co nanoparticles were also found to be altered in the CoCl_2 treatment. Within these genes, a significant enrichment of genes known as targets of the HIF1 α (hypoxia inducible factor) transcription factor or genes coding proteins that are involved in response to hypoxia could be identified by pathway and gene set enrichment analyses. Cobalt ions are known to stabilise the transcription factor HIF1 α , which affects

appropriate downstream target genes. Hence, this study clearly indicates that leached cobalt ions play an important role in toxicity of WC-Co nanoparticles. The underlying mechanism for the enhanced toxicity of WC-Co in comparison to WC particles and dissolved cobalt, however, could not be explained by the genome wide transcription analysis (Chapter 5).

Concluding remarks and future directions

Nanotechnology industry, focussing on the development and production of new products for many fields of application, is rapidly growing. The emerging use of nanoparticles could lead to their release and emissions with potential negative consequences for occupational and environmental health. So far, nanoparticles are not specifically regulated and labelling of nanoparticle-containing products is not required. Potential health or environmental effects are assessed based on the properties of the bulk materials. The need to establish nanoparticle-specific regulations is controversially discussed. Finally, for risk assessment, both the hazardous potential and the exposure probability have to be considered. Therefore, successive analyses are necessary at which *in vitro* experiments contribute to identify acute toxic nanoparticles and potential modes of action as initial steps for the risk assessment. *In vitro* studies are economically and ethically desirable and provide evidence about possible hazardous potential. Especially for the toxicological screening of the huge palette of different nanoparticles, *in vivo* studies are inappropriate or not even feasible. Nevertheless, *in vitro* methods based on cell cultures still have a limited capacity to predict *in vivo* effects (Sayes et al. 2007). This is primarily caused by the specific uptake and translocation routes *in vivo*, which are difficult to be mimicked *in vitro*. Particles that enter an organism via the lung may lead to reactions that are a consequence of communication between several cell types and are not detectable in a single cell culture (e.g. inflammation due to immunological and defence responses independent of particle translocation). Co-cultures of several cell types, as recently demonstrated by a few studies (Brandenberger et al. 2010, Burguera et al. 2010), might provide an *in vitro* approach for future activities addressing these problems of systemic interactions. However, considering our knowledge so far, particles that are toxic *in vitro* should be handled accordingly and exposure should be avoided generally. Non

toxic particles (such as WC), that have been found to enter cells easily, have to be assessed *in vivo* due to their possible long term and systemic impacts on organisms.

Besides toxicological issues, estimating and analysing the particle uptake into cells is rather difficult, especially in a quantitative manner. Initial studies show that “Inductively Coupled Plasma - Mass Spectrometry” (ICP-MS) might be a useful tool to measure intracellular particle contents (Limbach et al. 2005, Wang et al. 2008a, Xia et al. 2008). However, for this method the chemical destruction of the particles is necessary, which is not trivial for hard materials such as tungsten. Furthermore, the detection and distinction of free or particle-bound ions in comparison to solid particles is not possible. Therefore, further investigations are necessary to establish a system to measure absolute amounts of particles within cells. Studies should focus on the development or adaptation of methods for the quantitative determination of intracellular nanoparticles and leached components to better link toxicological effects to internal particle or ion concentrations. Furthermore, exposure scenarios for humans and the environment have to be generated to estimate relevant exposure concentrations and the abilities to measure nanoparticles qualitatively and quantitatively in air and the environment have to be improved.

The research of this thesis shows that toxicological investigations of engineered nanoparticles *in vitro* are possible and appropriate for the understanding of interactions between technical nanoparticles and cells. Based on these data, further activities should focus on the role of the potential carrier function of nanoparticles and consider questions of bioaccumulation and intracellular effect concentrations.

Untersuchungen zur Toxizität technischer Nanopartikel in Vertebratenzellen *in vitro*

Die Nanotechnologie ist eine der am stärksten wachsenden Technologien der heutigen Zeit. Da technische Nanopartikel andere chemische und physikalische Eigenschaften im Vergleich zum gleichen Material in grober Form aufweisen (z.B. ein stark vergrößertes Oberflächen/Volumen Verhältnis), werden sie für verschiedenste Anwendungen entwickelt, hergestellt und verwendet. Eine Risikobewertung für Nanopartikel ist insbesondere dann erforderlich, wenn die Partikel mit Mensch oder Umwelt in Kontakt kommen können. Deshalb war es Ziel dieser Arbeit, die toxikologischen Wirkungen von technischen Nanopartikeln *in vitro* in Vertebratenzellen zu untersuchen. Die Aufnahme von verschiedenen Nanopartikeln in verschiedene Arten isolierter Zellen konnte eindeutig nachgewiesen werden. Zudem wurde gezeigt, dass selbst Partikel, welche in agglomerierter Form im Expositionsmedium vorlagen, von Zellen aufgenommen wurden. Für Wolframcarbid (WC) and Wolframcarbid-Cobalt (WC-Co) Nanopartikel, welche aufgrund ihres Einsatzes in der Hartmetall-Industrie und damit ihres Auftretens an Arbeitsplätzen von besonderer Relevanz sind, konnte aus den toxikologischen Studien eine besondere Rolle des metallischen Cobalts in Verbindung mit Wolframcarbid abgeleitet werden. Mit Hilfe einer genom-weiten Transkriptionsanalyse wurden Änderungen der Expression verschiedener Gene festgestellt, welche größtenteils auf das vorhandene Cobalt in WC-Co Nanopartikeln zurückgeführt werden konnten. Die Ergebnisse dieser Arbeit unterstreichen somit auch die Bedeutung der chemischen Partikelzusammensetzung für die Bestimmung und Interpretation toxikologischer Effekte.

Kurzbeschreibung der Ergebnisse

Technische Nanopartikel werden in verschiedene Säugerzelltypen aufgenommen

Toxikologische Wirkungen von Nanopartikeln entstehen entweder aufgrund von Wechselwirkungen mit Zelloberflächen oder durch die Aufnahme von Partikeln in das Zellplasma oder sub-zelluläre Strukturen. Deshalb wurde zunächst untersucht, ob verschiedene Nanopartikel von Säugerzellen aufgenommen werden können. Für diese Studie wurden unterschiedliche Zelltypen und sechs verschiedene technische Nanopartikel mit unterschiedlichen Eigenschaften in Betracht gezogen (Kapitel 2). Mit Hilfe von Licht- und Elektronenmikroskopie konnte gezeigt werden, dass alle Nanopartikel von allen Zelltypen aufgenommen wurden. Die Partikel wurden im Zellplasma, aber nicht im Zellkern gefunden. Eine Co-Lokalisation der Partikel mit lysosomalen Strukturen deutet auf eine Anreicherung der Partikel in den Lysosomen der Zellen hin. Eine relative Quantifizierung der Partikelaufnahme wurde durch Messungen am Durchflußzytometer (FACS) möglich, da Partikel im Zellinneren die Granularität der Zellen verändern und damit das Licht des Lasers anders ablenken als Zellen ohne Partikel. Veränderungen der zellulären Granularität aufgrund von Partikelaufnahme waren stets stärker vom Partikeltyp als vom Zelltyp abhängig. Dies deutet auf einen Einfluss der Partikeleigenschaften auf die Partikelaufnahme in die Zellen, oder aber auch auf die Messung der Granularität, hin. Allerdings konnte nur nach kurzer Expositionszeit eine schwache Korrelation zwischen den relativen Granularitätsmesswerten und der Primärpartikelgröße nachgewiesen werden. Dies deutet darauf hin, dass weitere Partikeleigenschaften die Granularitätsmessung beeinflussen können, welche in zukünftigen Studien berücksichtigt werden sollten. Ein Einfluss eines Aktin- (und damit Zytoskelett-) Inhibitors (Cytochalasin D) auf die Partikelaufnahme wurde nur für wenige Zelltypen bestätigt; in keinem Falle wurde die Partikelaufnahme komplett gehemmt. Damit wurde gezeigt, dass technische Nanopartikel in verschiedene Säugerzellen aufgenommen werden und zwar unabhängig davon, ob diese Zellen phagozytieren können oder nicht. Allerdings müssen die genauen Mechanismen der Partikelaufnahme in die Zellen noch aufgeklärt werden. Unter den Bedingungen dieser *in vitro* Studie konnte kein Partikelexport aus den Zellen beobachtet werden, trotzdem sollten Aspekte des Partikel-Transports innerhalb und aus Organismen heraus in zukünftigen Studien

genauer untersucht werden. Zudem sollte der potenziellen Langzeitwirkung von Partikeln in Zellen besondere Beachtung geschenkt werden.

Toxizität Wolfram-basierter Nanopartikel

Um die akut toxischen Wirkungen von technischen Nanopartikeln zu bewerten, wurden im Rahmen der hier vorliegenden Arbeit Analysen zu WC und WC-Co Nanopartikeln mit humanen (Kapitel 3) und Fischzellen (Kapitel 4) durchgeführt. Die Charakterisierung der Partikel zeigte, dass diese durch Serumproteine, insbesondere Albumin, stabilisiert werden, wodurch eine Agglomeration der Partikel im Medium verhindert wird. Es konnte gezeigt werden, dass sich das Cobalt zu gewissen Anteilen aus den WC-Co Partikeln herauslöst. Dieses Verhalten wurde berücksichtigt, indem vergleichende Untersuchungen mit CoCl_2 durchgeführt wurden. Humane Lungen-, Haut- und Darmzellen waren in ihrer Zellvitalität und Membranintegrität durch WC Nanopartikel bis zu einer Konzentration von $30 \mu\text{g/ml}$ nicht beeinflusst. Im Gegensatz dazu wirkte WC-Co leicht toxisch, wobei die Darmzellen am sensitivsten reagierten. Die zytotoxische Wirkung der WC-Co Partikel war dabei stets stärker als die von CoCl_2 oder WC+ CoCl_2 in äquivalenten Konzentrationen (Kapitel 3). Eine erhöhte Toxizität für WC-Co konnte auch in Fischkiemenzellen nachgewiesen werden (Kapitel 4). WC und WC-Co Nanopartikel wurden im Zellplasma der Fischzelllinie nachgewiesen und zwar unabhängig davon, ob die Partikel im Expositionsmedium agglomeriert vorlagen oder nicht. Der Agglomerationszustand wurde dabei durch den Einsatz verschieden komplexer Medien, z.B. mit oder ohne Serumproteine, bestimmt. Die Komplexität der Medien hatte einen Einfluss auf die toxische Wirkung sowohl des CoCl_2 als auch der Nanopartikel, wobei kein eindeutiger Trend zwischen Medienzusammensetzung und Toxizität erkennbar war. Die toxische Wirkung der WC-basierten Partikel konnte aber in keinem Falle auf Cobalt allein zurückgeführt werden. Zusammenfassend zeigte diese Studie, dass die Agglomeration von Nanopartikeln im Expositionsmedium die Aufnahme und Toxizität, zumindest von WC-basierten Partikeln, nicht verhindern kann und, dass sowohl die Partikel selbst, als auch die herausgelösten Ionen für die toxikologische Beurteilung berücksichtigt werden müssen.

Veränderte Genexpression und die Rolle gelöster Ionen

Um die Wirkungen der WC und WC-Co Nanopartikel genauer zu untersuchen und die verstärkt toxische Wirkung von WC-Co mechanistisch zu erklären, wurden Genexpressionsstudien unter Verwendung humaner Hautzellen durchgeführt (Kapitel 5). Dabei wurden die Zellen neben den Nanopartikeln auch gegenüber CoCl_2 exponiert, um die Genexpressionsmuster der Partikel mit denen der frei gelösten Ionen zu vergleichen. Dazu wurden Microarrays verwendet, die das gesamte humane Genom abbilden. Mit Hilfe umfassender Daten- und Signalweganalysen konnten einzelne betroffene Gene und Signalwege identifiziert werden. Die größte Anzahl verändert regulierter Gene wurde nach der Exposition mit CoCl_2 detektiert. Auch die Behandlung mit WC-Co Nanopartikeln führte zu einer großen Anzahl verändert regulierter Gene. Im Gegensatz dazu zeigten Zellen, die mit WC Nanopartikeln behandelt wurden, kaum Veränderungen auf Ebene der Genexpression. Dies zeigt eindrucksvoll, dass die Partikelaufnahme und damit verbundene Signalwege auf Transkriptionsebene, zumindest für WC-basierte Partikel, kaum detektierbar sind. Fast alle Gene die durch WC-Co reguliert wurden waren auch mit CoCl_2 beeinflusst. Signalweganalysen zeigten eine signifikante Anreicherung von Genen die für Hypoxie-relevante Proteine kodieren und/oder als Zielgene des HIF1 α (hypoxia inducible factor) Transkriptionsfaktors bekannt sind. Es ist bekannt, dass Cobalt-Ionen zur Stabilisierung von HIF1 α beitragen. Dadurch werden weitere Zielgene („downstream targets“) aktiviert oder blockiert. Diese Studie zeigt damit eindeutig, dass frei werdende Cobalt-Ionen aus WC-Co Nanopartikeln eine wichtige Rolle bei der Wirkung dieser Partikel spielen. Dennoch konnte die erhöhte Toxizität der WC-Co Partikel im Vergleich zu den Einzelbestandteilen (WC, Cobalt) nicht im Detail aufgeklärt werden (Kapitel 5).

Schlussfolgerungen und Ausblick

Diese Arbeit zeigt, dass Wechselwirkungen zwischen Zellen und technischen Nanopartikeln mit Hilfe von *in vitro* Methoden identifiziert werden können. Eine klare Unterscheidung zwischen potentiell toxischen und nicht toxischen Partikeln sowie die Darstellung von Wirkmechanismen ist gelungen. Dennoch bleiben Fragen hinsichtlich relevanter Expositions- und tatsächlicher Effektkonzentrationen, sowie potentieller Langzeiteffekte offen, welche im Rahmen einer vollständigen Risikobewertung, aufbauend auf den vorhandenen Ergebnissen, noch zu bearbeiten sind.

REFERENCES

- Aardema MJ, MacGregor JT (2002) Toxicology and genetic toxicology in the new era of "toxicogenomics": impact of "-omics" technologies. *Mutation Research/Fundamental and Molecular Mechanisms of Mutagenesis* 499:13-25
- Andrew AS, Warren AJ, Barchowsky A, Temple KA, Klei L, Soucy NV, O'Hara KA, Hamilton JW (2003) Genomic and proteomic profiling of responses to toxic metals in human lung cells. *Environ Health Perspect* 111:825-835
- Ashwood P, Thompson RP, Powell JJ (2007) Fine particles that adsorb lipopolysaccharide via bridging calcium cations may mimic bacterial pathogenicity towards cells. *Exp Biol Med (Maywood)* 232:107-117
- Bao L, Chen S, Wu L, Hei TK, Wu Y, Yu Z, Xu A (2007) Mutagenicity of diesel exhaust particles mediated by cell-particle interaction in mammalian cells. *Toxicology* 229:91-100
- Bastian S, Busch W, Kühnel D, Springer A, Meißner T, Holke R, Scholz S, Iwe M, Pompe W, Gelinsky M, Potthoff A, Richter V, Ikonomidou C, Schirmer K (2009) Toxicity of tungsten carbide and cobalt-doped tungsten carbide nanoparticles in mammalian cells *in vitro*. *Environ Health Perspect* 117:530-536
- Baun A, Sorensen SN, Rasmussen RF, Hartmann NB, Koch CB (2008) Toxicity and bioaccumulation of xenobiotic organic compounds in the presence of aqueous suspensions of aggregates of nano-C(60). *Aquat Toxicol* 86:379-387
- Beyersmann D, Hartwig A (2008) Carcinogenic metal compounds: recent insight into molecular and cellular mechanisms. *Arch Toxicol* 82:493-512
- Bhattacharya K, Davoren M, Boertz J, Schins RP, Hoffmann E, Dopp E (2009) Titanium dioxide nanoparticles induce oxidative stress and DNA-adduct formation but not DNA-breakage in human lung cells. *Part Fibre Toxicol* 6:17
- Blanco E, Kessinger CW, Sumer BD, Gao J (2009) Multifunctional Micellar Nanomedicine for Cancer Therapy. *Experimental Biology and Medicine* 234:123-131
- Bols NC, Barlian A, Chirinotrejo M, Caldwell SJ, Goegan P, Lee LEJ (1994) Development of a Cell-Line from Primary Cultures of Rainbow-Trout, *Oncorhynchus Mykiss* (Walbaum), Gills. *J Fish Dis* 17:601-611
- Bols NC, Dayeh VR, Lee LEJ, Schirmer K (2005) Use of fish cell lines in the toxicology and ecotoxicology of fish. In: Mohn, T.W., Mommsen, T.P. (Eds.), *Biochemistry and Molecular Biology of Fishes Vol. 6*. Elsevier Sciences, Amsterdam, Netherlands, ISBN 044518339.
- Boukamp P, Petrussevska RT, Breitkreutz D, Hornung J, Markham A, Fusenig NE (1988) Normal keratinization in a spontaneously immortalized aneuploid human keratinocyte cell line. *J Cell Biol* 106:761-771
- Brandenberger C, Rothen-Rutishauser B, Mühlfeld C, Schmid O, Ferron GA, Maier KL, Gehr P, Lenz AG (2010) Effects and uptake of gold nanoparticles deposited at the air-liquid interface of a human epithelial airway model. *Toxicology and Applied Pharmacology* 242:56-65
- Bruick RK, McKnight SL (2001) A conserved family of prolyl-4-hydroxylases that modify HIF. *Science* 294:1337-1340
- Brunner TJ, Wick P, Manser P, Spohn P, Grass RN, Limbach LK, Bruinink A, Stark WJ (2006) *In vitro* cytotoxicity of oxide nanoparticles: comparison to asbestos, silica, and the effect of particle solubility. *Environ Sci Technol* 40:4374-4381

- Burguera EF, Bitar M, Bruinink A (2010) Novel *in vitro* co-culture methodology to investigate heterotypic cell-cell interactions. *Eur Cell Mater* 19:166-179
- Busch W, Kühnel D, Schirmer K, Scholz S (2010) Tungsten carbide cobalt nanoparticles exert hypoxia-like effects on the gene expression level in human keratinocytes. *BMC Genomics* 11:65
- Campbell A, Oldham M, Becaria A, Bondy SC, Meacher D, Sioutas C, Misra C, Mendez LB, Kleinman M (2005) Particulate matter in polluted air may increase biomarkers of inflammation in mouse brain. *Neurotoxicology* 26:133-140
- Cedervall T, Lynch I, Lindman S, Berggard T, Thulin E, Nilsson H, Dawson KA, Linse S (2007) Understanding the nanoparticle-protein corona using methods to quantify exchange rates and affinities of proteins for nanoparticles. *Proc Natl Acad Sci USA* 104:2050-2055
- Chandel NS, Maltepe E, Goldwasser E, Mathieu CE, Simon MC, Schumacker PT (1998) Mitochondrial reactive oxygen species trigger hypoxia-induced transcription. *Proc Natl Acad Sci USA* 95:11715-11720
- Chang GH, Barbaro NM, Pieper RO (2000) Phosphatidylserine-dependent phagocytosis of apoptotic glioma cells by normal human microglia, astrocytes, and glioma cells. *Neuro Oncol* 2:174-183
- Chen M, von Mikecz A (2005) Formation of nucleoplasmic protein aggregates impairs nuclear function in response to SiO₂ nanoparticles. *Exp Cell Res* 305:51-62
- Chithrani BD, Ghazani AA, Chan WC (2006) Determining the size and shape dependence of gold nanoparticle uptake into mammalian cells. *Nano Lett* 6:662-668
- Colvin VL (2003) The potential environmental impact of engineered nanomaterials. *Nat Biotechnol* 21:1166-1170
- Dayeh VR, Lynn DH, Bols NC (2005) Cytotoxicity of metals common in mining effluent to rainbow trout cell lines and to the ciliated protozoan, *Tetrahymena thermophila*. *Toxicol In Vitro* 19:399-410
- Dayeh VR, Schirmer K, Bols NC (2002) Applying whole-water samples directly to fish cell cultures in order to evaluate the toxicity of industrial effluent. *Water Res* 36:3727-3738
- Deguchi S, Yamazaki T, Mukai SA, Usami R, Horikoshi K (2007) Stabilization of C60 nanoparticles by protein adsorption and its implications for toxicity studies. *Chem Res Toxicol* 20:854-858
- DIN ISO 13321 (2004-10) Partikelgrößenanalyse - Photonenkorrelationsspektroskopie.
- Doherty GJ, McMahon HT (2009) Mechanisms of endocytosis. *Annu Rev Biochem* 78:857-902
- Dringen R, Pawlowski PG, Hirrlinger J (2005) Peroxide detoxification by brain cells. *J Neurosci Res* 79:157-165
- Duffin R, Tran L, Brown D, Stone V, Donaldson K (2007) Proinflammatory effects of low-toxicity and metal nanoparticles *in vivo* and *in vitro*: highlighting the role of particle surface area and surface reactivity. *Inhal Toxicol* 19:849-856
- Ermolli M, Menne C, Pozzi G, Serra MA, Clerici LA (2001) Nickel, cobalt and chromium-induced cytotoxicity and intracellular accumulation in human hacaT keratinocytes. *Toxicology* 159:23-31
- Federici G, Shaw BJ, Handy RD (2007) Toxicity of titanium dioxide nanoparticles to rainbow trout (*Oncorhynchus mykiss*): gill injury, oxidative stress, and other physiological effects. *Aquat Toxicol* 84:415-430
- Fedoroff S, Richardson A (1997) *Protocols for Neural Cell Culture*. Totowa, NJ, Humana Press

- Feeney CJ, Frantseva MV, Carlen PL, Pennefather PS, Shulyakova N, Shniffer C, Mills LR (2008) Vulnerability of glial cells to hydrogen peroxide in cultured hippocampal slices. *Brain Res* 1198:1-15
- Feynman R (1991) There's plenty of room at the bottom (original from 1995). *Science* 254:1300-1301
- Geiser M, Casaulta M, Kupferschmid B, Schulz H, Semmler-Behnke M, Kreyling W (2008) The role of macrophages in the clearance of inhaled ultrafine titanium dioxide particles. *Am J Respir Cell Mol Biol* 38:371-376
- Geiser M, Rothen-Rutishauser B, Kapp N, Schurch S, Kreyling W, Schulz H, Semmler M, Im Hof V, Heyder J, Gehr P (2005) Ultrafine particles cross cellular membranes by nonphagocytic mechanisms in lungs and in cultured cells. *Environ Health Perspect* 113:1555-1560
- Gojova A, Guo B, Kota RS, Rutledge JC, Kennedy IM, Barakat AI (2007) Induction of inflammation in vascular endothelial cells by metal oxide nanoparticles: effect of particle composition. *Environ Health Perspect* 115:403-409
- Gordon S, Akopyan G, Garban H, Bonavida B (2006) Transcription factor YY1: structure, function, and therapeutic implications in cancer biology. *Oncogene* 25:1125-1142
- Gottipolu RR, Wallenborn JG, Karoly ED, Schladweiler MC, Ledbetter AD, Krantz T, Linak WP, Nyska A, Johnson JA, Thomas R, Richards JE, Jaskot RH, Kodavanti UP (2009) One-month diesel exhaust inhalation produces hypertensive gene expression pattern in healthy rats. *Environ Health Perspect* 117:38-46
- Gottschalk F, Sonderer T, Scholz RW, Nowack B (2009) Modeled environmental concentrations of engineered nanomaterials (TiO₂, ZnO, Ag, CNT, Fullerenes) for different regions. *Environ Sci Technol* 43:9216-9222
- Gratton SE, Ropp PA, Pohlhaus PD, Luft JC, Madden VJ, Napier ME, DeSimone JM (2008) The effect of particle design on cellular internalization pathways. *Proc Natl Acad Sci USA* 105:11613-11618
- Greber B, Lehrach H, Adjaye J (2007) Silencing of core transcription factors in human EC cells highlights the importance of autocrine FGF signaling for self-renewal. *BMC Dev Biol* 7:46
- Gries B, Prakash LJ (2007) Acute inhalation toxicity by contact corrosion - the case of WC-Co. Euro PM 2007, Powder Metallurgy World Congress & Exhibition, Toulouse (France), *Hard Mater.* 1:189-196
- Griffitt RJ, Hyndman K, Denslow ND, Barber DS (2009) Comparison of molecular and histological changes in zebrafish gills exposed to metallic nanoparticles. *Toxicol Sci* 107:404-415
- Griffitt RJ, Luo J, Gao J, Bonzongo JC, Barber DS (2008) Effects of particle composition and species on toxicity of metallic nanomaterials in aquatic organisms. *Environ Toxicol Chem* 27:1972-1978
- Griffitt RJ, Weil R, Hyndman KA, Denslow ND, Powers K, Taylor D, Barber DS (2007) Exposure to copper nanoparticles causes gill injury and acute lethality in zebrafish (*Danio rerio*). *Environ Sci Technol* 41:8178-8186
- Haberzettl P, Duffin R, Kramer U, Hohl D, Schins RP, Borm PJ, Albrecht C (2007) Actin plays a crucial role in the phagocytosis and biological response to respirable quartz particles in macrophages. *Arch Toxicol* 81:459-470
- Handy RD, von der Kammer F, Lead JR, Hasselov M, Owen R, Crane M (2008) The ecotoxicology and chemistry of manufactured nanoparticles. *Ecotoxicology* 17:287-314

- Harush-Frenkel O, Rozentur E, Benita S, Altschuler Y (2008) Surface charge of nanoparticles determines their endocytic and transcytotic pathway in polarized MDCK cells. *Biomacromolecules* 9:435-443
- Hildebrand H, Kühnel D, Potthoff A, Mackenzie K, Springer A, Schirmer K (2009) Evaluating the cytotoxicity of palladium/magnetite nano-catalysts intended for wastewater treatment. *Environ Pollut* 158:65-73
- Hoet PH, Roesems G, Demedts MG, Nemery B (2002) Activation of the hexose monophosphate shunt in rat type II pneumocytes as an early marker of oxidative stress caused by cobalt particles. *Arch Toxicol* 76:1-7
- Huang DW, Sherman BT, Lempicki RA (2009) Systematic and integrative analysis of large gene lists using DAVID bioinformatics resources. *Nat Protoc* 4:44-57
- International Agency for Research on Cancer (IARC) (2006) Cobalt in hard-metals and cobalt sulfate, gallium arsenide, indium phosphide and vanadium pentoxide. IARC, Monographs on the Evaluation of Carcinogenic Risks to Humans 86
- Jiang BH, Rue E, Wang GL, Roe R, Semenza GL (1996) Dimerization, DNA binding, and transactivation properties of hypoxia-inducible factor 1. *J Biol Chem* 271:17771-17778
- Jiang JK, Oberdörster G, Biswas P (2009) Characterization of size, surface charge, and agglomeration state of nanoparticle dispersions for toxicological studies. *J Nanopart Res* 11:77-89
- Jin HO, An S, Lee HC, Woo SH, Seo SK, Choe TB, Yoo DH, Lee SB, Um HD, Lee SJ, Park MJ, Kim JI, Hong SI, Rhee CH, Park IC (2007) Hypoxic condition- and high cell density-induced expression of Redd1 is regulated by activation of hypoxia-inducible factor-1 α and Sp1 through the phosphatidylinositol 3-kinase/Akt signaling pathway. *Cell Signal* 19:1393-1403
- Jobling S, Tyler CR (2003) Endocrine disruption, parasites and pollutants in wild freshwater fish. *Parasitology* 126 Suppl:S103-108
- Johnsen S, Widder EA (1999) The Physical Basis of Transparency in Biological Tissue: Ultrastructure and the Minimization of Light Scattering. *J Theor Biol* 199:181-198
- Kaczmarek M, Cachau RE, Topol IA, Kasprzak KS, Ghio A, Salnikow K (2009) Metal ion-stimulated iron oxidation in hydroxylases facilitates stabilization of HIF-1 α protein. *Toxicol Sci* 107:394-403
- Kaksonen M, Toret CP, Drubin DG (2006) Harnessing actin dynamics for clathrin-mediated endocytosis. *Nat Rev Mol Cell Biol* 7:404-414
- Kanno S, Furuyama A, Hirano S (2007) A murine scavenger receptor MARCO recognizes polystyrene nanoparticles. *Toxicol Sci* 97:398-406
- Karlsson HL, Cronholm P, Gustafsson J, Moller L (2008) Copper oxide nanoparticles are highly toxic: a comparison between metal oxide nanoparticles and carbon nanotubes. *Chem Res Toxicol* 21:1726-1732
- Karovic O, Tonazzini I, Rebola N, Edstrom E, Lovdahl C, Fredholm BB, Dare E (2007) Toxic effects of cobalt in primary cultures of mouse astrocytes. Similarities with hypoxia and role of HIF-1 α . *Biochem Pharmacol* 73:694-708
- Kasten U, Hartwig A, Beyersmann D (1992) Mechanisms of cobalt(II) uptake into V79 Chinese hamster cells. *Arch Toxicol* 66:592-597
- Kasten U, Mullenders LH, Hartwig A (1997) Cobalt(II) inhibits the incision and the polymerization step of nucleotide excision repair in human fibroblasts. *Mutat Res* 383:81-89

- Khammanit R, Chantakru S, Kitiyanant Y, Saikhun J (2008) Effect of serum starvation and chemical inhibitors on cell cycle synchronization of canine dermal fibroblasts. *Theriogenology* 70:27-34
- Kim JB, Zaehres H, Wu G, Gentile L, Ko K, Sebastiano V, Arauzo-Bravo MJ, Ruau D, Han DW, Zenke M, Scholer HR (2008) Pluripotent stem cells induced from adult neural stem cells by reprogramming with two factors. *Nature* 454:646-650
- Kopera E, Schwerdtle T, Hartwig A, Bal W (2004) Co(II) and Cd(II) substitute for Zn(II) in the zinc finger derived from the DNA repair protein XPA, demonstrating a variety of potential mechanisms of toxicity. *Chem Res Toxicol* 17:1452-1458
- Kreuter J, Shamenkov D, Petrov V, Ramge P, Cychutek K, Koch-Brandt C, Alyautdin R (2002) Apolipoprotein-mediated transport of nanoparticle-bound drugs across the blood-brain barrier. *J Drug Target* 10:317-325
- Kreyling WG, Semmler M, Erbe F, Mayer P, Takenaka S, Schulz H, Oberdörster G, Ziesenis A (2002) Translocation of ultrafine insoluble iridium particles from lung epithelium to extrapulmonary organs is size dependent but very low. *J Toxicol Environ Health A* 65:1513-1530
- Kühnel D, Busch W, Meißner T, Springer A, Potthoff A, Richter V, Gelinsky M, Scholz S, Schirmer K (2009) Agglomeration of tungsten carbide nanoparticles in exposure medium does not prevent uptake and toxicity toward a rainbow trout gill cell line. *Aquat Toxicol* 93:91-99
- Lasfargues G, Lardot C, Delos M, Lauwerys R, Lison D (1995) The delayed lung responses to single and repeated intratracheal administration of pure cobalt and hard metal powder in the rat. *Environ Res* 69:108-121
- Lasfargues G, Lison D, Maldague P, Lauwerys R (1992) Comparative study of the acute lung toxicity of pure cobalt powder and cobalt-tungsten carbide mixture in rat. *Toxicol Appl Pharmacol* 112:41-50
- Lee LE, Dayeh VR, Schirmer K, Bols NC (2009) Applications and potential uses of fish gill cell lines: examples with RTgill-W1. *In Vitro Cell Dev Biol Anim* 45:127-134
- Lee LE, Van Es SJ, Walsh SK, Rainnie DJ, Donay N, Summerfield R, Cawthorn RJ (2006) High yield and rapid growth of *Neoparamoeba pemaquidensis* in co-culture with a rainbow trout gill-derived cell line RTgill-W1. *J Fish Dis* 29:467-480
- Li H, Zhang J, Wang T, Luo W, Zhou Q, Jiang G (2008a) Elemental selenium particles at nano-size (Nano-Se) are more toxic to Medaka (*Oryzias latipes*) as a consequence of hyper-accumulation of selenium: a comparison with sodium selenite. *Aquat Toxicol* 89:251-256
- Li N, Xia T, Nel AE (2008b) The role of oxidative stress in ambient particulate matter-induced lung diseases and its implications in the toxicity of engineered nanoparticles. *Free Radic Biol Med* 44:1689-1699
- Limbach LK, Li Y, Grass RN, Brunner TJ, Hintermann MA, Muller M, Gunther D, Stark WJ (2005) Oxide nanoparticle uptake in human lung fibroblasts: effects of particle size, agglomeration, and diffusion at low concentrations. *Environ Sci Technol* 39:9370-9376
- Limbach LK, Wick P, Manser P, Grass RN, Bruinink A, Stark WJ (2007) Exposure of engineered nanoparticles to human lung epithelial cells: influence of chemical composition and catalytic activity on oxidative stress. *Environ Sci Technol* 41:4158-4163
- Lison D (1996) Human toxicity of cobalt-containing dust and experimental studies on the mechanism of interstitial lung disease (hard metal disease). *Crit Rev Toxicol* 26:585-616

- Lison D, Carbonnelle P, Mollo L, Lauwerys R, Fubini B (1995) Physicochemical mechanism of the interaction between cobalt metal and carbide particles to generate toxic activated oxygen species. *Chem Res Toxicol* 8:600-606
- Lison D, De Boeck M, Verougstraete V, Kirsch-Volders M (2001) Update on the genotoxicity and carcinogenicity of cobalt compounds. *Occup Environ Med* 58:619-625
- Lison D, Lauwerys R (1990) *In vitro* cytotoxic effects of cobalt-containing dusts on mouse peritoneal and rat alveolar macrophages. *Environ Res* 52:187-198
- Lison D, Lauwerys R (1992) Study of the mechanism responsible for the elective toxicity of tungsten carbide-cobalt powder toward macrophages. *Toxicol Lett* 60:203-210
- Lison D, Lauwerys R (1993) Evaluation of the role of reactive oxygen species in the interactive toxicity of carbide-cobalt mixtures on macrophages in culture. *Arch Toxicol* 67:347-351
- Loh YH, Ng JH, Ng HH (2008) Molecular framework underlying pluripotency. *Cell Cycle* 7:885-891
- Lombaert N, De Boeck M, Decordier I, Cundari E, Lison D, Kirsch-Volders M (2004) Evaluation of the apoptogenic potential of hard metal dust (WC-Co), tungsten carbide and metallic cobalt. *Toxicol Lett* 154:23-34
- Lombaert N, Lison D, Van Hummelen P, Kirsch-Volders M (2008) *In vitro* expression of hard metal dust (WC-Co)-responsive genes in human peripheral blood mononucleated cells. *Toxicol Appl Pharmacol* 227:299-312
- Long TC, Saleh N, Tilton RD, Lowry GV, Veronesi B (2006) Titanium dioxide (P25) produces reactive oxygen species in immortalized brain microglia (BV2): implications for nanoparticle neurotoxicity. *Environ Sci Technol* 40:4346-4352
- Lundqvist M, Stigler J, Elia G, Lynch I, Cedervall T, Dawson KA (2008) Nanoparticle size and surface properties determine the protein corona with possible implications for biological impacts. *Proc Natl Acad Sci USA* 105:14265-14270
- Manalo DJ, Rowan A, Lavoie T, Natarajan L, Kelly BD, Ye SQ, Garcia JG, Semenza GL (2005) Transcriptional regulation of vascular endothelial cell responses to hypoxia by HIF-1. *Blood* 105:659-669
- Maynard AD, Aitken RJ, Butz T, Colvin V, Donaldson K, Oberdörster G, Philbert MA, Ryan J, Seaton A, Stone V, Tinkle SS, Tran L, Walker NJ, Warheit DB (2006) Safe handling of nanotechnology. *Nature* 444:267-269
- Maynard AD, Kuempel ED (2005) Airborne nanostructured particles and occupational health. *J Nanopart Res* 7:587-614
- Medina C, Santos-Martinez MJ, Radomski A, Corrigan OI, Radomski MW (2007) Nanoparticles: pharmacological and toxicological significance. *Br J Pharmacol* 150:552-558
- Meißner T, Kühnel D, Busch W, Oswald S, Richter V, Michaelis A, Schirmer K, Potthoff A (2010) Physical-chemical characterization of tungsten carbide nanoparticles as a basis for toxicological investigations. *Nanotoxicology* 4: 196-206
- Meißner T, Potthoff A, Richter V (2009) Physico-chemical characterization in the light of toxicological effects. *Inhal Toxicol* 21 Suppl 1:35-39
- Mense SM, Sengupta A, Zhou M, Lan C, Bentsman G, Volsky DJ, Zhang L (2006) Gene expression profiling reveals the profound upregulation of hypoxia-responsive genes in primary human astrocytes. *Physiol Genomics* 25:435-449
- Moore MN (2006) Do nanoparticles present ecotoxicological risks for the health of the aquatic environment? *Environ Int* 32:967-976

- Mootha VK, Lindgren CM, Eriksson KF, Subramanian A, Sihag S, Lehar J, Puigserver P, Carlsson E, Ridderstrale M, Laurila E, Houstis N, Daly MJ, Patterson N, Mesirov JP, Golub TR, Tamayo P, Spiegelman B, Lander ES, Hirschhorn JN, Altshuler D, Groop LC (2003) PGC-1 alpha-responsive genes involved in oxidative phosphorylation are coordinately downregulated in human diabetes. *Nat Genet* 34:267-273
- Moroz E, Carlin S, Dyomina K, Burke S, Thaler HT, Blasberg R, Serganova I (2009) Real-time imaging of HIF-1alpha stabilization and degradation. *PLoS One* 4:e5077
- Mottet D, Dumont V, Decache Y, Demazy C, Ninane N, Raes M, Michiels C (2003) Regulation of Hypoxia-inducible Factor-1{alpha} Protein Level during Hypoxic Conditions by the Phosphatidylinositol 3-Kinase/Akt/Glycogen Synthase Kinase 3{beta} Pathway in HepG2 Cells. *J Biol Chem* 278:31277-31285
- Moulin JJ, Wild P, Romazini S, Lasfargues G, Peltier A, Bozec C, Deguerry P, Pellet F, Perdrix A (1998) Lung cancer risk in hard-metal workers. *Am J Epidemiol* 148:241-248
- Mueller NC, Nowack B (2008) Exposure modeling of engineered nanoparticles in the environment. *Environ Sci Technol* 42:4447-4453
- Muir DCG, Norstrom RJ (2000) Geographical differences and time trends of persistent organic pollutants in the Arctic. *Toxicol Lett* 112-113:93-101
- Muir DCG, Norstrom RJ, Simon M (1988) Organochlorine contaminants in arctic marine food chains: accumulation of specific polychlorinated biphenyls and chlordane-related compounds. *Environ Sci Technol* 22:1071-1079
- Murdock RC, Braydich-Stolle L, Schrand AM, Schlager JJ, Hussain SM (2008) Characterization of nanomaterial dispersion in solution prior to *in vitro* exposure using dynamic light scattering technique. *Toxicol Sci* 101:239-253
- Na G, Bridges PJ, Koo Y, Ko C (2008) Role of hypoxia in the regulation of periovulatory EDN2 expression in the mouse. *Can J Physiol Pharmacol* 86:310-319
- Naß R, Albayrak S, Aslan M, Schmidt H (1994) Colloidal Processing and Sintering of Nano-Scale TiN. *Int Conf Ceramic Processing, Science and Technology, Friedrichshafen, Germany*
- Navarro E, Piccapietra F, Wagner B, Marconi F, Kaegi R, Odzak N, Sigg L, Behra R (2008) Toxicity of silver nanoparticles to *Chlamydomonas reinhardtii*. *Environ Sci Technol* 42:8959-8964
- Nel A, Xia T, Madler L, Li N (2006) Toxic potential of materials at the nanolevel. *Science* 311:622-627
- Nemmar A, Hoet PH, Vanquickenborne B, Dinsdale D, Thomeer M, Hoylaerts MF, Vanbilloen H, Mortelmans L, Nemery B (2002) Passage of inhaled particles into the blood circulation in humans. *Circulation* 105:411-414
- Nemmar A, Vanbilloen H, Hoylaerts MF, Hoet PH, Verbruggen A, Nemery B (2001) Passage of intratracheally instilled ultrafine particles from the lung into the systemic circulation in hamster. *Am J Respir Crit Care Med* 164:1665-1668
- Nie S, Xing Y, Kim GJ, Simons JW (2007) Nanotechnology Applications in Cancer. *Annu Rev Biomed Eng* 9:257-288
- Oaks JL, Gilbert M, Virani MZ, Watson RT, Meteyer CU, Rideout BA, Shivaprasad HL, Ahmed S, Chaudhry MJ, Arshad M, Mahmood S, Ali A, Khan AA (2004) Diclofenac residues as the cause of vulture population decline in Pakistan. *Nature* 427:630-633
- Oberdörster G, Oberdörster E, Oberdörster J (2005) Nanotoxicology: an emerging discipline evolving from studies of ultrafine particles. *Environ Health Perspect* 113:823-839

- Oberdörster G, Sharp Z, Atudorei V, Elder A, Gelein R, Kreyling W, Cox C (2004) Translocation of inhaled ultrafine particles to the brain. *Inhal Toxicol* 16:437-445
- Oetken M, Bachmann J, Schulte-Oehlmann U, Oehlmann J (2004) Evidence for endocrine disruption in invertebrates. *Int Rev Cytol* 236:1-44
- Oh JM, Choi SJ, Lee GE, Kim JE, Choy JH (2009) Inorganic metal hydroxide nanoparticles for targeted cellular uptake through clathrin-mediated endocytosis. *Chem Asian J* 4:67-73
- Olbryt M, Jarzab M, Jazowiecka-Rakus J, Simek K, Szala S, Sochanik A (2006) Gene expression profile of B 16 (F10) murine melanoma cells exposed to hypoxic conditions *in vitro*. *Gene Expr* 13:191-203
- Ortega R, Bresson C, Fraysse A, Sandre C, Deves G, Gombert C, Tabarant M, Bleuet P, Sez nec H, Simionovici A, Moretto P, Moulin C (2009) Cobalt distribution in keratinocyte cells indicates nuclear and perinuclear accumulation and interaction with magnesium and zinc homeostasis. *Toxicol Lett* 188:26-32
- Papageorgiou I, Brown C, Schins R, Singh S, Newson R, Davis S, Fisher J, Ingham E, Case CP (2007) The effect of nano- and micron-sized particles of cobalt-chromium alloy on human fibroblasts *in vitro*. *Biomaterials* 28:2946-2958
- Papis E, Rossi F, Raspanti M, Dalle-Donne I, Colombo G, Milzani A, Bernardini G, Gornati R (2009) Engineered cobalt oxide nanoparticles readily enter cells. *Toxicol Lett* 189:253-259
- Pei D (2009) Regulation of pluripotency and reprogramming by transcription factors. *J Biol Chem* 284:3365-3369
- Pelkmans L, Fava E, Grabner H, Hannus M, Habermann B, Krausz E, Zerial M (2005) Genome-wide analysis of human kinases in clathrin- and caveolae/raft-mediated endocytosis. *Nature* 436:78-86
- Peters A, Skorkovsky J, Kotesovec F, Brynda J, Spix C, Wichmann HE, Heinrich J (2000) Associations between mortality and air pollution in central Europe. *Environ Health Perspect* 108:283-287
- Peters A, Veronesi B, Calderon-Garciduenas L, Gehr P, Chen LC, Geiser M, Reed W, Rothen-Rutishauser B, Schurch S, Schulz H (2006) Translocation and potential neurological effects of fine and ultrafine particles a critical update. *Part Fibre Toxicol* 3:13
- Pisanic TR, 2nd, Blackwell JD, Shubayev VI, Finones RR, Jin S (2007) Nanotoxicity of iron oxide nanoparticle internalization in growing neurons. *Biomaterials* 28:2572-2581
- Pope CA, 3rd, Burnett RT, Thun MJ, Calle EE, Krewski D, Ito K, Thurston GD (2002) Lung cancer, cardiopulmonary mortality, and long-term exposure to fine particulate air pollution. *JAMA* 287:1132-1141
- Potthoff A, Meißner T, Richter V, Busch W, Kühnel D, Bastian S, Iwe M, Springer A (2009) Evaluation of health risks of nanoparticles - a contribution to a sustainable development of nanotechnology. *Solid State Phenomena* 151: 183-189
- Razani B, Woodman SE, Lisanti MP (2002) Caveolae: from cell biology to animal physiology. *Pharmacol Rev* 54:431-467
- Rejman J, Oberle V, Zuhorn IS, Hoekstra D (2004) Size-dependent internalization of particles via the pathways of clathrin- and caveolae-mediated endocytosis. *Biochem J* 377:159-169
- Reyes L, Davidson MK, Thomas LC, Davis JK (1999) Effects of *Mycoplasma fermentans incognitus* on differentiation of THP-1 cells. *Infect Immun* 67:3188-3192

- Richter V, Von Ruthendorf M (1999) On hardness and toughness of ultrafine and nanocrystalline hard materials. *International Journal of Refractory Metals & Hard Materials* 17:141-152
- Roesems G, Hoet PH, Dinsdale D, Demedts M, Nemery B (2000) *In vitro* cytotoxicity of various forms of cobalt for rat alveolar macrophages and type II pneumocytes. *Toxicol Appl Pharmacol* 162:2-9
- Roldan A, Gogg S, Ferrini M, Schillaci R, De Nicola AF (1997) Glucocorticoid regulation of *in vitro* astrocyte phagocytosis. *Biocell* 21:83-89
- Rozen S, Skaletsky H (2000) Primer3 on the WWW for general users and for biologist programmers. *Methods Mol Biol* 132:365-386
- Saeed AI, Sharov V, White J, Li J, Liang W, Bhagabati N, Braisted J, Klapa M, Currier T, Thiagarajan M, Sturn A, Snuffin M, Rezantsev A, Popov D, Ryltsov A, Kostukovich E, Borisovsky I, Liu Z, Vinsavich A, Trush V, Quackenbush J (2003) TM4: a free, open-source system for microarray data management and analysis. *Biotechniques* 34:374-378
- Salata O (2004) Applications of nanoparticles in biology and medicine. *J Nanobiotechnology* 2:3
- Sanchez-Elsner T, Botella LM, Velasco B, Langa C, Bernabeu C (2002) Endoglin expression is regulated by transcriptional cooperation between the hypoxia and transforming growth factor-beta pathways. *J Biol Chem* 277:43799-43808
- Sayes CM, Reed KL, Warheit DB (2007) Assessing Toxicity of Fine and Nanoparticles: Comparing *In Vitro* Measurements to *In Vivo* Pulmonary Toxicity Profiles. *Toxicol. Sci.* 97:163-180
- Schirmer K, Chan AGJ, Greenberg BM, Dixon DG, Bols NC (1997) Methodology for demonstrating and measuring the photocytotoxicity of fluoranthene to fish cells in culture. *Toxicol In Vitro* 11:107-119
- Schubert W, Frank PG, Razani B, Park DS, Chow CW, Lisanti MP (2001) Caveolae-deficient endothelial cells show defects in the uptake and transport of albumin *in vivo*. *J Biol Chem* 276:48619-48622
- Schulze C, Kroll A, Lehr CM, Schäfer UF, Becker K, Schnekenburger J, Isfort CS, Landsiedel R, Wohlleben W (2008) Not ready to use - overcoming pitfalls when dispersing nanoparticles in physiological media. *Nanotoxicology* 2:51-61
- Seaton A, MacNee W, Donaldson K, Godden D (1995) Particulate air pollution and acute health effects. *Lancet* 345:176-178
- Semenza GL (2001) Hypoxia-inducible factor 1: oxygen homeostasis and disease pathophysiology. *Trends Mol Med* 7:345-350
- Semmler M, Seitz J, Erbe F, Mayer P, Heyder J, Oberdörster G, Kreyling WG (2004) Long-term clearance kinetics of inhaled ultrafine insoluble iridium particles from the rat lung, including transient translocation into secondary organs. *Inhal Toxicol* 16:453-459
- Shi-Wen X, Denton CP, Dashwood MR, Holmes AM, Bou-Gharios G, Pearson JD, Black CM, Abraham DJ (2001) Fibroblast matrix gene expression and connective tissue remodeling: role of endothelin-1. *J Invest Dermatol* 116:417-425
- Smith CJ, Shaw BJ, Handy RD (2007) Toxicity of single walled carbon nanotubes to rainbow trout, (*Oncorhynchus mykiss*): respiratory toxicity, organ pathologies, and other physiological effects. *Aquat Toxicol* 82:94-109
- Spurr AR (1969) A low-viscosity epoxy resin embedding medium for electron microscopy. *J Ultrastruct Res* 26:31-43

- Stearns RC, Paulauskis JD, Godleski JJ (2001) Endocytosis of ultrafine particles by A549 cells. *Am J Respir Cell Mol Biol* 24:108-115
- Stefaniak AB, Virji MA, Day GA (2009) Characterization of exposures among cemented tungsten carbide workers. Part I: Size-fractionated exposures to airborne cobalt and tungsten particles. *J Expo Sci Environ Epidemiol* 19:475-491
- Sterrenburg E, Turk R, Boer JM, van Ommen GB, den Dunnen JT (2002) A common reference for cDNA microarray hybridizations. *Nucleic Acids Res* 30:e116
- Stierum R, Heijne W, Kienhuis A, van Ommen B, Groten J (2005) Toxicogenomics concepts and applications to study hepatic effects of food additives and chemicals. *Toxicol Appl Pharmacol* 207:179-188
- Stoeger T, Takenaka S, Frankenberger B, Ritter B, Karg E, Maier K, Schulz H, Schmid O (2009) Deducing *in vivo* toxicity of combustion-derived nanoparticles from a cell-free oxidative potency assay and metabolic activation of organic compounds. *Environ Health Perspect* 117:54-60
- Stringer B, Imrich A, Kobzik L (1995) Flow cytometric assay of lung macrophage uptake of environmental particulates. *Cytometry* 20:23-32
- Subramanian A, Tamayo P, Mootha VK, Mukherjee S, Ebert BL, Gillette MA, Paulovich A, Pomeroy SL, Golub TR, Lander ES, Mesirov JP (2005) Gene set enrichment analysis: a knowledge-based approach for interpreting genome-wide expression profiles. *Proc Natl Acad Sci USA* 102:15545-15550
- Takenaka S, Karg E, Roth C, Schulz H, Ziesenis A, Heinzmann U, Schramel P, Heyder J (2001) Pulmonary and systemic distribution of inhaled ultrafine silver particles in rats. *Environ Health Perspect* 109 Suppl 4:547-551
- Tang TT, Lasky LA (2003) The forkhead transcription factor FOXO4 induces the down-regulation of hypoxia-inducible factor 1 alpha by a von Hippel-Lindau protein-independent mechanism. *J Biol Chem* 278:30125-30135
- The Royal Society and the Royal Academy of Engineering (2004) *Nanoscience and Nanotechnologies: Opportunities and Uncertainties*. Royal Society Publications, London
- Thomas WE (1992) Brain macrophages: evaluation of microglia and their functions. *Brain Res Brain Res Rev* 17:61-74
- Thomson EM, Williams A, Yauk CL, Vincent R (2009) Toxicogenomic analysis of susceptibility to inhaled urban particulate matter in mice with chronic lung inflammation. *Part Fibre Toxicol* 6:6
- Tusher VG, Tibshirani R, Chu G (2001) Significance analysis of microarrays applied to the ionizing radiation response. *Proc Natl Acad Sci USA* 98:5116-5121
- Van Goethem F, Lison D, Kirsch-Volders M (1997) Comparative evaluation of the *in vitro* micronucleus test and the alkaline single cell gel electrophoresis assay for the detection of DNA damaging agents: genotoxic effects of cobalt powder, tungsten carbide and cobalt-tungsten carbide. *Mutat Res* 392:31-43
- Vengellur A, LaPres JJ (2004) The role of hypoxia inducible factor 1 alpha in cobalt chloride induced cell death in mouse embryonic fibroblasts. *Toxicol Sci* 82:638-646
- Vengellur A, Phillips JM, Hogenesch JB, LaPres JJ (2005) Gene expression profiling of hypoxia signaling in human hepatocellular carcinoma cells. *Physiol Genomics* 22:308-318
- Vevers WF, Jha AN (2008) Genotoxic and cytotoxic potential of titanium dioxide (TiO₂) nanoparticles on fish cells *in vitro*. *Ecotoxicology* 17:410-420

- Wang J, Chen C, Liu Y, Jiao F, Li W, Lao F, Li Y, Li B, Ge C, Zhou G, Gao Y, Zhao Y, Chai Z (2008a) Potential neurological lesion after nasal instillation of TiO₂ nanoparticles in the anatase and rutile crystal phases. *Toxicol Lett* 183:72-80
- Wang X, Li C, Chen Y, Hao Y, Zhou W, Chen C, Yu Z (2008b) Hypoxia enhances CXCR4 expression favoring microglia migration via HIF-1[alpha] activation. *Biochem Biophys Res Commun* 371:283-288
- Warheit DB (2008) How meaningful are the results of nanotoxicity studies in the absence of adequate material characterization? *Toxicol Sci* 101:183-185
- Waring JF, Gum R, Morfitt D, Jolly RA, Ciurlionis R, Heindel M, Gallenberg L, Buratto B, Ulrich RG (2002) Identifying toxic mechanisms using DNA microarrays: evidence that an experimental inhibitor of cell adhesion molecule expression signals through the aryl hydrocarbon nuclear receptor. *Toxicology* 181-182:537-550
- Waters KM, Masiello LM, Zangar RC, Tarasevich BJ, Karin NJ, Quesenberry RD, Bandyopadhyay S, Teeguarden JG, Pounds JG, Thrall BD (2009) Macrophage responses to silica nanoparticles are highly conserved across particle sizes. *Toxicol Sci* 107:553-569
- Waxman S, Wurmbach E (2007) De-regulation of common housekeeping genes in hepatocellular carcinoma. *BMC Genomics* 8:243
- Wenger RH (2002) Cellular adaptation to hypoxia: O₂-sensing protein hydroxylases, hypoxia-inducible transcription factors, and O₂-regulated gene expression. *FASEB J* 16:1151-1162
- Wörle-Knirsch JM, Kern K, Schleh C, Adelhelm C, Feldmann C, Krug HF (2007) Nanoparticulate vanadium oxide potentiated vanadium toxicity in human lung cells. *Environ Sci Technol* 41:331-336
- Xia T, Kovochich M, Brant J, Hotze M, Sempf J, Oberley T, Sioutas C, Yeh JI, Wiesner MR, Nel AE (2006) Comparison of the abilities of ambient and manufactured nanoparticles to induce cellular toxicity according to an oxidative stress paradigm. *Nano Lett* 6:1794-1807
- Xia T, Kovochich M, Liong M, Madler L, Gilbert B, Shi H, Yeh JI, Zink JI, Nel AE (2008) Comparison of the mechanism of toxicity of zinc oxide and cerium oxide nanoparticles based on dissolution and oxidative stress properties. *ACS Nano* 2:2121-2134
- Yamashita K, Discher DJ, Hu J, Bishopric NH, Webster KA (2001) Molecular regulation of the endothelin-1 gene by hypoxia. Contributions of hypoxia-inducible factor-1, activator protein-1, GATA-2, AND p300/CBP. *J Biol Chem* 276:12645-12653
- Yuan Y, Hilliard G, Ferguson T, Millhorn DE (2003) Cobalt inhibits the interaction between hypoxia-inducible factor-alpha and von Hippel-Lindau protein by direct binding to hypoxia-inducible factor-alpha. *J Biol Chem* 278:15911-15916
- Yumoto R, Nishikawa H, Okamoto M, Katayama H, Nagai J, Takano M (2006) Clathrin-mediated endocytosis of FITC-albumin in alveolar type II epithelial cell line RLE-6TN. *Am J Physiol Lung Cell Mol Physiol* 290:L946-955
- Zegura B, Volcic M, Lah TT, Filipic M (2008) Different sensitivities of human colon adenocarcinoma (CaCo-2), astrocytoma (IPDDC-A2) and lymphoblastoid (NCNC) cell lines to microcystin-LR induced reactive oxygen species and DNA damage. *Toxicol* 52:518-525
- Zhang LW, Monteiro-Riviere NA (2009) Mechanisms of quantum dot nanoparticle cellular uptake. *Toxicol Sci* 110:138-155

- Zhang Q, Kusaka Y, Zhu X, Sato K, Mo Y, Kluz T, Donaldson K (2003) Comparative toxicity of standard nickel and ultrafine nickel in lung after intratracheal instillation. *J Occup Health* 45:23-30
- Zhang QW, Kusaka Y, Donaldson K (2000) Comparative pulmonary responses caused by exposure to standard cobalt and ultrafine cobalt. *J Occup Health* 42:179-184
- Zhu S, Oberdörster E, Haasch ML (2006) Toxicity of an engineered nanoparticle (fullerene, C60) in two aquatic species, *Daphnia* and fathead minnow. *Mar Environ Res* 62 Suppl:S5-9
- Zou W, Yan M, Xu W, Huo H, Sun L, Zheng Z, Liu X (2001) Cobalt chloride induces PC12 cells apoptosis through reactive oxygen species and accompanied by AP-1 activation. *J Neurosci Res* 64:646-653

APPENDIX

Chapter 5, Table 3. Genes with most prominent changes in expression levels[†].

WC 3h	WCCo 3h	CoCl2 3h	WC 3d	WCCo 3d	CoCl2 3d	Gene Name	Accession	Description
	up	up	up	up	up	PPFIA4	NM_015053	protein tyrosine phosphatase, receptor type, f polypeptide (PTPRF), interacting protein (liprin), alpha 4 (PPFIA4), mRNA [NM_015053]
		up	up	up	up	BNIP3	NM_004052	BCL2/adenovirus E1B 19kDa interacting protein 3 (BNIP3), nuclear gene encoding mitochondrial protein, mRNA [NM_004052]
		up	up	up	up	PDK1	NM_002610	pyruvate dehydrogenase kinase, isozyme 1 (PDK1), nuclear gene encoding mitochondrial protein, mRNA [NM_002610]
		up	up	up	up	CA9	NM_001216	carbonic anhydrase IX (CA9), mRNA [NM_001216]
		up	up	up	up	EGLN3	NM_022073	egl nine homolog 3 (C. elegans) (EGLN3), mRNA [NM_022073]
		up	up	up	up	LOXL2	NM_002318	lysyl oxidase-like 2 (LOXL2), mRNA [NM_002318]
			up	up	up	THC2369600	THC2369600	ALU6_HUMAN (P39193) Alu subfamily SP sequence contamination warning entry, partial (12%) [THC2369600]
			up	up	up	PLOD2	NM_182943	procollagen-lysine, 2-oxoglutarate 5-dioxygenase 2 (PLOD2), transcript variant 1, mRNA [NM_182943]
			up	up	up	PPP1R3C	NM_005398	protein phosphatase 1, regulatory (inhibitor) subunit 3C (PPP1R3C), mRNA [NM_005398]
			up	up	up	CST6	NM_001323	cystatin E/M (CST6), mRNA [NM_001323]
			up	up	up	FN1	NM_212482	fibronectin 1 (FN1), transcript variant 1, mRNA [NM_212482]
			up	up	up	THC2316753	THC2316753	Q91TG6 (Q91TG6) T130, partial (7%) [THC2316753]
			up	up	up	VLDLR	NM_003383	very low density lipoprotein receptor (VLDLR), transcript variant 1, mRNA [NM_003383]
			up	up	up	AML1a	ENST00000358356	mRNA for AML1a protein, complete cds. [D43967]
			up	up	up	HK2	NM_000189	hexokinase 2 (HK2), mRNA [NM_000189]
			up	up	up	PTGS2	NM_000963	prostaglandin-endoperoxide synthase 2 (prostaglandin G/H synthase and cyclooxygenase) (PTGS2), mRNA [NM_000963]
			up	up	up	SLC2A14	BC060766	solute carrier family 2 (facilitated glucose transporter), member 14, mRNA (cDNA clone MGC:71510 IMAGE:5297510), complete cds. [BC060766]
			up	up	up	GPI	NM_000175	glucose phosphate isomerase (GPI), mRNA [NM_000175]
			up	up	up	ENO2	NM_001975	enolase 2 (gamma, neuronal) (ENO2), mRNA [NM_001975]
			up	up	up	CDH2	NM_001792	cadherin 2, type 1, N-cadherin (neuronal) (CDH2), mRNA [NM_001792]
			up	up	up	AK021874	ENST00000366930	cDNA FLJ11812 fis, clone HEMBA1006364. [AK021874]
	up	up	up	up	up	ASB2	NM_016150	ankyrin repeat and SOCS box-containing 2 (ASB2), mRNA [NM_016150]
	up	up	up	up	up	ANGPTL4	NM_139314	angiopoietin-like 4 (ANGPTL4), transcript variant 1, mRNA [NM_139314]
	up	up	up	up	up	LOC653068	XM_925841	PREDICTED: similar to TBP-associated factor 9L (LOC653068), mRNA [XM_925841]
		up		up	up	TCF19	BC033086	transcription factor 19 (SC1), mRNA (cDNA clone MGC:45652 IMAGE:3160434), complete cds. [BC033086]
		up		up	up	AIPL1	NM_014336	aryl hydrocarbon receptor interacting protein-like 1 (AIPL1), transcript variant 1, mRNA [NM_014336]
		up		up	up	LOC200726	XM_117266	PREDICTED: hypothetical LOC200726 (LOC200726), mRNA [XM_117266]
		up		up	up	LUZPP1	AJ312775	mRNA for leucine zipper protein 3 (LUZP3 gene). [AJ312775]
		up		up	up	C9orf65	NM_138818	chromosome 9 open reading frame 65 (C9orf65), mRNA [NM_138818]
		up		up	up	THC2411387	THC2411387	ALU8_HUMAN (P39195) Alu subfamily SX sequence contamination warning entry, partial (9%) [THC2411387]
		up		up	up	SOX6	NM_033326	SRY (sex determining region Y)-box 6 (SOX6), transcript variant 2, mRNA [NM_033326]
		up		up	up	SULT2A1	NM_003167	sulfotransferase family, cytosolic, 2A, dehydroepiandrosterone (DHEA)-preferring, member 1 (SULT2A1), mRNA [NM_003167]
		up		up	up	C1orf67	BC042869	cDNA clone IMAGE:5270407. [BC042869]
		up		up	up	CRB1	NM_201253	crumbs homolog 1 (Drosophila) (CRB1), mRNA [NM_201253]
	up	up		up	up	EDN2	NM_001956	endothelin 2 (EDN2), mRNA [NM_001956]
			up	up	up	CBLN4	NM_080617	cerebellin 4 precursor (CBLN4), mRNA [NM_080617]
			up	up	up	G65686	ENST00000332107	A117 Human STS cDNA, sequence tagged site. [G65686]
			up	up	up	XAGE2	NM_130777	X antigen family, member 2 (XAGE2), mRNA [NM_130777]
			up	up	up	PELO	AF118075	PRO1770 mRNA, complete cds. [AF118075]
			up	up	up	SAA3P	AY209188	truncated serum amyloid A3 precursor (SAA3) mRNA, complete cds. [AY209188]
			up	up	up	ITIHS	NM_030569	inter-alpha (globulin) inhibitor H5 (ITIHS), transcript variant 1, mRNA [NM_030569]
			up	up	up	MCHR1	NM_005297	melanin-concentrating hormone receptor 1 (MCHR1), mRNA [NM_005297]
			up	up	up	MGAT4A	NM_012214	mannosyl (alpha-1,3-)-glycoprotein beta-1,4-N-acetylglucosaminyltransferase, isozyme A (MGAT4A), mRNA [NM_012214]
			up	up	up	GPR65	NM_003608	G protein-coupled receptor 65 (GPR65), mRNA [NM_003608]
			up	up	up	DFNB31	AK056190	cDNA FLJ31628 fis, clone NT2RI2003344, weakly similar to PRESYNAPTIC PROTEIN SAP97. [AK056190]
			up	up	up	LRP8	NM_033300	low density lipoprotein receptor-related protein 8, apolipoprotein E receptor (LRP8), transcript variant 2, mRNA [NM_033300]
dn		up	up	up	up	SORCS3	NM_014978	sortilin-related VPS10 domain containing receptor 3 (SORCS3), mRNA [NM_014978]
dn		up		up	up	HLA-DPA1	NM_033554	major histocompatibility complex, class II, DP alpha 1 (HLA-DPA1), mRNA [NM_033554]
		up	dn	dn	up	AKR1C1	BC040210	aldo-keto reductase family 1, member C1, mRNA (cDNA clone MGC:42600 IMAGE:4825338), complete cds. [BC040210]
		up		dn	up	WDR64	NM_144625	WD repeat domain 64 (WDR64), mRNA [NM_144625]
		dn		up	up	ESCO2	NM_001017420	establishment of cohesion 1 homolog 2 (S. cerevisiae) (ESCO2), mRNA [NM_001017420]
		dn		up	up	CACNG5	NM_145811	calcium channel, voltage-dependent, gamma subunit 5 (CACNG5), transcript variant 1, mRNA [NM_145811]
		dn		up	up	ANPEP	NM_001150	alanyl (membrane) aminopeptidase (aminopeptidase N, aminopeptidase M, microsomal aminopeptidase, CD13, p150) (ANPEP), mRNA [NM_001150]
			dn	up	up	GPX7	NM_015696	glutathione peroxidase 7 (GPX7), mRNA [NM_015696]
			dn	dn	up	TLL7	NM_024686	tubulin tyrosine ligase-like family, member 7 (TLL7), mRNA [NM_024686]
			dn	dn	up	THC2371963	THC2371963	AIP1_HUMAN (Q86UL8) Atrophin-1 interacting protein 1 (Atrophin-1 interacting protein A) (MAGI-2), partial (3%) [THC2371963]
	up		dn	dn	up	GDF15	NM_004864	growth differentiation factor 15 (GDF15), mRNA [NM_004864]

Chapter 5, Table 3. Genes with most prominent changes in expression levels[#] - continued.

WC 3h	WCCo 3h	CoCl2 3h	WC 3d	WCCo 3d	CoCl2 3d	Gene Name	Accession	Description
			<i>dn</i>		<i>dn</i>	ALDH1A1	NM_000689	aldehyde dehydrogenase 1 family, member A1 (ALDH1A1), mRNA [NM_000689]
			<i>dn</i>		<i>dn</i>	DCN	NM_001920	decorin (DCN), transcript variant A1, mRNA [NM_001920]
			<i>dn</i>		<i>dn</i>	SOX2	NM_003106	SRY (sex determining region Y)-box 2 (SOX2), mRNA [NM_003106]
			<i>dn</i>		<i>dn</i>	TAF9B	NM_015975	TAF9B RNA polymerase II, TATA box binding protein (TBP)-associated factor, 31kDa (TAF9B), mRNA [NM_015975]
			<i>dn</i>		<i>dn</i>	THC2302184	THC2302184	GAL2_HUMAN (Q01415) N-acetylgalactosamine kinase (GalNAc kinase) (Galactokinase 2), partial (21%) [THC2302184]
			<i>dn</i>		<i>dn</i>	PTPRZ1	NM_002851	protein tyrosine phosphatase, receptor-type, Z polypeptide 1 (PTPRZ1), mRNA [NM_002851]
			<i>dn</i>		<i>dn</i>	DMRT2	NM_006557	doublesex and mab-3 related transcription factor 2 (DMRT2), transcript variant 1, mRNA [NM_006557]
			<i>dn</i>		<i>dn</i>	CLEC3A	NM_005752	C-type lectin domain family 3, member A (CLEC3A), mRNA [NM_005752]
			<i>dn</i>		<i>dn</i>	ATP10B	AB018258	mRNA for KIAA0715 protein, partial cds. [AB018258]
			<i>dn</i>		<i>dn</i>	PROS1	NM_000313	protein S (alpha) (PROS1), mRNA [NM_000313]
			<i>dn</i>		<i>dn</i>	RAXLX	NM_001008494	RAX-like homeobox (RAXLX), mRNA [NM_001008494]
			<i>dn</i>		<i>dn</i>	OLFM4	NM_006418	olfactomedin 4 (OLFM4), mRNA [NM_006418]
			<i>dn</i>		<i>dn</i>	DSG4	NM_177986	desmoglein 4 (DSG4), mRNA [NM_177986]
			<i>dn</i>	<i>dn</i>	<i>dn</i>	IQGAP2	NM_006633	IQ motif containing GTPase activating protein 2 (IQGAP2), mRNA [NM_006633]
			<i>dn</i>	<i>dn</i>	<i>dn</i>	MAL	NM_002371	mal, T-cell differentiation protein (MAL), transcript variant a, mRNA [NM_002371]
			<i>dn</i>	<i>dn</i>	<i>dn</i>	KRT1	NM_006121	keratin 1 (epidermolytic hyperkeratosis) (KRT1), mRNA [NM_006121]
			<i>dn</i>	<i>dn</i>	<i>dn</i>	MMP1	NM_002421	matrix metalloproteinase 1 (interstitial collagenase) (MMP1), mRNA [NM_002421]
	<i>dn</i>		<i>dn</i>	<i>dn</i>	<i>dn</i>	LAMP3	NM_014398	lysosomal-associated membrane protein 3 (LAMP3), mRNA [NM_014398]
	<i>dn</i>		<i>dn</i>	<i>dn</i>	<i>dn</i>	HLA-DMB	NM_002118	major histocompatibility complex, class II, DM beta (HLA-DMB), mRNA [NM_002118]
	<i>dn</i>		<i>dn</i>	<i>dn</i>	<i>dn</i>	HERC5	NM_016323	hect domain and RLD 5 (HERC5), mRNA [NM_016323]
				<i>dn</i>	<i>dn</i>	BTN3A3	NM_006994	butyrophilin, subfamily 3, member A3 (BTN3A3), transcript variant 1, mRNA [NM_006994]
				<i>dn</i>	<i>dn</i>	C6orf130	NM_145063	chromosome 6 open reading frame 130 (C6orf130), mRNA [NM_145063]
				<i>dn</i>	<i>dn</i>	CRY2	NM_021117	cryptochrome 2 (photolyase-like) (CRY2), mRNA [NM_021117]
				<i>dn</i>	<i>dn</i>	TMEM140	NM_018295	transmembrane protein 140 (TMEM140), mRNA [NM_018295]
				<i>dn</i>	<i>dn</i>	ZNF438	NM_182755	zinc finger protein 438 (ZNF438), mRNA [NM_182755]
				<i>dn</i>	<i>dn</i>	DNMT3L	NM_013369	DNA (cytosine-5)-methyltransferase 3-like (DNMT3L), transcript variant 1, mRNA [NM_013369]
	<i>dn</i>					CTAGE3	AF338231	CTAGE-3 protein mRNA, complete cds. [AF338231]
	<i>dn</i>					MOSPD2	NM_152581	motile sperm domain containing 2 (MOSPD2), mRNA [NM_152581]
	<i>dn</i>					OR4N4	NM_001005241	olfactory receptor, family 4, subfamily N, member 4 (OR4N4), mRNA [NM_001005241]
	<i>dn</i>					SPATA7	NM_018418	spermatogenesis associated 7 (SPATA7), transcript variant 1, mRNA [NM_018418]
	<i>dn</i>					TMC1	NM_138691	transmembrane channel-like 1 (TMC1), mRNA [NM_138691]

[#] listed genes were statistically significant different and exhibited at least a 5fold induction or repression in one of the treatments (with respect to controls and based on normalised fluorescence intensity ratios in the microarray analysis); type of gene regulation is indicated as “up” for induction (> 2fold) and “dn” for repression (> 2fold); fields are empty when induction or repression was < 2fold; full table is provided as Additional File 1 (<http://www.biomedcentral.com/content/supplementary/1471-2164-11-65-S1.XLS>).

Chapter 5, Table 4. Gene sets with strongest overlaps with observed differentially expressed genes.*

up-regulated gene sets	description	WC 3h	WCCo 3h	CoCl2 3h	WC 3d	WCCo 3d	CoCl2 3d
hypoxia related gene sets							
HIF1_TARGETS	Hif-1 (hypoxia-inducible factor 1) transcriptional targets		0.17			0.01	
HIFPATHWAY	BIOCARTA: Under normal conditions, HIF-1 is degraded; under hypoxic conditions, it activates transcription of genes controlled by hypoxic response elements (HREs)					0.02	0.20
HYPOXIA_FIBRO_UP	Up-regulated by hypoxia in normal fibroblasts from both young and old donors		0.20		0.65	0.05	
HYPOXIA_NORMAL_UP	Up-regulated by hypoxia in normal, RPTEC renal cells		0.50			0.02	
HYPOXIA_REG_UP	Up-regulated by hypoxia in renal cells, and down-regulated with reoxygenation		0.05			0.01	0.03
HYPOXIA_REVIEW	Genes known to be induced by hypoxia		0.22		0.75	0.00	
MANALO_HYPOXIA_UP	Genes up-regulated in human pulmonary endothelial cells under hypoxic conditions or after exposure to AdCA5, an adenovirus carrying constitutively active hypoxia-inducible factor 1 (HIF-1alpha)		0.24			0.01	0.21
MENSE_HYPOXIA_UP	List of Hypoxia-induced genes found in both Astrocytes and HeLa Cell		0.00			0.02	0.13
RESPONSE_TO_HYPOXIA	GO:0001666. Change in state or activity of a cell or an organism (in terms of movement, secretion, enzyme production, gene expression, etc.) as a result of a stimulus indicating lowered oxygen tension					0.12	0.08
carbohydrate metabolism							
POLYSACCHARIDE_METABOLIC_PROCESS	GO:0005976. Chemical reactions and pathways involving polysaccharides, a polymer of more than 10 monosaccharide residues joined by glycosidic linkages					0.06	
FRUCTOSE_AND_MANNOSE_METABOLISM	Genes involved in fructose and mannose metabolism		0.21			0.02	
HSA00010_GLYCOLYSIS_AND_GLUONEOGENESIS	KEGG: Genes involved in glycolysis and gluconeogenesis					0.00	0.14
GLYCOGEN_METABOLISM	Genes involved in glycogen metabolism					0.04	
GALACTOSE_METABOLISM	Genes involved in galactose metabolism					0.04	
PENTOSE_PHOSPHATE_PATHWAY	Genes involved in pentose phosphate pathway				0.61	0.14	
STARCH_AND_SUCROSE_METABOLISM	Genes involved in starch and sucrose metabolism					0.01	0.50
endocrine metabolism							
GN_CAMP_GRANULOSA_UP	Up-regulated in human granulosa cells by the gonadotropins LH and FSH, as well as by cAMP-stimulator forskolin					0.01	0.17
LH_GRANULOSA_UP	Up-regulated in human granulosa cells stimulated with luteinizing hormone (LH)					0.01	
FSH_GRANULOSA_UP	Up-regulated in human granulosa cells stimulated with follicle stimulation hormone (FSH)					0.01	
BREAST_CANCER_ESTROGEN_SIGNALING	Genes preferentially expressed in breast cancers, especially those involved in estrogen-receptor-dependent signal transduction					0.05	
PROSTAGLANDIN_SYNTHESIS_REGULATION	WIKIPATHWAYS: Prostaglandin Synthesis and Regulation		0.09				
HSA04150_MTOR_SIGNALING_PATHWAY	KEGG: Genes involved in mTOR signalling pathway		0.19				
cell adhesion, structure, cytoskeleton							
HSA04510_FOCAL_ADHESION	KEGG: Genes involved in focal adhesion					0.07	0.46
ACTIN_CYTOSKELETON	GO:0015629. Part of the cytoskeleton (the internal framework of a cell) composed of actin and associated proteins					0.04	
ACTIN_BINDING	GO:0003779. Interacting selectively with monomeric or multimeric forms of actin, including actin filaments					0.06	
CYTOSKELETON_DEPENDENT_INTRACELLULAR_TRANSPORT	GO:0030705. The directed movement of substances along cytoskeletal elements such as microfilaments or microtubules within a cell					0.07	
ANATOMICAL_STRUCTURE_FORMATION	GO:0048646. Process pertaining to the initial formation of an anatomical structure from unspecified parts					0.04	
VASCULATURE_DEVELOPMENT	GO:0001944. Process whose specific outcome is the progression of the vasculature over time, from its formation to the mature structure					0.04	
ANGIOGENESIS	GO:0001525. Blood vessel formation when new vessels emerge from the proliferation of pre-existing blood vessels					0.05	
HSA04512_ECM_RECEPTOR_INTERACTION	KEGG: Genes involved in ECM-receptor interaction					0.06	0.29
miscellaneous							
G13_SIGNALING_PATHWAY	G13 signaling pathway					0.10	0.51
NUCLEOTIDE_BIOSYNTHETIC_PROCESS	GO:0009165. Chemical reactions and pathways resulting in the formation of nucleotides					0.09	
CARBON_CARBON_LYASE_ACTIVITY	GO:0016830. Catalysis of the cleavage of C-C bonds by other means than by hydrolysis or oxidation, or conversely adding a group to a double bond					0.10	
ALKPATWAY	Activin receptor-like kinase 3 (ALK3) is required during gestation for cardiac muscle development						0.29
CARDIACEGFPATWAY	BIOCARTA: Cardiac hypertrophy, a response to high blood pressure, is stimulated by GPCR ligands such as angiotensin II that activate the EGF pathway		0.21			0.01	
WNT_SIGNALING	Wnt signaling genes					0.01	
HSA05211_RENAL_CELL_CARCINOMA	Genes involved in renal cell carcinoma					0.07	
NKTPATWAY	BIOCARTA: T cell differentiation into Th1 and Th2 cells occurs by differential chemokine receptor expression, which mediates tissue localization and immune response						0.29
BIOGENIC_AMINE_SYNTHESIS	WIKIPATHWAYS: Genes involved in synthesis of biogenic amines		0.23				
HSA00591_LINOLEIC_ACID_METABOLISM	Genes involved in linoleic acid metabolism		0.22				
HSA00361_GAMMA_HEXACHLOROCYCLOHEXANE_DEGRADATION	KEGG: Genes involved in gamma-hexachlorocyclohexane degradation		0.17				

Chapter 5, Table 4. Gene sets with strongest overlaps with observed differentially expressed genes.*

down-regulated gene sets	description	WC 3h	WCCo 3h	CoCl2 3h	WC 3d	WCCo 3d	CoCl2 3d
<i>RNA metabolism and processing</i>							
MRNA_METABOLIC_PROCESS	GO:0016071. Chemical reactions and pathways involving mRNA		0.23				
RIBONUCLEOPROTEIN_COMPLEX_BIOGENESIS_AND_ASSEMBLY	GO:0022613. The cellular process by which a complex containing RNA and proteins, is synthesized, aggregates, and bonds together		0.25				
RNA_PROCESSING	GO:0006396. Any process involved in the conversion of one or more primary RNA transcripts into one or more mature RNA molecules		0.20				
RNA_SPLICING_VIA_TRANSESTERIFICATION_REACTIONS	GO:0000375. Splicing of RNA via a series of two transesterification reactions		0.20				
SEQUENCE_SPECIFIC_DNA_BINDING	GO:0043565. Interacting selectively with DNA of a specific nucleotide composition, e.g. GC-rich DNA binding, or with a specific sequence motif or type of DNA e.g. promotor binding or rDNA binding		0.33				
TRNA_METABOLIC_PROCESS	GO:0006399. Chemical reactions and pathways involving tRNA		0.27				
<i>nucleus and the nuclear membrane related gene sets</i>							
PORE_COMPLEX	GO:0046930. Any small opening in a membrane that allows the passage of gases and/or liquids.		0.28				
NUCLEAR_PORE	GO:0005643. Any of the numerous similar discrete openings in the nuclear envelope of a eukaryotic cell, where the inner and outer nuclear membranes are joined		0.19				
NUCLEAR_LUMEN	GO:0031981. The volume enclosed by the nuclear inner membrane		0.31				
NUCLEAR_MEMBRANE	GO:0031965. Either of the lipid bilayers that surround the nucleus and form the nuclear envelope; excludes the intermembrane space		0.31				
<i>enzyme and receptor activity</i>							
UBIQUITIN_PROTEIN_LIGASE_ACTIVITY	GO:0004842. Catalysis of the reaction: ATP + ubiquitin + protein lysine = AMP + diphosphate + protein N-ubiquityllysine		0.32				
SMALL_PROTEIN_CONJUGATING_ENZYME_ACTIVITY	GO:0008639. Catalysis of the covalent attachment of small proteins, such as ubiquitin or ubiquitin-like proteins, to lysine residues on a target protein. This function may be performed alone or in conjunction with an E3, ubiquitin-like protein ligase		0.21				
CASPASEPATHWAY	BIOCARTA: Caspases are cysteine proteases active in apoptosis				0.30		

* identified by GSEA (gene set enrichment analysis), using the databases MSigDB C2 and C5; number of entries is limited to gene sets with a false discovery rate (FDR)<0.35 in at least one of the treatments and FDR<0.1 for the WC-Co 3d treatment; only gene sets obviously related to biochemical pathways or cellular organelles were selected; full table provided as Additional File 3 (<http://www.biomedcentral.com/content/supplementary/1471-2164-11-65-S3.XLS>).

AUTHORS' CONTRIBUTIONS TO THE MANUSCRIPTS

The research of this thesis was part of an interdisciplinary project funded by the BMBF. Groups with expertise in particle production and chemistry (Fraunhofer IKTS; Dresden), electron microscopy (Max Bergman Centre for Biomaterials - MBZ, TU Dresden), isolation and toxicology of rat brain cells (Medical Faculty, TU Dresden) and (Eco)toxicology of particles and chemicals (Helmholtz Centre for Environmental Research - UFZ, Leipzig) contributed to a coherent, integrated assessment of the behaviour and toxicity of the nanoparticles as proposed by the main applicants. Four Ph.D. students and two postdoctoral scientists carried out the research in the different groups based on their respective expertise. Thus, the results of the project were, in most cases, published jointly. For all of my research on uptake and toxicity of the nanoparticles, I received particle suspensions by the material scientist (IKTS) who also provided the physico-chemical characterisation of the particles. For visualisation by electron microscopy, samples were prepared by me but processed by the colleagues of the MBZ. A detailed explanation of my contributions to each of the chapters of my Ph.D. thesis is given below.

Chapter 2 - Internalisation of engineered nanoparticles into mammalian cells in vitro: influence of cell type and particle properties

As the first author of this article, I prepared and submitted the manuscript. I conducted the flow cytometry experiments and performed all experiments regarding particle uptake into the human cell lines and partly also for PBMC and OLN93 cells. I conducted light microscopy studies together with one of the co-authors and compiled the video. Experiments with rat brain cells and parts of experiments with monocytes and lung cells were carried out by co-authors. I analysed most of the data and merged data for the manuscript.

Chapter 3 - Toxicity of tungsten carbide and cobalt-doped tungsten carbide nanoparticles in mammalian cells in vitro

I am one of the equally contributing first authors that are listed in alphabetical order. The toxicological experiments with human cells were carried out by me. I performed data analyses and prepared the results section of the manuscript for that part of the study. I

was also involved in writing the introduction and discussion of the article, whereas the final preparation and editing of the entire article was done by Kristin Schirmer (the last author). The other equally contributing first authors were involved in particle preparation and characterisation, toxicological experiments with rat brain cells and electron microscopy.

Chapter 4 - Agglomeration of tungsten carbide nanoparticles in exposure medium does not prevent uptake and toxicity toward a rainbow trout gill cell line

I am the second author of this article. All experiments as well as data analyses were jointly carried out by Dana Kühnel (the first author) and me with equal contributions. I participated partly in the preparation of the manuscript. The main part of the manuscript was prepared and submitted by the first author.

Chapter 5 - Tungsten carbide cobalt nanoparticles exert hypoxia-like effects on the gene expression level in human keratinocytes

As the first author of the article I carried out all experiments as well as the computational data analyses and statistics. I prepared and submitted the manuscript.

Further publications related to this thesis:

Meißner T., Kühnel D., **Busch W.**, Oswald S., Richter V., Schirmer K., Potthoff A. (2010) Physical-chemical characterization of tungsten carbide nanoparticles as a basis for toxicological investigations. *Nanotoxicology* 4: 196-206

Potthoff A., Meißner T., Richter V., **Busch W.**, Kühnel D., Bastian S., Iwe M., Springer A. (2009). Evaluation of health risks of nanoparticles - a contribution to a sustainable development of nanotechnology. *Solid State Phenomena* 151: 183-189

CURRICULUM VITAE

WIBKE BUSCH

Name Wibke Busch; married, two children
Place and Date of Birth Freiberg, Germany; November 1st, 1978

Research Associate at the Helmholtz Centre for Environmental Research (UFZ)

Since May 2010 Department of Bioanalytical Ecotoxicology, Helmholtz Centre for Environmental Research (UFZ), Leipzig, Germany

BMBF-funded Project: "Iron-based nanoparticles and nano-composite structures for contaminant removal of ground and waste waters (Fe-NANOSIT).

PhD student at the Helmholtz Centre for Environmental Research (UFZ)

Feb. 2006 – Apr. 2010 Department of Bioanalytical Ecotoxicology (former Cell Toxicology), Helmholtz Centre for Environmental Research (UFZ), Leipzig, Germany

BMBF-funded Project: "Identification and Assessment of the Effects of Engineered Nanoparticles on Human and Environmental Health (INOS)"

Award PhD proposal was awarded additional financial support by the "Max-Buchner-Forschungsstiftung"

Diploma in Biotechnology (Graduate Engineer)

Sep. 1999 – Feb. 2005 Study of Biotechnology, FH Jena (University of Applied Sciences), Jena, Germany

May 2003 – Dec. 2004 Placement and diploma thesis, Dept. of Molecular Biochemistry, Institute of Biochemistry, Faculty of Medicine, University of Leipzig, Germany

Title of diploma thesis: "Structural and functional evolution of the V2-Vasopressin receptor"

Nov. 1998 – Jul. 1999 Stay abroad (Australia)

Oct. 1997 – Sep. 1999 Study of process engineering, Technical University of Dresden, Germany

1997 Abitur at the "Geschwister Scholl Gymnasium" Freiberg

1992-1997 "Geschwister Scholl Gymnasium" Freiberg, Germany

1985-1992 Primary and Secondary School Weißenborn, Germany

Place, Date

Wibke Busch

EIDESSTATTLICHE ERKLÄRUNG

Hiermit versichere ich eidesstattlich, dass die vorliegende Arbeit ohne unzulässige Hilfe Dritter und ohne Benutzung anderer als der angegebenen Hilfsmittel angefertigt habe; die aus fremden Quellen direkt oder indirekt übernommenen Gedanken sind als solche kenntlich gemacht. Die Arbeit wurde bisher weder im Inland noch im Ausland in gleicher oder ähnlicher Form einer anderen Prüfungsbehörde vorgelegt.

.....

Ort, Datum

.....

Wibke Busch

DANKSAGUNG

Ich möchte mich ganz herzlich bei allen bedanken, die zum Entstehen und Gelingen dieser Arbeit beigetragen haben und durch Ihre Aktionen und Diskussionen das, ohnehin schon schöne, Arbeitsklima im Department noch angenehmer werden ließen.

Ganz besonders möchte ich mich bei Prof. Kristin Schirmer und Dr. Stefan Scholz bedanken, die es mir ermöglichten ans UFZ zu kommen und diese Arbeit durchzuführen. Beiden danke ich für die wundervolle Betreuung und Unterstützung während der gesamten Zeit und für ihren unermüdlichen Einsatz beim Korrekturlesen.

Prof. Krauß danke ich herzlich für die Betreuung der Arbeit von Seiten der Universität Halle und für die angeregten Diskussionen und Hinweise im AG Seminar in Halle.

Ein besonderer Dank gilt den Projektpartnern, ohne deren einwandfreie Kooperation diese Arbeit nicht in dieser Form entstanden wäre. Ich danke Dr. Armin Springer für großartige elektronen-mikroskopische Aufnahmen, Tobias Meißner für die schnelle und unproblematische Bereitstellung der Nanopartikel und die kurzfristigen Antworten auf die vielen kleinen und großen Fragen. Susanne Bastian danke ich fürs gegenseitige Motivieren, Diskutieren, und die effektive Zusammenarbeit. Dr. Irina Lehmann danke ich für die Weiterbildung am FACS und die gute Zusammenarbeit. Ich möchte mich auch bei Dr. Hajo Stärk bedanken, für seine Motivation die widerspenstigen Partikel kaputt zu bekommen und zu quantifizieren.

Außerdem möchte ich mich bei allen Mitarbeitern des Departments Bioanalytische Ökotoxikologie und des früheren Departments Zelltoxikologie für ihre Offenheit und die angenehme Arbeitsatmosphäre bedanken, besonders bei Dr. Rolf Altenburger für den unproblematischen Übergang ins neue Department. Peggy danke ich für ihre Hilfe und Expertise in der Zellkultur. Kelly und Matthias danke ich für ihre Unterstützung im Labor. Bei Nils und Uli bedanke ich mich für die fachlichen Diskussionen und die wertvollen Hinweise auf viele kleine Fragen. Janet danke ich fürs allwöchentliche Philosophieren über die Wissenschaft und sonstige weltbewegende Fragen. Meinen

ehemaligen Büromitbewohnern Stephan und Till danke ich für ihr Interesse an meiner Arbeit, für tolle Gespräche und alle sportlichen und kulinarischen Aktionen.

Mein größter Dank gilt Dana, meiner Projektpartnerin, Büromitbewohnerin und Freundin, die immer ein offenes Ohr hatte und mir jederzeit hilfsbereit zur Seite stand. Ich danke ihr für all die Diskussionen, das gemeinsame Freuen und Fluchen über Erfolge und Misserfolge, die gute Zusammenarbeit und die gemeinsame Zeit auch außerhalb des UFZ.

Von ganzem Herzen möchte ich mich bei meiner Familie bedanken, bei Ralf-Uwe, Lena und Pepe für ihre Geduld, ihr Verständnis und ihre Unterstützung und bei meinen Eltern und Schwiegereltern für die liebevolle Kinderbetreuung in Zeiten von Krankheit, Ferien oder Dienstreisen.